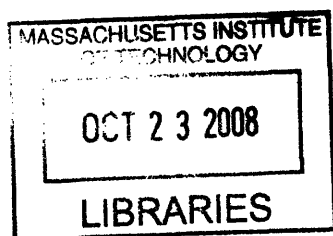


Quantifying Effects of Substrata Chemomechanical Properties on Eukaryotic and Prokaryotic Cell Adhesion and Morphology

By
Michael Todd Thompson
B.S., Biochemistry and Mathematics
University of Arizona Honors College, 1999

SUBMITTED TO THE DIVISION OF HEALTH SCIENCES AND TECHNOLOGY
IN PARTIAL FULFILLMENT OF THE REQUIREMENTS FOR THE DEGREE OF

Doctor of Philosophy in Biomedical Engineering/Medical Physics
at the
MASSACHUSETTS INSTITUTE OF TECHNOLOGY



© Michael Todd Thompson, 2008
All rights reserved.

The author hereby grants to MIT permission to reproduce
and to distribute publicly paper and electronic
copies of this thesis document in whole or in part
in any medium now known or hereafter created.

Signature of Author: _____
Harvard-MIT Division of Health Sciences and Technology
August 8, 2008

Certified by: _____
Thomas Lord Assistant Professor of Materials Science and Engineering
Krystyn J. Van Vliet
Thesis Supervisor

Certified by: _____
Michael F. Rubner, Ph.D.
Director of the Center for Materials Science and Engineering
Professor of Materials Science and Engineering
Thesis Chair

Accepted by: _____
Martha L. Gray, Ph.D.
Edward Hood Taplin Professor of Medical and Electrical Engineering
Director, Harvard-MIT Division of Health Sciences and Technology

Quantifying Effects of Substrata Chemomechanical Properties on Eukaryotic and Prokaryotic Cell Adhesion and Morphology

By

Michael Todd Thompson

Submitted to the Division of Health Sciences and Technology
On August 8th, 2008 in Partial Fulfillment of the
Requirements for the Degree of Doctor Philosophy
in Biomedical Engineering/Medical Physics

ABSTRACT

It is now widely accepted that cells are capable of processing both mechanical and chemical signals from the extracellular environment. Exactly how these two factors affect the cell biology in the context of physiological circumstances is an area of intense interest that has given rise to an entire field of study called cell mechanotransduction. The unambiguous decoupling of mechanical and chemical properties that stimulate cell development and phenotypic change is challenging from an experimental standpoint. This thesis describes some of the first studies of chemomechanical coupling arising from anchorage-dependent forces between cells and a versatile class of chemically and mechanically tunable polymer thin films, termed polyelectrolyte multilayers. Specifically, investigation of the effects of extracellular chemomechanical stimulation on cell morphology and adhesion in the eukaryotic cells such as vascular endothelial cells and fibroblasts; and the adhesion of prokaryotic cells *S. epidermidis* and *E. coli* are presented.

Endothelial cells (EC) comprise a major portion of the cell population in the human body. Because of the extensive distribution of endothelial cells in various tissues, they function across a broad range of mechanical and chemical environments. Furthermore, a general understanding of how mechanical forces contribute to the development of cellular function is an important aspect in the development of therapeutic techniques and materials capable of addressing a wide spectrum of human diseases and injuries. Cell adhesion to extracellular matrices and tissues can be indicative of underlying molecular processes in both healthy and disease states. Through the use of a mechanically tunable class of polymer thin films called polyelectrolyte multilayers (PEMs) developed by Rubner et al., we have demonstrated that the adhesion and morphology of human microvascular endothelial cells depend directly on the mechanical stiffness of these synthetic substrates, as quantified by the nominal elastic modulus E . Characterization of the mechanical properties and surface features of PEMs is attained via scanning probe microscopy (SPM) and SPM-enabled nanoindentation. Typical cellular response to increased substrata stiffness includes increased number of cells adhered per unit substratum area. We have further demonstrated that the chemical and mechanical signals imposed at the cell-substrata interface can be decoupled, thereby providing two independent parameters capable of controlling cell behavior. This capacity of the cell to sense and/or exert chemical and mechanical forces, in addition to initiating a sustained molecular response, is termed the chemomechanical response element. Finally, adhesion dependent mechanosensation in bacteria is explored, with respect to the chemomechanical response elements common to eukaryotic and prokaryotic cells. Potential applications towards the development of therapeutic materials and compounds for treatment of various disease states are discussed, with particular attention to limiting hospital acquired infections.

Thesis Committee:

Krystyn J. Van Vliet

Thomas Lord Assistant Professor of Materials Science and Engineering
Thesis Supervisor

Michael F. Rubner, Ph.D.

Director of the Center for Materials Science and Engineering
Professor of Materials Science and Engineering
Thesis Chair

Dr. William Aird, M.D.

Associate Professor of Medicine
Department of Medicine
Beth Israel Deaconess Medical Center

Shiladitya Sengupta, Ph.D. M.Sc.

Assistant Professor of Medicine and HST
Brigham and Women's Hospital
Massachusetts Institute of Technology

BIOGRAPHICAL NOTE

Michael Todd Thompson was born in Phoenix, Arizona on November 11, 1976 to Debra Mitchell and Michael L. Thompson. Growing up in the "Valley of the Sun" afforded him many opportunities to experience the Arizona desert and contributed to an early fascination with science and nature. After graduating high school, where he met his future wife Julia, Michael traveled south to Tucson, AZ. There, he completed his Bachelor's of Science in Mathematics and Biochemistry at the University of Arizona Honor's College. During that time, Michael and Julia saw the birth of their first child, Daughter Lauren. It was also during this time that Michael decided on a career in the sciences. Michael came to Massachusetts in the summer of 1999 to begin a Ph.D. in Chemistry. Since his arrival at MIT, Michael and Julia have celebrated the birth of two sons, Michael Alexander and William. Soon after beginning his program in Chemistry, Michael left to go on medical leave. During this time he underwent four major surgeries and struggled with life-threatening complications from one of them. His experiences as a patient in the medical field left Michael with a strong desire to apply his skills as a scientist to improving healthcare. In 2002, Michael was accepted into the Harvard-MIT Division of Health Sciences and Technology Medical Engineering/Medical Physics program.

ACKNOWLEDGEMENTS

I would like to thank my thesis advisor and thesis chair, Prof. Krystyn Van Vliet and Prof. Michael Rubner. I am one of the fortunate students, able to honestly say that I had opportunities and learned things that I could not have found working for anyone else. I am honored to have worked with such exceptional scientists, and hope that I may work with them again some day. Prof. Rubner was always a source of positivity and inspiration. I always felt able to conquer any problem after talking to him. I also admire his ability to see clearly the heart of any experiment and ask direct, insightful questions about the data. He brings clarity to every discussion, and that is something I aspire to match.

Krystyn has taught me valuable lessons over the years and helped shape me into a more effective researcher. When we first started working together, I had only a vague idea of what engineering entailed, since my training up to that point was more in the way of classical sciences. She immediately challenged me with new approaches to problem solving, and within the span of a few meetings, Krystyn had me thinking like an engineer. I have enjoyed our discussions over the years, as lively and “jousty” as they may have been at times. I am truly saddened to leave those times behind, but I look forward to starting a new chapter at square one. I also have to say that I marvel at her organization and thoroughness. Throughout our time together, Krystyn has taught me to “put words in word places”, so-to-speak. I have learned so much about the art of presentation and performance from her.

Prof. Shiladit Sengupta has been an unparalleled mentor and a great friend over the years. Shiladit’s evaluations of my thesis work helped me refine experiments and challenge myself to think about my work in new ways. His friendship and advice over the years have also been invaluable. I look back fondly at our old lunchtime conversations and hope that we can someday pick them back up.

Dr. William Aird was a fabulous mentor that I could always count on for invigorating conversations. His ideas on evolutionary medicine were challenging, but enlightening. I’ve often found myself searching for “Aird-worthy” hypotheses when reasoning through experimental data. Thanks to Dr. Aird, I’ll also never forget the most important answer in endothelial cell behavior is epigenetics. Dr. Aird is more than just a great scientist. I’m thankful for his interest in my family and personal life outside of work.

I am also indebted to my collaborators, Ms. Jenny Lichter and Dr. Mike C. Berg. Mike Berg helped trained me to work with PEMs and helped me through those first experiments. Looking back, I am extremely grateful for all the time he selflessly gave making PEMs while finishing up his own Ph.D. I enjoyed our “down-

time” discussions over shared interests in superheroes, comic books, and generally geeky things. So very cool, Dr. Berg.

Jenny Lichter’s intensity as a scientist is matched equally well by her warmth and friendliness. Throughout our work together on the bacteria project, I found her to be a constant source of inspiration and at times a much needed “antagonist” to my ideas. This thesis simply wouldn’t be what is without her valuable contributions. Like Mike Berg, we also had some great times between experiments... though Jenny more put up with my geek side than shared in it. She is a gracious person, a

Irene Tobias and Maricela Delgadillo were hands-down, two of the greatest UROPs that I’ve had the pleasure of knowing. Our group was better for having had the two of you as members. I will always value working with each one of you, and I look forward to watching your continued success in the future. I’d also like to thank Kay Furman for her hard work and dedication in Prof. Yet-Ming Chiang’s course. I’m pleased to have had a positive influence in her time at MIT and Harvard. She is now a fellow student in the HST program, and I’m confident in her ability to make significant contributions to the medical field,.

I would like to thank every member of the Van Vliet group for their support over the years – I can’t begin to express how grateful I am for each and every one of you. Catherine Tweedie has been a model of hard work and adventuring spirit, and it was a highlight of my time in the group to watch as she pushed further towards her dreams. Sunyoung Lee is an exceptional experimentalist and wonderful lab mate with an infectious smile. Emily Walton and Jack Milwid were always ready to “chalk-talk” through crazy experimental ideas and provide much needed constructive criticism. To everyone else in the group: Binu, Ranjani, Georgios, Dessy, Tim, and all the others – I sincerely thank you for your friendship and wish you continued success.

Thanks go to Dr. Alan Schwartzmann for assistance, and the MIT Laboratory for Nanomechanical Study for access and use of resources. I would also like to acknowledge the Center for Materials Science and Engineering for use of facilities and resources.

Thanks go to everyone at Asylum Research for technical support and critical guidance on MFP 3D experiments. In particular, Jason Beemis was extremely helpful in creating macros for data analysis. A major thank you goes to Alejandro, Flavio-Bonilla. Who helped me numerous times in the last year and half with tricky force pulling experiments and navigation through machine and software upgrades.

I’d also like to thank Larry Stern for his support and guidance as my advisor early in my tenure as a Chemistry Ph.D. candidate. He is one of the best experimental scientists I have ever met, and he helped me become the scientist I am today. Jen Stone, Greg Carven, and Mia Rushe were all wonderful

collaborators and a pleasure to work with. Prof. Herman Eisen and Prof. Jianzhou Chen provided valuable advice and mentoring during my time in the Stern group for which I am truly grateful.

I want to thank my Grandmother and Grandfather Thompson, for their continued support over the years. They have, at various points in my time here, dropped everything to come take care of me when I was ill and Julia had to work. They drove me out to Cambridge when I was too anemic to fly. It's hard to imagine my life without them. My Brother Mark was a great outlet to talk to when times were rough. It's been a pleasure watching him grow into the Naval Officer he is today. My Mom, Dad, Stepfather Steve, and Stepmother Diane: their unconditional love and support has kept me going and kept me smiling.

To the friends and family that were with me when I started, but couldn't come along to see the end – I love you and I miss you all. Keith Goljan was an inspiration as a brother, a friend, and an uncle to my children. I always felt a little taller around him, as he was the kind of man whose spirit lifted the shoulders and straightened the back. His final, greatest lesson was also his most tragic; I carry it with me today and for the rest of life. Polly, beautiful friend and mother to my beloved Aunt Diane, was the life of every party and a source of wisdom over the years. She showed me what grace in the face of extreme adversity looks like, lessons that I have relied upon during my own struggles with failing health.

No acknowledgement could be complete without mentioning my family. They have been with me along the way, completely on board with every demand: through long hours, missed plays and beach trips, and lots of late-night keyboard tapping (sorry Julie). There is no way – I'm not exaggerating here – absolutely no way I could have done this without them. I'm not always the easiest person to live with, and they put up with, no questions asked. More than that, they continue to astound me with their creativity, ambition, and accomplishments. If I had nothing else in my life, I would already have everything I need in them. My wife, the molecular biologist who finds time to be the world's greatest mother? Check. Three beautiful, brainy children that somehow challenge and satisfy me in every way? Check. Every morning I'm just thankful to be their husband and father. To borrow an old expression, my sun rises and sets with you guys. I love you.

Finally, to everyone mentioned above: I hope that I have made you proud with this work; that all of you can look back on what you've given me and know that it was worth the effort - that I was worth your time and effort. I promise to keep working to earn that. Thank you so very much.

TABLE OF CONTENTS

ABSTRACT	2
BIOGRAPHICAL NOTE.....	4
ACKNOWLEDGEMENTS.....	5
TABLE OF CONTENTS	8
LIST OF FIGURES.....	12
SELECTED TERMINOLOGY AND ABBREVIATIONS.....	18
CHAPTER 1 INTRODUCTION.....	21
1.1 Chemomechanical Stimuli in Biomedical Engineering and Materials Design	21
1.2 Thin Films as Tools to Explore Interfacial Chemistry and Mechanics	26
1.3 Eukaryotic and Prokaryotic Cells in Mechanotransduction	33
1.4 Thesis Scope	35
CHAPTER 2 PAA/PAH POLYELECTROLYTE MULTILAYERS CHEMICAL AND MECHANICAL PROPERTIES.....	38
2.1 Background and Motivation	38
2.2 Polyelectrolyte Multilayers Thin Films as Tunable Cell Adhesive Substrata	41
2.3 Mechanical Analysis of PEMs.....	46
2.4 Analysis of Nanoindentation Response	48
2.5 Contact Angle Measurement Based Calculation of Surface Interaction Energies.....	54
2.6 Calculation of Surface Charge Density from Electrostatic Model.....	57
2.7 Summary	60
CHAPTER 3 PHYSICOCHEMICAL CONTROL OF HMVEC ADHESION TO POLYELECTROLYTE MULTILAYERS	63
3.1 Background and Motivation	63
3.1.1 Endothelial Cell Structures and Mechanoselective Behavior	63

3.1.2 Integrins as Mechanosensitive Mediators of Eukaryotic Cell Interactions in the Extracellular Environment.....	67
3.1.3 Cellular Response to Substrata Stiffness	70
3.2 Materials and Methods.....	73
3.2.1 PEM Assembly and Materials.....	73
3.2.2 Mechanical Testing and Data Analysis of PAA/PAH Multilayers	74
3.2.3 Cell Culture, Attachment and Proliferation Assays	75
3.3 Results and Discussion.....	76
3.3.1 Effect of Multilayer Assembly pH on Mechanical Compliance	76
3.3.2 Effect of Substrate Compliance and Assembly pH on Cell Attachment and Proliferation	78
3.3.3 Limits of Nanoindentation Experiments and Analysis.....	83
3.3.4 Effects of E_s on Cell Attachment and Proliferation.....	87
3.5 Summary	89
CHAPTER 4 CHEMICAL AND MECHANICAL PROPERTIES AS INDEPENDENT MODULATORS OF CELL ADHESION	91
4.1 Background and Motivation	91
4.1.1 Chemically and Mechanically Guided Cell Behavior	91
4.1.2 Biomaterial Fabrication for Decoupling Chemistry and Mechanics in the Extracellular Space	93
4.2 Materials and Methods.....	95
4.2.1 PEM Assembly and Materials.....	95
4.2.2 Mechanical Testing and Data Analysis of PAA/PAA _m Multilayers	96
4.2.3 PEM Film Thickness Measurement.....	97
4.2.4 Cell Attachment to Modified PEM Substrata	98
4.3 Results and Discussion.....	99
4.3.1 Biochemical Functionalization of Polymeric Cell Substrata Can Alter Mechanical Compliance	99
4.3.2 Effect of Surface Functionalization on Mechanical Compliance	100

4.3.3 Consideration of PEM Film Thickness.....	102
4.3.4 Effect of Surface Functionalization on Cell Attachment.....	109
4.4 Summary	112
CHAPTER 5 EXTRACELLULAR PHYSICOCHEMICAL AND MECHANICAL FACTORS IN BACTERIAL ADHESION TO PEMS	115
5.1 Background and Motivation	115
5.1.1 Controlling Microbial Adhesion: a Critical Unmet Need	115
5.1.2 Properties of Gram (+) and Gram (-) Bacteria: Cell Envelope Shape, Chemical Composition, and Elasticity	118
5.1.3 <i>S. epidermidis</i> and <i>E. coli</i> as Model Organisms	126
5.1.4 Coupled Interactions of Cell-Material Properties In Bacterial Adhesion	130
5.2 Materials and Methods.....	137
5.2.1 PEM Assembly and Materials.....	137
5.2.2 Mechanical Testing and Data Analysis of PAA/PAH Multilayers	138
5.2.3 Substrata Surface Energy and Interaction Energy	138
5.2.4 Substrata Surface Charge Density	140
5.2.5 Determination of Relative Free Carboxylic Acid Presence at the PEM Surface.....	141
5.2.6 Bacterial Attachment Assays.....	142
5.2.7 Colony Image Analysis.....	143
5.3 Results and Discussion.....	144
5.3.1 Substrata Mechanical Stiffness Can Regulate Adhesion of Viable <i>S. epidermidis</i> Bacteria.....	144
5.3.1.1 Bacterial Colonization can be Reduced by Material Substrata Modifications.....	144
5.3.1.2 Weak Polyelectrolyte Multilayers Modulate Stable Adhesion of <i>S. epidermidis</i> Bacteria	145
5.3.1.3 Characterization of Polymeric Substrata Properties	147

5.3.1.4 <i>S. epidermidis</i> Adhesion Modulated Chiefly by Substrata Mechanical Compliance.....	151
5.3.1.5 Mechanoselective Adhesion is Independent of Monovalent Ion Concentration.....	155
5.3.2 Substrata Mechanical Stiffness can Regulate Adhesion of Viable Wild-type <i>Escherichia coli</i> K-12 Bacteria and a $\Delta mreB$ Spherical Mutant	157
5.3.2.1 <i>E. coli</i> Adhesion Modulated Chiefly by Substrata Mechanical Compliance.....	157
5.3.2.1 Adhesion of a Spherical <i>E. coli</i> Mutant Lacking Actin-like MreB is Modulated Chiefly by Substrata Mechanical Compliance.....	161
5.4 Summary	163
CHAPTER 6 CONCLUSIONS AND DIRECTION FOR POTENTIAL FUTURE PROJECTS	165
APPENDIX A.1 SOURCE CODE FOR DATA EXTRACTION FROM MFP EXPERIMENT FILES	170
APPENDIX A.2 SOURCE CODE FOR LOADING/UNLOADING CURVE EXTRACTION AND SURFACE CHARGE ANALYSIS PRE-PROCESSING.....	176
APPENDIX A.3 SUPPLEMENTAL DATA TABLE RELATED TO DETERMINATION OF THE MICROBE-PEM INTERACTION ENERGY	188
APPENDIX A.4 SUPPLEMENTAL INFORMATION RELATED TO THE DIFFERENCES BETWEEN E MEASURED IN DEIONIZED WATER VERSUS SALT	190
APPENDIX A.5 NOTE ABOUT STATISTICAL ANNOTATION FOR EXPERIMENTAL DATA.....	192
REFERENCES.....	193

LIST OF FIGURES

Schematic 1.1 Eukaryotic signal transduction pathways implicated in mechanotransduction (Left) G-coupled protein receptors (GCPR's) respond via mechanical deformation to switch associated $\alpha\beta\gamma$ G proteins to the activated state. Downstream of this activation, induction of the Ras/Rac pathway and recruitment of protein kinase C activates the mitogen-activated protein kinases (MAPK), leading to rapid changes in gene expression. (Right) Physical deformation of receptor-tyrosine kinases and cytoskeletal-associated integrins leads to activation of the MAPK pathway independently of the GCPR-based pathway. (see abbreviations for a more extensive list of relevant abbreviated names. Figure rendered using Paracel Pathworks pre-rendered pathway models.)

Figure 2.1 Layer-by-layer assembly of polyelectrolyte multilayers A glass slide is dipped in a dilute, pH-calibrated polyanion solution and allowed to equilibrate for 15 minutes. The slide is then washed for 1-2 minutes, three times sequentially in individual deionized water baths. The slide is then dipped in dilute, pH-calibrated polycation solution for an additional 15 minutes, sequentially washed 3 times in separate deionized water baths, and the cycle is reiterated until all layers have been deposited. A single completed dipping cycle deposits 1 bilayer. The order of polyion addition by dipping can be changed depending on properties of the slide, such as the presence of pre-adsorbed/conjugated ionizable groups (e.g., amines). The slide is kept hydrated throughout the process to prevent aberrant deposition of the multilayer.

Figure 2.2 Polyelectrolytes components used in this study In ionically crosslinked PEMs, poly(allylamine hydrochloride) (PAH) is used as the polycation. For thermally crosslinked, weakly hydrogen-bonded PEMs the counter polyelectrolyte is polyacrylamide (PAAm). Poly(acrylic acid) (PAA) is used as the polyanion for all PEMs in this thesis.

Figure 2.3 Polyelectrolyte multilayer structure. For high charge density cation-anion paired polymer chains and high charge compensation result in thinner films (*top*). Low charge density for either the cation or anion, or poor charge compensation in the assembled film leads to loop-rich, highly swellable structures (*bottom*).

Figure 2.4 Schematic of AFM indenter Indentation of hydrated PEMs is carried out using a commercial atomic force microscope. Deflection of a cantilever with a known spring constant is measured by detecting the positional change of a light source reflected from the cantilever tip. The AFM base is capable of translation normal to the surface via a piezoactuator, and controls the approach and retraction of the sample probe relative to the sample surface. Indentation depth, Δ , is restricted to < 20 nm to approximate indentation by a spherical probe. (*Inset*) The silicon nitride AFM sample probe has a nominal radius ranging 25-50 nm. The PAA/PAH multilayer is an interpenetrating network of polycation and polyanion polymer chains (1).

Figure 2.5 Ideal and representative MFP data (A) Representative force-displacement $P-\Delta$ responses of PEMs as a function of assembly pH (solid, pH = 6.5; dash, pH = 4.0; dot, pH = 2.0). (B) Logarithmic representation used to extract indentation modulus E_s .

Figure 3.1 Indentation elastic modulus E_s as a function of assembly pH of polyanion and polycation solutions, pH = 6.5, 4.0, and 2.0 The terminal or top layer of the PEM is indicated as polyanion PAA (solid black) or polycation PAH (solid gray). Polyacrylamide multilayers (PAAm, striped) and polystyrene (TCPS, cross-hatched) are shown for reference, and used as negative and positive controls, respectively. Standard deviation is shown for each sample ($n = 15$).

Figure 3.2 Total number of cells harvested from 60 mm-diameter Petri dishes at seven days post-seeding, as a function of PEM assembly pH The terminal or top layer of the PEM indicated as polyanion PAA (solid black) or polycation (solid gray). Polyacrylamide multilayers (PAAm) and polystyrene (TCPS) are negative and positive controls of cell attachment, respectively. Standard deviation is indicated for each sample ($n = 3$).

Figure 3.3 Spatial density of cells attached as a function of days in culture Cell density measured through optical imaging analysis of a specific area of 6.25 mm^2 for each sample. Cells seeded at $84,000$ cells/sample or ~ 30 cells/ mm^2 if uniform density assumed. Sample legend: PAA/PAH 2.0/2.0 (black diamond); 4.0/4.0 (black square); 6.5/6.5 (black triangle); and tissue culture polystyrene (gray square).

Figure 4.1 Wild-type NR6 fibroblast attachment as a function of RGD concentration PAA/PAH PEMs at 48 h post-seeding, where the PEM surface was modified via polymer-on-polymer stamping of PAH in a vertical line pattern (dashed rectangles show three representative linewidths) followed by RGD conjugation via a heterobifunctional crosslinker. Cells do not adhere as readily on PAA/PAAm PEM lines functionalized with low RGD concentrations of $\sim 53,000$ molecules/ μm^2 (A), but do adhere readily to the same PAA/PAAm lines functionalized with a higher RGD concentration of 152,000 molecules/ μm^2 (B). Scalebars = 50 μm . These materials, cell culture methods, and cell adhesion results are detailed in Ref. (75).

Figure 4.2 Representative force-depth responses Traces acquired during nanoindentation of PAA/PAAm PEMs in 150 mM phosphate buffered saline. PAA/PAAm/adsorbed PAH, 15 min (solid black); PAA/PAAm/adsorbed PAH + RGD (solid gray); unmodified PAA/PAAm (dashed black); PAA/PAAm/stamped PAH, 30 sec (dashed gray).

Figure 4.3 Nominal elastic moduli E of surface modified PAA/PAAm PEMs PEMs were indented to a depth of 20 nm using a scanning probe microscope in fluid (150 mM PBS, pH = 7.4) at room temperature. Error bars represent standard deviation among at least 50 measurements on a single sample. All samples except * were statistically significantly different from the unmodified PAA/PAAm PEM termed the null sample ($p < 0.0001$, ANOVA and ad hoc Fischer PLSD).

Fig. 4.4 PEM sample thickness and RMS surface roughness +/- adsorbed PAH Changes in mechanical stiffness in PAH adsorbed, PAA/PAAm PEMs is not due to differences in sample nm-scale thickness relative to as-deposited PAA/PAAm multilayers (grey, left axis), or to differences in RMS surface roughness (green, right axis).

Table 4.1 Properties of PAA/PAAm polymer multilayer derivatives

Figure 4.5 Murine NIH 3T3 fibroblast attachment at day 3 as a function of surface functionalization TCPS is tissue culture polystyrene; surface functionalization of PAA/PAAm (null) as indicated in Table 4.1. Growth area for stamped samples is $0.25 \mu\text{m}^2$, whereas growth area for all other samples is $9.6 \mu\text{m}^2$. Area is expressed in units of functionalized surface area (mean +/- standard deviation).

Figure 4.6 Chemical and mechanical properties orthogonally modulate cell adhesion to PEMs For all samples with increased E (red diamonds) relative to the compliant native PEM show marked increases in adhered cells, while samples predicted to be cytophilic via presentation of adhesion peptides also show good cell adhesion despite the magnitude of the sample compliance. Finally, cells show increased adherence to substrates that are chemically disfavor adhesion as sample stiffness is increased relative to the native PEM. E (red diamonds), cells/cm² (grey bars).

Figure 5.1 Chemical crosslinking in the bacterial cell wall Carbohydrate polymers composed of dimers of NAG and NAM are crosslinked throughout the cell wall via peptide bridges. In many Gram (+) cells the peptide bridge has a highly flexible, pentaglycine linker sequence. In *E. coli*, a Gram (-) rod, there is no pentapeptide linker; carbohydrate polymers are directly linked through the transpeptide side chains. NAG, N-acetyl glucosamine; NAM, N-acetyl muramic acid; G, glycine; D-GluNH₂, D-glutamine; D-GluCOOH; D-glutamic acid; D-Ala; D-alanine; L-Lys; L-lysine (1).

Schematic 5.1 Architecture of the Gram-positive cell coat The cell sheath consists of a thick peptidoglycan cell wall with embedded teichoic acid polymers (red, orange modular structures. Lipoteichoic acid polymers are embedded in the inner cell membrane and assist in anchoring the cell wall to the membrane. Penicillin-binding proteins anchored in the peptidoglycan cell wall (PBP, blue receptor). Ion channels of the transient receptor potential protein superfamily are embedded in the inner membrane, and open in response to hypo-osmotic shock induced lateral cell membrane tension. A wide variety of additional proteins are also embedded in the inner membrane (green, IM, rendered in *Paracel Pathworks*).

Schematic 5.2 Architecture of the Gram-negative cell coat The cell sheath consist of an outer membrane with embedded proteins (green, white ovals), some of which interact with the so-called penicillin-binding proteins (PBP, blue receptor). PBPs are anchored in the peptidoglycan cell wall, and interact with the MreC, a member of the trimeric protein complex comprised of gene products from the MreBCD operon. MreC and MreD are anchored in the inner cell membrane. MreB is associated on the cytoplasmic side of the inner membrane and forms helical filamentous structures with ATPase activity (yellow sphere, ATP/GTP). Ion channels of the transient receptor potential protein superfamily are also embedded in the inner membrane, and open in response to hypo-osmotic shock induced lateral cell membrane tension. (rendered in *Paracel Pathworks*).

Schematic 5.3 The two-step kinetic binding mechanism Bacteria adhere to surface according to a two step kinetic process. The first stage of binding is governed by mid-long range forces on approach, such as van der Waals attraction, and hydrophylic repulsion and electrostatic repulsion. Fimbriae play a role in overcoming the repulsive interactions in this region, as the force acting on the fimbrial tip is small because of the very small tip radius ($r = 1-5$ nm). Adhesion in this phase is fast, reversible, and weak; cells eventually adhere as the number of fimbrial-material interactions grow. In the second phase, specific molecular interactions take place between ligands and their cognate receptors on both the bacterial and host-material surfaces. For abiotic surfaces, the second step is restricted to molecular recognition of specific chemical moieties, or pre-patterned molecular agents (1).

Figure 5.2 PEMs reduce bacterial adhesion on medical grade titanium Adhesion of waterborne *S. epidermidis* is reduced by coating with a pH-tunable polyelectrolyte multilayer (PEM) film of PAA and PAH assembled at pH 2.0, and is stable at both 2 h (inset; circle indicates one such colony) and 4 h incubation duration. Scale bars = 5 mm.

Figure 5.3 Bacterial colonies observed for $10^3 - 10^8$ *S. epidermidis*/mL in 150 mM NaCl PBS (A) Average colony number per unit substrata area increased with increasing incubation concentration for greater than 10^5 cells/mL; for all concentrations, the density of colonies observed on the PEM substrata assembled at pH 6.5 (●) was significantly greater than that observed on the substrata assembled at pH 2.0 (▼). (B) For given initial concentration, colony number was greater and colony size was smaller on stiffer substrata, supporting a model whereby bacteria attachment is modulated in part by substrata stiffness, but subsequent growth is affected predominantly by available space and nutrients. Scalebars = 500 μ m.

Table 5.1 PEMs used to test physicochemical and mechanical properties affecting bacterial attachment Assembly pH of polyanion and polycation indicated, respectively, for PEMs assembled to ~ 50 nm dry thickness (≥ 57 nm hydrated thickness) with PAA as the last layer. All properties measured in deionized water. Total interaction energy ΔG_{MWP} of the microbe-water-polymer system, interaction energy for *microbe*-water-PEM are listed as indicated; root mean square (RMS) surface roughness; and nominal elastic moduli E . Data expressed as average \pm standard deviation. Symbols used throughout to indicate the corresponding PEM in all figures.

Figure 5.4 Colony density as a function of various surface parameters (A) Colony density varies directly with substrata elastic moduli E . All sample differences statistically significant (1-way ANOVA, $\alpha = 0.05$, $P = 0.0059$). (B) Colony density is independent of RMS surface roughness of the substrata. Scale bar = 5 μm . (C) Total interaction energy ΔG_{MWP} for the microbe-water-PEM system is statistically indistinguishable among all substrata considered (1-way ANOVA, $\alpha = 0.05$, $P = 0.987$). (D) Surface charge density Q , as measured via electrostatic repulsion of a carboxylated spherical probe in Milli-Q water (see Methods), is within standard deviation for PEMs assembled at pH 2.0 (compliant) and pH 6.5 (stiff). Representative charge repulsion curve (solid) and constant-surface-charge model fit (dashed) are shown. Symbols refer to the following PEMs: PAA/PAH 2.0/2.0 (\blacktriangledown), 4.0/4.0 (\times) in A to consider intermediate substrata stiffness, 6.5/6.5 (\bullet), 3.5/7.5 (\blacklozenge), and 3.5/8.6 (\blacksquare).

Figure 5.5 Multilayer addition to modulate composite substrata stiffness Addition of 0.5 and 1 bilayer of PAA/PAH at pH 2.0 onto a stiff PEM (pH 6.5) decreases the effective mechanical stiffness of the substrata (grey circles) and decreases the bacterial colony density (black columns). Addition of one bilayer of pH 6.5 PAA/PAH to a compliant PEM (pH 2.0) increases effective stiffness (black triangles) and bacterial colony density (grey columns). Substrata were incubated with bacteria at concentrations of 10^7 cells/mL for 1 hr. We observed statistically significant differences in the colony densities among the masked PEM 6.5 substrata and among the masked PEM 2.0 substrata, respectively. (1-way ANOVA, $\alpha = 0.05$ with $P = 0.00027$ and 0.0031 , respectively).

Figure 5.6 Bacterial colony density on compliant substrata (black, $E \sim 1$ MPa) is lower than that on stiff substrata (gray, $E \sim 100$ MPa), regardless of solution monovalent ion concentration in which 10^7 cells/mL incubated with substrata.

Figure 5.7 Colony density as a function of various surface parameters Fig. (A-B) Representative colonies for wild-type *E. coli* K-12 on PEM 6.5 (stiff) and PEM 2.0 (compliant), respectively. Scale bar = 1 mm. (C) Colony density varies directly with substrata elastic moduli E . (D) Colony density is independent of RMS surface roughness of the substrata. (E) Total interaction energy ΔG_{MWP} for the microbe-water-PEM system. Symbols refer to the following PEMs: PAA/PAH 2.0/2.0 (\blacktriangledown), 6.5/6.5 (\bullet), 3.5/7.5 (\blacklozenge), and 3.5/8.6 (\blacksquare).

Figure 5.8 Adhesion of ΔmreB *E. coli* Final colony density for spherical mutant ΔmreB *E. coli* cells grown on PEM 6.5 (black, stiff) versus PEM 2.0 (gray, compliant.) Inset: Representative photos of colonies grown on PEM 6.5 (left), and PEM 2.0 (right). Scalebar = 1 mm.

SELECTED TERMINOLOGY AND ABBREVIATIONS

AFM	<i>Atomic Force Microscopy</i>
cAMP	cyclic adenosine monophosphate
ANOVA	<i>analysis of variance</i>
cGMP	cyclic guanine monophosphate
CI	confidence interval (<i>see appendix A.5</i>)
CSK	cytoskeleton
Δ	indentation depth, displacement
δ	cantilever deflection
E	elastic modulus, Young's modulus
E_r	reduced elastic modulus
EC	<i>Endothelial Cell</i>
ECM	<i>ExtraCellular Matrix</i>
ERK	extracellular-regulated kinase
FA	focal adhesion
FAK	Focal adhesion kinase
FtsZ	<i>filamentous temperature sensitive protein Z</i>
GIT	G protein coupled receptor interacting protein
GPCR	G protein coupled receptor
G protein	member of the family of cGMP activated/inactivated proteins

HMVEC	H uman M icro V ascular E ndothelial C ell
HUVEC	H uman U mbilical V ascular E ndothelial C ell
<i>I</i>	ionic strength
InvOLS	I nverse O ptical L ever S ensitivity
IP ₃	inositol-triphosphate, <i>see</i> <i>PI</i> ₃
ITP	inositol-triphosphate, <i>see</i> <i>PI</i> ₃
<i>k_c</i>	cantilever spring constant
LbL	layer-by-layer (assembly)
MAPK	m itogen – a ctivated p rotein k inase
MAPK-K	MAPK kinase, kinase that phosphorylates MAPK (<i>also seen as MAPKK</i>)
Mbl	MreB -like
MFP	Molecular Force Probe (3D), Asylum Research, CA
<i>min</i>	operon responsible for the min icell phenotype, originally discovered in <i>E. coli</i> . Comprised of the gene cluster MinCDE
MinD	Min protein D , from the <i>min</i> operon. Membrane ATPase, activates MinC.
MreB	Murein cluster B (gene and gene product)
MreBH	MreB -homolog
MWP	m icrobe- w ater- P EM
P	sample load, $P = k\delta$
Pd	photodiode, MFP detection source
ParM	P artitioning loci M otor protein, a bacterial cytoskeletal element
PEMs	p olyelectrolyte m ultilayers

PAH	poly(allylamine hydrochloride)
PAA	poly(acrylic acid)
PAAm	polyacrylamide (<i>also seen as PAA_m</i>)
PI ₃	inositol-triphosphate
PKC	protein kinase C
P-value	quantitative statistic that measures the likelihood that two or more data sets are related with respect to their individual probability distributions (<i>see appendix A.5</i>)
Q	surface charge density
R _p	probe radius, radius of the cantilever tip-probe
r	radius
RMS	root mean square
RPTP _α	receptor-like protein tyrosine phosphatase-α
(n)RTK	(non)receptor tyrosine kinase
SD	standard deviation (<i>see appendix A.5</i>)
SE	standard error (<i>see appendix A.5</i>)
SLD	super-luminescent diode , MFP optical sensor
Species	basic unit of taxonomic rank
SPM	scanning probe microscopy
TPSD	thermal power spectral density
V	voltage
Wt	wild type, the cell line or strain from which mutants are derived

CHAPTER 1 INTRODUCTION

1.1 Chemomechanical Stimuli in Biomedical Engineering and Materials Design

Eukaryotic and prokaryotic cell growth *in vivo* occurs under complex physical, mechanical and chemical extracellular conditions. Though extracellular environmental conditions may be modeled using *in vitro* model systems, there exists no perfect mimetic with which to probe the extent to which these parameters influence cell behavior. It is widely accepted that chemical and mechanical cues from the extracellular milieu are not only important eukaryotic stimulatory factors in the normal cell response, but they are also necessary for the maintenance of cellular homeostasis (3, 4). The types of physiologic stresses and strains to which eukaryotic cells are subjected will depend upon the cell type, and its location with respect to other tissues. Some of the stresses applied to or by cells under physiological conditions include cyclic strain from stretching/contraction processes; fluid or semi-fluid shear stress from flow based processes; stress from cell migratory processes, which involve a careful balance of forces derived from cell protrusions with those derived from opposing and cooperative adhesive interactions (5); and, in non-motile cells, anchorage-dependent stress arising from the cell-cell and cell-matrix adhesion that occurs between adjacent surfaces. Specifically, in epithelial-type cells, mechanical strain and stress arise due to cell-cell adhesion and basolateral adhesion via cell-basement membrane

macromolecular focal contacts. Prokaryotic cells also behave differently under fluid shear stress, forming so-called catch-bonds or slip-bonds in a protein specific, and species specific manner (Section 5.1).

Mechanotransduction is the process by which mechanical stimuli are converted to chemical signals in the cell, and is a widely studied phenomenon within the field of study known as chemomechanics (or, alternatively, mechanobiology)(196). The degree to which the biochemical state is influenced by the sensing and response of the cell to applied forces is not completely understood, nor are the molecular mechanisms of mechanotransduction signaling pathways fully elaborated. Nevertheless, reports thus far provide significant insight into the potential mechanisms at work in cellular mechanosensation.

Mechanical signaling is known to occur through integrins, G-coupled protein receptors, and ion channels of the class known as transient receptor potential channels (6, 7). The common pathways involved in active remodeling of the cytoskeleton feed into the MAPK (mitogen-activated protein kinase) kinase system, a phosphorylation cascade that results in the activation of effector proteins in the cytosol and of transcription factors in the nucleus (8, 9). There are many molecular routes leading to the activation of the MAPK pathway, but a key component in almost all of those routes involves the release of phosphatidyl-inositol(3,4,5)-triphosphate [PtdIns(3,4,5)P₃] from the plasmalemmal side of the membrane and the recruitment of ITP3-kinase (ITP3-K) to convert it to the active (1,4,5) form of inositol-triphosphate (ITP/PI₃) (8, 9). This is important because PI₃ kinases are

known to associate closely with cytoskeletal components, and may therefore be critical in the cellular mechanical response via this interaction. Release of $\text{PtdIns}(3,4,5)\text{P}_3$ from the membrane occurs near membrane anchored proteins, including receptor and non-receptor tyrosine kinases (RTK and non-RTK, respectively) (8, 9). It is well known that endothelial cells under shear stress alter numerous phenotypic markers such as cell surface receptors, secretion of cytokines, and actively remodel the cytoskeleton (4, 10). Shear stress is also implicated in critical regulation of gene expression levels and activation of the so-called inducible stress response element, a collection of genes and DNA binding proteins that show marked up- or down-regulation in response to applied shear flow. Previous studies have shown that fluid shear stresses can induce numerous signaling events and state changes in both eukaryotic and prokaryotic cells, including the activation of the endothelin/eNOS system (10, 11), release of intracellular calcium stores, and increased secretion of growth factor and surface expression of growth factor receptors (4, 12-16). Additionally, cyclic strain is able to induce the mobilization of intracellular stores of matrix metalloproteinases, as well as elevate intracellular levels of the second messenger inositol triphosphate (IP_3) (4, 17). It has been proposed that mechanical deformation of membrane bound receptors and activation of stretch-induced ion channels play an important role in some of these changes (13, 18-20). Additional reports on the mechanical response of tumor cells have implicated members of the Ras superfamily of small guanine triphosphatases (GTPases), of which the cytoskeletal associated proteins Rho and Rac are members (8, 9, 21).

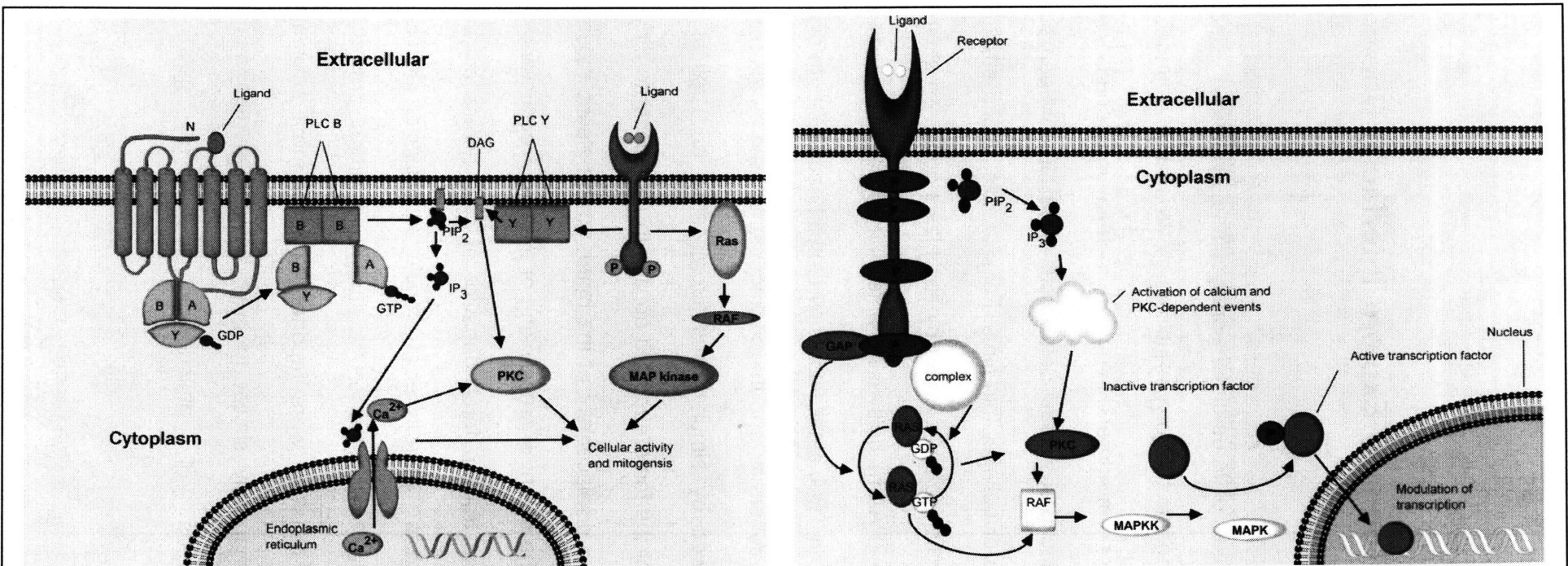
However, studies involving shear stresses derived from a combination of fluid flow and cell-cell contact show more complex behavior that cannot be explained by simple mechanical deformation, and suggests the possibility that kinetic and thermodynamic properties of the adhesive interaction are simultaneously modified by the application of external force (4, 22, 23). Such reports illustrate an important challenge in the area of mechanotransduction; namely, distinguishing chemical and mechanical influences on cell behavior in an unambiguous manner. Classical treatment of the extracellular chemical environment is conceptualized in terms of chemical potentials, primarily described by biomolecular gradients along which signals move to stimulate cell growth/development, maintain morphology, or induce cell turnover/death. Such signals may be soluble, as in the case of hormones or chemokines; or anchored, such as the glycoproteins and proteoglycans that comprise the extracellular matrix (ECM.) Under such a system, specific molecular interactions with cell surface receptors trigger cytosolic signaling kinase cascades that result in transcriptional events in the nucleus. However, Kramer, Bell, and others established a model of cell-cell interactions that shifts the focus from purely chemical considerations towards explicitly dealing with the presence of applied force in the determination of cellular interactions in two or more dimensions (24-27). Their work established that the chemical kinetics and thermodynamics of biomolecular interactions could be linked quantitatively to the mechanical forces applied to a cell or to individual molecules. In addition to the previously stated observations of purely mechanically induced changes in cellular behavior, it is evident that care must be taken to

accurately account for the individual contributions of both chemical and mechanical input to the cell.

Another major type of applied force in cell biology can be described by anchorage dependent processes, which include forces applied by cells in motion and those applied by cells in stable adherence to another surface. Typically, anchorage dependent forces are complex in physiological settings: they are three-dimensional, often involve specific molecular interactions, and can be dynamically altered through chemical or mechanical signals. Under standard *in vitro* culture conditions, the complexity of the extracellular environment can be drastically reduced both chemically and mechanically, thus facilitating studies of the specific interactions between a cell and its chemomechanical environment. Although one may introduce any number of additional mechanical stresses by experimental design, anchorage dependent stresses are intrinsically present under *in vitro* culture conditions. Many *in vitro* culture systems can be considered quasi-two-dimensional. Recent reports by Weaver et al. and Zaman et al. have begun to address the role that anchorage dependent forces play in the induction and maintenance of pathogenic states (tumor migration, general abnormal cell growth) in two and three dimensions (21, 28-35). They have found that tumor cells are able to evade apoptosis during migration in a manner correlated with extracellular stiffness and involving mechanically induced recruitment of integrins and the downstream activation of proteins such as Rac and NF κ B (nuclear factor kappa B), suggesting that malignant phenotypes are directly affected by the surrounding tissue stiffness (21, 35).

1.2 Thin Films as Tools to Explore Interfacial Chemistry and Mechanics

While the incorporation of three-dimensional culture systems to describe mechanically induced pathogenic phenotypes utilized by Weaver et al. and Zaman et al. is an area that is both promising and intriguing, modulation of phenotype and cell mechanical cues via anchorage dependent forces have largely been studied using thin flexible substrata or polymer thin films. For example, Wang et al., have extensively detailed the traction forces exerted by fibroblasts grown on chemically crosslinked polyacrylamide (PAAm) gels using a technique called traction force microscopy (TFM) (36, 37). In TFM, small fluorescent latex beads (0.2 μm diameter) are embedded in a flexible substrate, and the displacement of the beads resulting from cell traction is followed by simultaneous fluorescence and optical video microscopy. Computation of the force each cell applies to the substrate may then be computed by relating the displacement of the beads to the elastic modulus of the substrate. By varying the extent of crosslinking of the film, Pelham and Wang observed the migration and traction force behavior of cells across a range of substrate mechanical stiffness. Janmey et al., employed a similar technique to chemically crosslink flexible PAA_m films for the study of neuronal growth in the presence of astrocytes. Neurons were reported to grow most efficiently on compliant substrates mechanically similar to brain tissue, whereas astrocytes exhibited higher degrees of attachment to stiffer gels (38).



Schematic 1.1 Eukaryotic Signal Transduction Pathways Implicated in Mechanotransduction (Left) G-coupled protein receptors (GPCR's) respond via mechanical deformation to switch associated $\alpha\beta\gamma$ G proteins to the activated state. Downstream of this activation, induction of the Ras/Rac pathway and recruitment of protein kinase C activates the mitogen-activated protein kinases (MAPK), leading to rapid changes in gene expression. (Right) Physical deformation of receptor-tyrosine kinases and cytoskeletal-associated integrins leads to activation of the MAPK pathway independently of the GPCR-based pathway. (see abbreviations for a more extensive list of relevant abbreviated names. Figure rendered using Paracel Pathworks pre-rendered pathway models.)

These differences were also seen on chemically treated fibrin gels, utilized specifically for the purpose of development as an implantable material. Sheetz et al., further reported that migration of fibroblasts grown on similar, chemically treated PAA_m gels is at least partially mediated by the integrin $\alpha_v\beta_3$ and the receptor-like protein tyrosine phosphatase- α (RPTP α) (39).

Material systems like those described above necessitate changing the film's chemical composition as the means of controlling the mechanical properties of the film. Such changes may include altering the molecular composition of polymer molecules by varying the extent of covalent crosslinking and introduction of new molecular agents to induce crosslinking. This means of mechanical modulation poses a problem or unambiguous interpretation of mechanical cues: namely, the extent of covalent crosslinks within the film and availability of functional groups at the film surface (chemical), as well as the topography (physical) become variables in the experimental system. It can therefore be argued that such systems disallow direct evaluation of chemomechanical cell responses via isolation of mechanical properties, because the underlying effect from the sample physical and chemical variation is unknown. This problem is generally considered inescapable from the standpoint of material design, since it is nearly impossible to alter the mechanical properties of a material without simultaneously changing the chemical or physical properties of the material. However, one can limit the impact of physical, chemical, and mechanical interdependence by systematically varying each property under well-defined experimental conditions, and then determining which variations bear

minimal effect on observable cellular behavior. Such an approach was successfully demonstrated by Mendelsohn et al. using a class of ultrathin polymer films known as polyelectrolyte multilayers (PEMs) as a culture surface, where the authors showed that systematic perturbation of chemical and physical properties of the films had no effect on cell attachment, save for the “swellability” of the polymer films (40). Thus, rather than attempting the extremely challenging task of isolating mechanical variation from physicochemical properties directly, Mendelsohn et al. engineered an experimental system where such variation became irrelevant, and cell attachment could be correlated with a single, experimentally quantifiable feature. Furthermore, the PEM system was demonstrated to be tunable by simple, cost-effective variations of assembly conditions. The critical importance of these features to the work described in this thesis, and to the field of mechanotransduction as a whole, will be discussed in greater detail in Chapter 2.

A wide variety of PEMs have been employed to examine questions related to cell adhesion, cell migration, and cell phenotype (41-48). The early work described in this thesis was among a series of reports from several independent research groups between 2004-2006, in which a clear correlation between cell adhesion and quantifiable mechanical properties of the underlying substrata was established (42, 44-46, 49-53). Among these reports, Engler et al. demonstrated that smooth muscle cells grown on hyaluronic acid/poly-(*l*)-Lysine (HA/PLL) PEMs attach and spread more readily to substrates of higher stiffness (42), while

Schneider et al. made similar observations of increased attachment and growth on HA/PLL PEMs using chondrosarcoma cells (53). Discher et al. have further shown that myotube precursor cells are capable of exhibiting some myocyte differentiation markers when cultured on extracellular matrix protein-coated polyacrylamide (PAAm) hydrogels with stiffness proposed to match to that measured for *in vitro* tissue samples, i.e., stiffness of approximately 10-12 kPa (42). In a subsequent study, Engler et al. report that mesenchymal stem cells exhibit some genetic and protein markers of neural, muscle, and bone cell phenotype when grown on collagen-coated PAAm hydrogels of elastic moduli similar to that measured for *in vitro* tissue sections (51).

The finding that adhesion, morphology, and functional markers of cells can differ among substrates of varying mechanical stiffness is in accord with our observations, yet the reported range of nominal stiffness by these groups, characterized by the Young's elastic modulus E , differs from the range of stiffness reported in this thesis. The ability of cells to distinguish between polyacrylamide gels of E varying by only several kPa is difficult to rationalize, as instrumented measurements of stiffness by our group have demonstrated that local variation of E typically exceeds the few kPa range reported as a critical range in the experiments of Engler et al. To this end, the demonstration of differential cellular adhesion to PEMs varying in E over several orders of magnitude is a distinct contribution to the field, as is the concept of using mechanically tunable PEM interfaces. This is significant, as quantitative assessment of the mechanical properties of cellular

substrata is now a common feature in literature related to PEM-cell adhesion studies.

It is not unreasonable to postulate that biologically derived PEMs, while physiologically relevant, possess chemical attributes that facilitate cell attachment to compliant materials cooperatively with mechanically activated pathways. For example, Picart et al. report that chondrosarcoma cells adhere with in greater number to HA/PLL PEMs of high E relative to those of lower E ; yet chondrosarcoma cells express highly specific cell surface receptors for HA, leaving open the possibility that material-receptor interactions may mediate attachment to the compliant surfaces used in the study (54). Neither Discher et al. nor Picart et al. have addressed the fact that both compounds comprising the PEMs used in many of their studies are native to the *in vivo* extracellular milieu, and therefore may present unexpected chemical contributions to the attachment responses reported. Such examples therefore make it difficult to fully appreciate the manner in which cells use extracellular mechanical environment as a signal transducer in the absence of very thorough characterization of the cell-material interfacial properties.

PEMs have been extensively studied, and a number of techniques exist to characterize these films on the macroscale (44-46, 55-57, 68, 70-72). However, mechanical properties of such films in the fluid-immersed state are difficult to analyze by conventional means. Moreover, the nanoscale thickness of PEM thin

films used in our studies and those of other groups require use of nanomechanical tools, such as nanoindentation and scanning probe microscopy (SPM), to characterize material properties such as surface roughness, elastic modulus, adhesiveness, and swelling in fluid (55-57). Using nanoindentation and SPM, one can directly measure mechanical stiffness in terms of nominal elastic modulus E , and thus correlate cell behavior with the stiffness (or, inversely, compliance) of the cell substratum. Careful choice of the PEMs used in a given cell study allows one to probe such cell responses independently of the chemical composition at the cell-PEM interface. This is important, because it is impossible to completely separate the mechanical properties of a thin film from the chemical composition of the film. Rubner et al. have developed and characterized a system of poly(acrylic acid)/poly(allyl amine hydrochloride) (PAA/PAH) PEMs with the ability to swell in fluids by as much as 300%. This swelling in near neutral pH fluid is directly related to the magnitude of E and can be modulated by controlling aqueous polymer solution pH during PEM assembly. It must be noted that nominal values of E obtained via SPM-enabled nanoindentation range from 0.1-500 MPa. The substratum of highest nominal E approaches a stiffness probably experienced only by cells abutting mineralized bone *in vivo*, thus raising questions about the relevance of such PEMs in analysis of adhesion in cells accustomed to extracellular conditions of greater compliance *in vivo* (e.g., within ECM of soft tissues). However, the transitions in nominal E at each assembly pH are particularly well suited to exploring the dynamic range of mechanical environments

to which cells such as ECs are exposed. More importantly, the mechanical variation among PEMs at each assembly pH typically differs by order of magnitude for pH mod-2, and can be engineered to far exceed any chemical variation (polycation:polyanion ratio, total free acid content), a crucial factor for this type of study. Therefore, the PAA/PAH and PAA/PAAm PEM systems satisfy the criterion described above regarding the ability to unambiguously identify mechanically induced changes in cell behavior. Film thickness of the PAA/PAH PEM system can be varied down to ~100 nm with retention of the mechanical properties for a given assembly condition, which correlates to the approximate thickness of the extracellular matrix (ECM) in vascular beds *in vivo*; thus, this ensemble of PEM substrates is a useful model system for investigations of chemomechanical modulation of phenotype.

1.3 Eukaryotic and Prokaryotic Cells in Mechanotransduction

Vascular endothelial cells (ECs) are well suited for study in a variety of cell culture environments, and are particularly well suited for investigations of response to mechanical cues. *In vivo*, ECs operate in two-dimensional arrays e.g., in large blood vessels ECs where they line the vascular wall as a single cell sheet; and they also operate in solid , three-dimensional structures, such as capillary vessels

where the endothelium is enveloped by support cells and also responsible for penetration and subsequent migration of ECs into tissues during angiogenesis. Furthermore, as a cell class, ECs exist in close contact with cells comprising a diverse range of mechanical stiffness, such as in the highly compliant tissues of the lung and the much stiffer environment of mineralized bone. Numerous studies have demonstrated strong, persistent response to shear and stretch-induced strain as described above, and more recently to anchorage-dependent forces (4, 10, 11, 46, 58-60). It is well known that ECs, in particular, are potent transducers of mechanical force and mediate chemomechanical signals on a wide scale, acting in endocrine, paracrine, and autocrine fashion to induce chemical and various cellular architectural changes *in vivo*.

Prokaryotic cells, which lack the true nucleus found in eukaryotes, are interesting targets for the study of mechanotransduction. Among prokaryotes, there exist cells with and without ancestral precursors to the elements that are now known to mediate some mechanosensation in eukaryotes. For example, some bacteria possess a proto-cytoskeleton for which some elements dictate cell shape and coordinate cell division and DNA replication (61-63). Moreover, bacteria represent a major portion of Earth's biomass, and together with other microbial species are representative of a staggering collection of diversity in phenotype and genotype (64). Bacterial adhesion to material surfaces represents an area where unmet biomedical need coincides with mechanical processes amenable to study by chemomechanically defined substrates. As detailed in

greater depth in Chapter 5, hospital acquired infections are a major source of morbidity and mortality in the U.S and across the world, with associated costs totaling estimated \$4.5 billion annually for the U.S. healthcare system (20, 65-67). The primary causative agent of infection is the bacterium *Staphylococcus epidermidis* (*S. epidermidis*), and its major route of infection is the formation of a film-like material called a biofilm through the process known as bacterial colonization (or, simply colonization)(1). Another species often identified in hospital acquired infections is *Escherichia coli* (*E. coli*), an enteric organism that is widely studied in bioengineering because of its suitability for genotypic manipulation (1). *E. coli* also expresses cytoskeletal proteins homologous to the eukaryotic cytoskeletal protein, actin. Together, these species represent excellent tools to probe mechanosensation along paths both independent and analogous to those reported in eukaryotic cells.

1.4 Thesis Scope

This thesis investigates the effects of chemical and mechanical extracellular properties on eukaryotic and prokaryotic cell behavior. The overall goal of this thesis is to assess phenotypic changes in cells and cellular response induced through modulation of local properties of the extracellular environment. From an engineering perspective, it is helpful to identify key elements of the molecular mechanisms involved in cell behavior evoked by extracellular processes. This

provides a more complete understanding of cellular function in physiologic environments and potential prediction of pathogenesis in disease states. This thesis supports the hypothesis that external mechanical environment can alter cell functions including adhesion and morphology. This work details morphological differences in ECs during initial adhesion to PAA/PAH PEMs. Additionally, differences in cell proliferation during *in vitro* culture imply that the pathways involved in cell growth are also activated during EC adhesion to PEMs. Moreover, this work describes mechanoselective adhesion in prokaryotic systems and demonstrates that such bacterial cells are capable of distinguishing cellular substrata of differing stiffness by using an as-yet-unidentified mechanism distinct from analogous actin-based eukaryotic processes. Detailed introductions to each class of eukaryotic and prokaryotic cell are given in the appropriate chapters. Nevertheless, this work describes the response of a variety of cell types known for acting as both chemical and mechanical transducers of extracellular cues.

Chapter 2 presents the motivation for using weak polyelectrolyte multilayers to address chemomechanical effects on cell response. Results of mechanical characterizations of PEMs via atomic force microscope-enabled nanoindentation used throughout this study are presented, along with a brief discussion of issues related to the interpretation and usefulness of such analysis. Additionally, characterizations of several physicochemical properties of PEMs relevant to this thesis are discussed in detail in Chapter 2, and cell adhesion assays based upon those findings presented in Chapter 5.

Chapters 3 and 4 present results relating to eukaryotic cell behavior on mechanically and chemically tunable PEMs. Chapter 3 demonstrates that human vascular endothelial cells are responsive to changes in external mechanical cues (46). Chapter 4 shows that PEM ensembles can be engineered to independently modulate cell adhesion efficiency through chemical and mechanical signals (45). Both of these results also demonstrate that chemical and mechanical cues can work in tandem to enhance cell adhesion to a synthetic substrate, such as enhanced adhesion of cells to stiff PAA/PAH PEMs dependent on the net charge of the terminal polyelectrolyte (46), or adhesion of cells to compliant films the surface of which have been sufficiently conjugated with cell adhesion peptides (45).

Chapter 5 describes studies of prokaryotic adhesion to PEMs. A systematic investigation of the effect of physical, chemical and mechanical material properties on *S. epidermidis* adhesion to PAA/PAH PEMs is presented. Following those studies, data pertaining to cell adhesion as a function of differences in cell shape, cell species, and cell envelope chemistry are discussed using two different strains of the *E. coli*.

Finally, Chapter 6 presents a summary of the research, and a brief discussion of future directions and applications of the research, followed by several appendices to supplement important aspects pertaining to the research described in this thesis.

CHAPTER 2 PAA/PAH POLYELECTROLYTE MULTILAYERS CHEMICAL AND MECHANICAL PROPERTIES

Note: Portions of this chapter include sections previously published with contributions from the following publications and co-authors:

Biomaterials. Dec 2005;26(34):6836-6845, M.T. Thompson, M.C. Berg, I.S. Tobias, M.F. Rubner, and K.J. Van Vliet.

Biomacromolecules Jun 2006;7(6):1990-1995, M.T. Thompson, M.C. Berg, I.S. Tobias, J.A. Lichter, M.F. Rubner, and K.J. Van Vliet.

Biomacromolecules Jun 2008;9(6):1571-1578, J.A. Lichter, M.T. Thompson, M. Delgadillo, T. Nishikawa, M.F. Rubner, and K.J. Van Vliet.

2.1 Background and Motivation

Early investigation of mechanical effects on cell response was tested in a series of pilot experiments involving bovine capillary endothelial cells grown on hydrogels made from commercially available purified collagen (BD BioSciences) and on the commercially available product Matrigel™ (BD BioSciences), a mixture of proteins including laminin and fibrin that are present *in vivo* in extracellular

matrixes. However, the results of these pilot experiments were inconclusive, and the approach was quickly abandoned for reasons described below.

Drawbacks in the hydrogel system used in the pilot experiments provided insight for later experimental design. First, the assembly of hydrogel layers was subject to variations in gel thickness, and defects from the presence of air pockets and bubbles formed during the deposition process by pipette devices. Second, the assembly protocols offered little ability to control the uniformity of deposition of the gels. Hence, the physical properties (gel thickness, lateral and surface roughness, porosity, and chemical properties of the composite gel could vary significantly with each assembly batch. Third, the composition of commercial gels such as Matrigel™ is complex and proprietary, which makes standardization of the composition difficult to quantify. Finally, the appearance of the hydrogels via optical microscopy suggested the cells might be digesting and migrating into the gel, thus defeating the intended experimental design.

Thus, the hydrogel pilot experiments highlighted several key features the cell substrata should possess in order to quantify the effect of mechanical and chemical variation on cell phenotype and adhesion. First, the substrata should be thin and of uniform thickness and properties when deposited, in order to minimize effects from physical variation like differences in lateral or Z-scale root-mean-square (RMS) roughness. In addition, the thickness of each film-type should be controllable. This ensures that the cells are anchored to substrata of comparable thickness in any given study, and allows preparation of samples suitably thick so

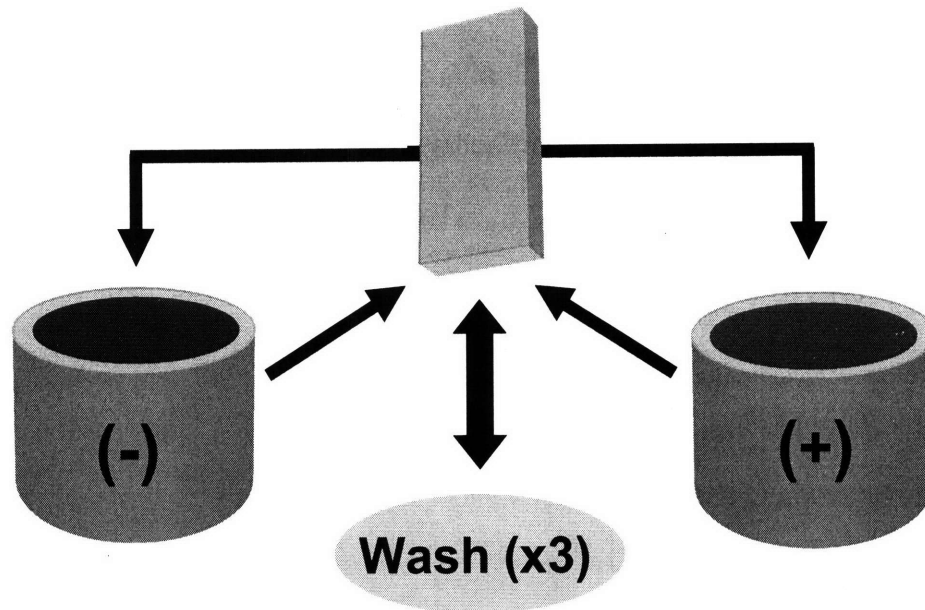


Figure 2.1 Layer-by-layer assembly of polyelectrolyte multilayers A glass slide is dipped in a dilute, pH-calibrated polyanion solution and allowed to equilibrate for 15 minutes. The slide is then washed for 1-2 minutes, three times sequentially in individual deionized water baths. The slide is then dipped in dilute, pH-calibrated polycation solution for an additional 15 minutes, sequentially washed 3 times in separate deionized water baths, and the cycle is reiterated until all layers have been deposited. A single completed dipping cycle deposits 1 bilayer. The order of polyion addition by dipping can be changed depending on properties of the slide, such as the presence of pre-adsorbed/conjugated ionizable groups (e.g., amines). The slide is kept hydrated throughout the process to prevent aberrant deposition of the multilayer.

as to prevent cells from sensing the substrate to which the films are anchored. The substrata must also be tunable with respect to mechanical stiffness, and this tunability must not significantly alter the chemical composition of the film or film interface. Chemical features of the film must include the ability to modify the interface to display adsorbed or covalently conjugated molecules. The films should be cytophilic, in at least some cases, or possess the ability to be modified such that

they are cytophilic. This implies that the films be compatible with conditions used in standard tissue culture protocols: that is thermal stability up to $\sim 37^\circ \text{C}$, stability in the presence of salt solutions approaching ionic strength $I = 0.15$, and stability at pH values ranging between 6.6-7.6. The class of ultrathin films known as polyelectrolyte multilayers (PEMs) satisfies each of these conditions. The remainder of this chapter describes the techniques used to quantify the tunable mechanical properties of PEMs that make them ideal for studying the complex interplay between chemical and mechanical signaling in cells.

2.2 Polyelectrolyte Multilayers Thin Films as Tunable Cell Adhesive Substrata

Polyelectrolyte multilayers are thin films comprising cationic and anionic polymer chains complexed through ionic bond crosslinking. Strong polyelectrolytes are those polymer chains that are fully ionized in solution and are relatively insensitive to changes in solution pH, while weak PEM chain ionization can be modulated by adjustment of assembly pH. In this way, the extent of charge across a given weak polyelectrolyte can be “tuned” by careful adjustment of the solution pH and limitation of factors that might skew the pH, such as diffusion of ambient CO_2 (68). Such interactions can include ionic-ionic crosslinking, such as those between carboxylate-amine containing PEMs; covalently bonded systems, via the use of crosslinking agents; hydrogen-bonded networks, such as poly(amide)-

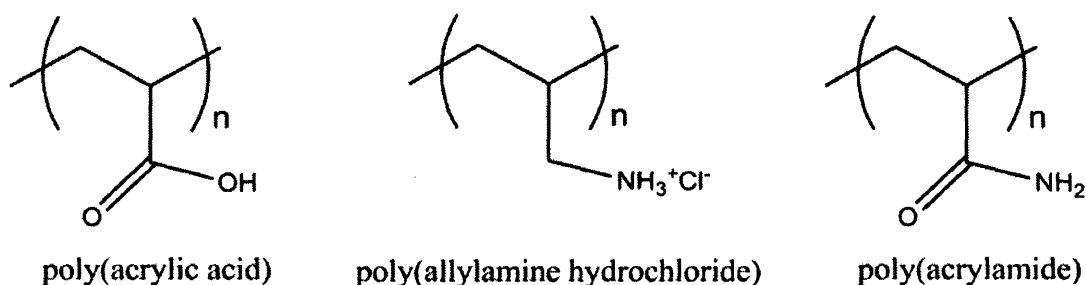


Figure 2.2 Polyelectrolytes components used in this study In ionically crosslinked PEMs, poly(allylamine hydrochloride) (PAH) is used as the polycation. For thermally crosslinked, weakly hydrogen-bonded PEMs the counter polyelectrolyte is polyacrylamide (PAAm). Poly(acrylic acid) (PAA) is used as the polyanion for all PEMs in this thesis.

poly(carboxylate) systems that may be further stabilized by limited covalent modification, typically by increasing the percent crosslinking; and hybrids of these systems (40, 69). The PEMs used in this thesis are assembled through a layer-by-layer (LbL) dipping process (Fig. 2.1), although alternative assembly techniques exist (e.g., spin coating). PEM samples are typically described in the literature by the chemical abbreviation of the cation/anion pair and the assembly pH for each polyelectrolyte, e.g., PAA/PAH 2.0/2.0 corresponding to a poly(acrylic acid)/poly(allylamine hydrochloride) PEM assembled at pH 2.0 for the cation and anion solution bath, respectively.

PEMs can be assembled in films of nanometer to micrometer scale thicknesses, depending on the number of dipping cycles and the swellability of the PEM at the pH of interest. The presence of biocompatible chemical moieties, such as amines and carboxylic acids, facilitates chemical modification within the polymer films as well as at the surface. Although the designation “multilayer” might evoke images of a striated structure, this is not the case for PEMs. Structurally,

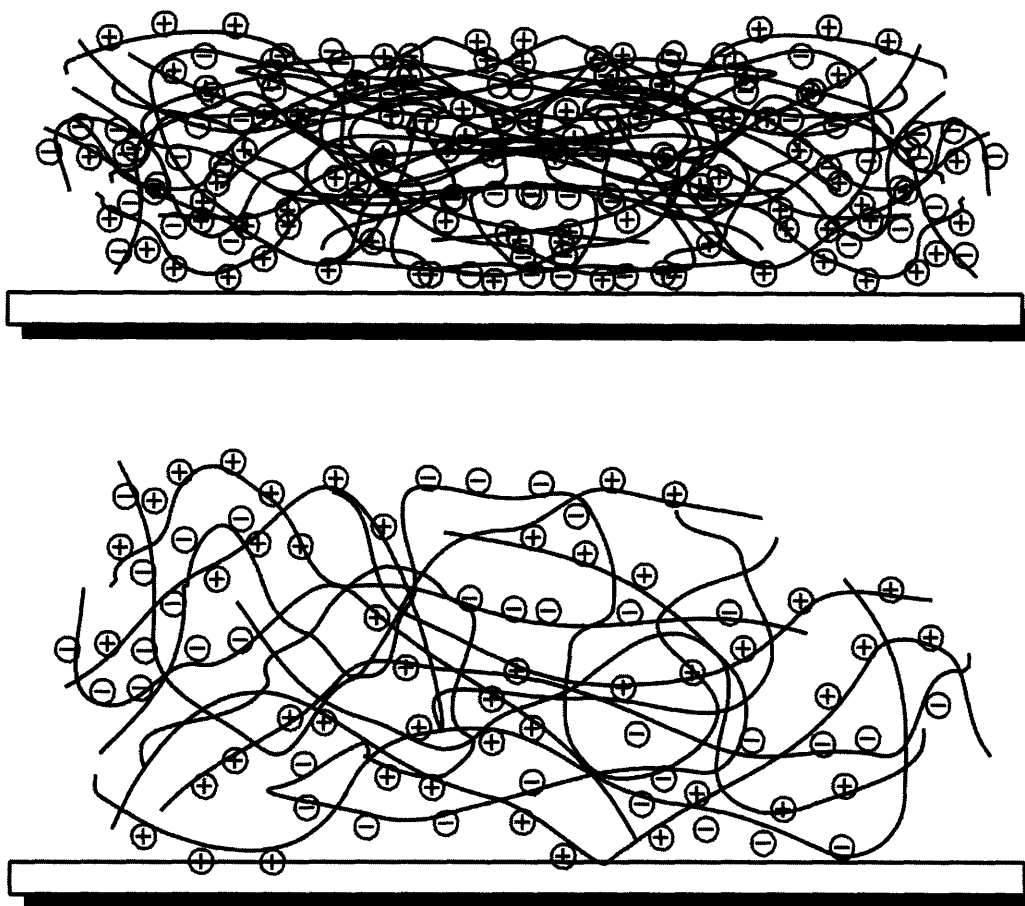


Figure 2.3 Polyelectrolyte multilayer structure. For high charge density cation-anion paired polymer chains and high charge compensation result in thinner films (*top*). Low charge density for either the cation or anion, or poor charge compensation in the assembled film leads to loop-rich, highly swellable structures (*bottom*).

PEMs are interpenetrating networks of polymers that are freely open to solvent diffusion, yet the pore size is small enough to restrict cells to the PEM surface (Fig. 2.3). Furthermore, PEMs are mechanically tunable through control of assembly conditions such as pH, temperature, and through adjustment of the mode of polymer chain deposition (45). Adjustment of the pH modulates the charge density

crosslinking across the polymer chains at the time of assembly. As the films are assembled via LbL-deposition, the excess charge from the previously deposited layer is compensated by the subsequent oppositely charged polymer. The extent of charge compensation by the next polymer layer determines the extent of ionic crosslinking in the PEM network, modulating the thickness of the film and the loop-like features throughout the network.

PEMs are capable of modification by covalent attachment of molecules to surface functional groups directly, or through a process known as polymer-on-polymer (POP) stamping (45, 47, 70-72). It should be noted that all POP-stamped PEMs used in this thesis were assembled by Dr. M.C. Berg or Ms. J.A. Lichter (73, 74). For surface-modified samples, PAH was first added to the surface by one of two routes. In the first case, surface modification was achieved via incubation of the PEM sample in a 0.01 M / pH = 9.0 polyelectrolyte solution at room temperature for 15 min or 30 sec (hereafter termed *adsorbed PAH*). In the second case, surface modification was achieved via polymer-on-polymer transfer with a patterned PDMS stamp inked with 0.05 M PAH / pH = 9.0 (hereafter termed *stamped PAH*), as described previously by Berg et al. (75). Briefly, PDMS polymer stamps were soaked in a 0.01 M solution of PAH and then allowed to physically contact the PAA/PAAm PEM surface for 30 sec before removal. The PEMs were then rinsed with 150 mM / pH = 7.4 phosphate buffered saline (PBS) several times under agitation, and allowed to dry in air for subsequent rehydration and use. Modification of PAH-treated PEMs with Arg-Gly-Asp (RGD) or a sequence that

does not illicit cell adhesion, Arg-Gly-Glu (RGE), was accomplished first by incubation of 0.5 mM Sulfo-LC-SPDP in the presence of PAH-treated PEMs for 30 min at room temperature. Following the addition of this heterobifunctional crosslinker, the samples were washed with PBS twice for 5 min. Incubation of 0.5 mM peptide solution (GRGDSPC or GRGESPC) in PBS for 8 hours at room temperature yielded RGD and RGE modified PAA/PAAm samples, ostensibly conjugated to the heterobifunctional crosslinker via a disulfide linkage. PEMs were rinsed several times in PBS under agitation, and allowed to dry in air for subsequent rehydration and use. The use of POP-stamping of PEMs, mechanical and physical characterization of the PEMs treated by this technique, and the affect of POP patterning versus chemical adsorption on cell adhesion are discussed in greater detail in Chapter 4.

One of the motivating principles of the early mechanical characterization of PEMs in this thesis relates to the property of swellability. When hydrated at near neutral pH, loosely cross-linked PEM films such as pH-assembled 2.0/2.0 PAA/PAH and pH 3.0/3.0 PAA/PAAm show significant swelling from fluid absorption. Early cell studies on these films reported that the capacity to which a film swelled when hydrated directly correlated with the eukaryotic cytophilicity or cytophobicity of the film (40, 47, 70-72, 75). Assessment of PEM film mechanical properties using nanoindentation was proposed as a means of providing a quantifiable parameter by which the cytophobicity or cytophilicity of these PEMs could be understood and possibly predicted.

2.3 Mechanical Analysis of PEMs

Nanoindentation of PAA/PAH multilayers assembled in 60 mm-diameter polystyrene Petri dishes (p60s) or on borosilicate glass slides (Sigma-Aldrich) was conducted using a commercially available scanning probe microscope (Molecular Force Probe 3D or MFP 3D, Asylum Research, Santa Barbara, CA). Unsharpened silicon nitride cantilever of nominal spring constant $k_c = 0.1$ N/m and nominal probe radius of 50 nm (MHCT-AUHW, Veeco Metrology Group, Sunnyvale, CA) were used to obtain the continuous force-displacement response of the PEMs in fluid, and silicon cantilevers of nominal $k_c = 0.7 - 3.8$ N/m and probe radius of 50 nm (AC-240, Olympus) were used to obtain the response on comparably rigid polystyrene. For the eukaryotic cell studies, p60s were used so that mechanical testing would occur using the same underlying tissue culture polystyrene substrata that cells would be exposed to during normal culture. In all other circumstances, mechanical testing was performed on slides composed of the indicated materials.

As the actual spring constant of each cantilever can vary from nominal values reported by the manufacturer, k_c was determined experimentally for each lever immediately prior to indentation as follows (See Fig. 2.3). First, cantilever free end-deflection δ was calibrated as a function of laser-photodiode voltage V through displacement of the cantilever against a rigid (glass or polystyrene) substrate, such

that there was a 1:1 correspondence between the downward displacement of the piezoactuated cantilever base and the upward displacement of the probe at the free end of the cantilever. Second, δ was recorded under thermal (room temperature) activation, and the Fourier transform (FFT) of cantilever amplitude as a function of oscillation frequency was fitted with the simple harmonic oscillator equation to determine k_c (76). This thermal power spectral density method is semi-automated within the instrument used herein. Experimentally determined values of k_c were implemented in subsequent data analysis, and did not exceed nominal values by more than 200%.

The experimental system was allowed to achieve thermal equilibration for a minimum of 1 hour inside of a customized acoustic isolation enclosure (Herzan, Inc.) prior to cantilever calibration and mechanical testing of the PEMs. This equilibration time was found necessary to minimize thermal drift of the laser-photodiode feedback response used to monitor the force-displacement response of the PEMs. Force-displacement (P - Δ) responses were recorded in deionized water at a velocity of 1 $\mu\text{m}/\text{sec}$ to a maximum cantilever deflection δ of <30 nm. This maximum deflection, corresponding to a maximum applied force $P \leq 5$ nN in the PEMs, was chosen such that the resulting penetration depth Δ did not exceed the displacement over which the mechanical contact between the probe of nominally 50 nm radius and the PEM substrate could be idealized as a sphere-on-flat contact geometry. Upon thermal equilibration of the experimental system, P - Δ responses

were recorded at distinct positions on the substrate surface, such that each response was generated at a different location. All indentations and cantilever calibrations were performed under force feedback control, which is a closed loop feedback method that precisely controls the specified load applied to the sample within ~ 0.1 nN (data not shown). A second closed feedback system is used by the MFP 3D positioning actuators, so that spatial control of indentation arrays is resolved < 1 nm (X-Y). The MFP 3D optical detection system is equipped with a super-luminescent diode (SLD) for maintenance of temperature stability in the AFM optics, and a linear closed-loop feedback system to maintain the SLD-photodiode calibration. Thus, once the system is calibrated and equilibrated, measurements can be made with high precision in a repeatable, controlled fashion.

2.4 Analysis of Nanoindentation Response

Mechanical output was analyzed offline using the scientific computing software IGOR (Wavemetrics, Lake Oswego, OR). Raw experimental data includes cantilever free-end deflection δ versus cantilever base displacement d , and requires straightforward conversion to force versus probe penetration depth, or P- Δ responses, where

$$P = k_c \delta \tag{2.1}$$

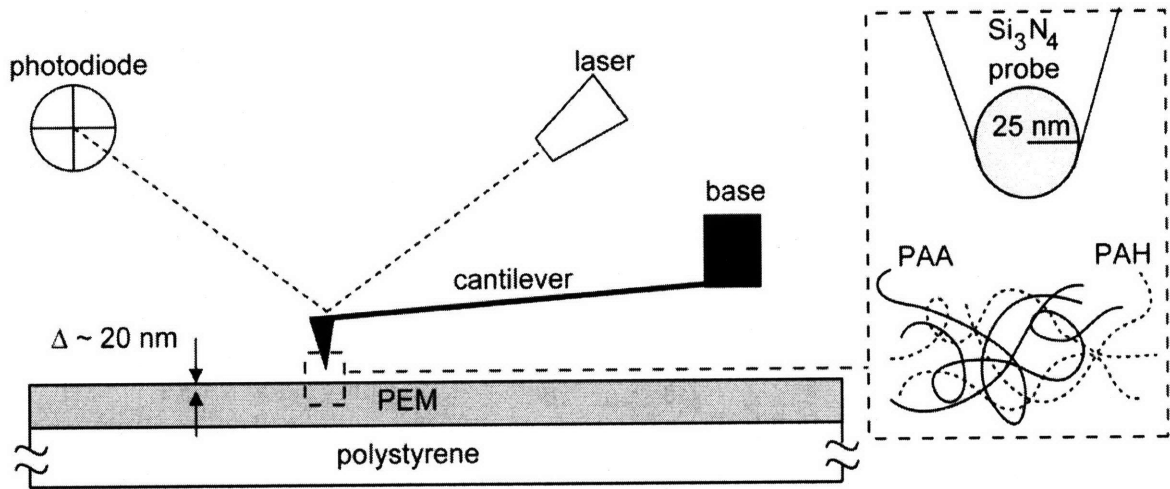


Figure 2.4 Schematic of AFM Indenter Indentation of hydrated PEMs is carried out using a commercial atomic force microscope. Deflection of a cantilever with a known spring constant is measured by detecting the positional change of a light source reflected from the cantilever tip. The AFM base is capable of translation normal to the surface via a piezoactuator, and controls the approach and retraction of the sample probe relative to the sample surface. Indentation depth, Δ , is restricted to $< 20 \text{ nm}$ to approximate indentation by a spherical probe. (*Inset*) The silicon nitride AFM sample probe has a nominal radius ranging 25-50 nm. The PAA/PAH multilayer is an interpenetrating network of polycation and polyanion polymer chains (1).

$$\Delta = d - \delta \quad (2.2)$$

For purposes of analysis, we describe the polymer substrata as a sphere of radius R_s and the cantilevered probe as a sphere of radius R_p , such that $R_s \gg R_p$. In this way, we can apply the Hertzian theory of elastic contact between spheres (77), which relates the force imposed by the cantilever P to the penetration depth within the substrate Δ as,

$$P = (4/3) E_r R_p^{1/2} \Delta^{3/2} \quad (2.3)$$

where R_p is the radius of curvature of the cantilevered probe, and E_r is the reduced elastic indentation modulus comprising the elastic response of both the substrate and the probe materials.

Experimentally, care was taken to acquire and analyze data within the range of indentation depth for which Hertzian analysis is reasonably valid. However, it should be noted that some loading curves showed a Hertzian elastic response beyond this estimated value of Δ_c , reflecting the uncertainty to which R_p is known. Equation (2.3) can be represented generally as,

$$P = C\Delta^{3/2}, \quad (2.4)$$

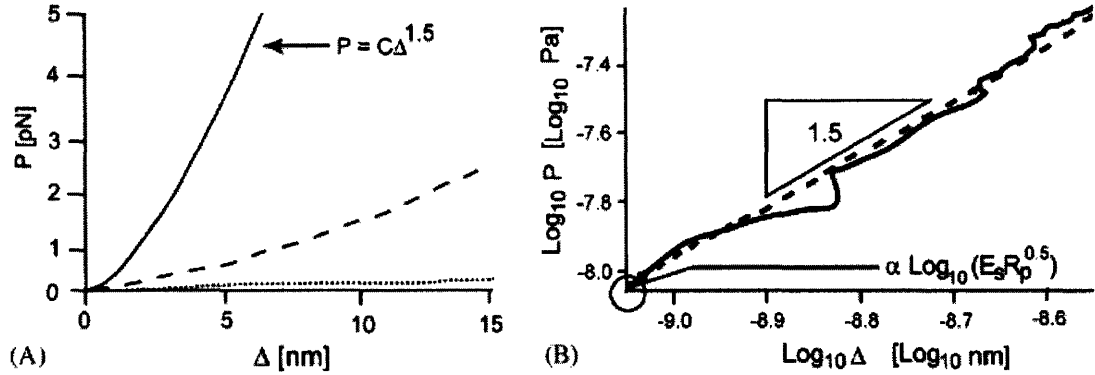


Figure 2.5 Ideal and representative MFP data (A) Representative force-displacement P - Δ responses of PEMs as a function of assembly pH (solid, pH = 6.5; dash, pH = 4.0; dot, pH = 2.0). (B) Logarithmic representation used to extract indentation modulus E_s .

where loading curvature C is qualitatively and quantitatively proportional to the elastic modulus of the indented sample E_s (See Fig. 2.4A). Taking the logarithm of Eq. (2.4) yields a linear representation of the form

$$\log_{10}P = \log_{10}C + 3/2 \log_{10}\Delta = a + b \log_{10}\Delta \quad (2.5)$$

from which the reduced modulus E_r can be calculated directly by reference to Eq. (2.5), as shown in Fig. 2.5B. The modulus of the substrata can be computed directly from E_r , where

$$E_r = [E_s(1 - \nu_s^2)^{-1} + E_p(1 - \nu_p^2)^{-1}] \quad (2.6)$$

where E_s , ν_s and E_p , ν_p are the Young's modulus and Poisson's ratio for the substrate material and the cantilevered probe material (Si_3N_4), respectively. Poisson's ratio was not measured experimentally, and was maintained fixed at a value of 0.33 and 0.45 for Si_3N_4 and the polymer substrata, respectively; $E_p = 310$ GPa. Here, it is equally reasonable to assume $E_p \rightarrow \infty$, such that $E_r = E_s$, with little effect on the calculated compliance. Through linear regression of the P - Δ response for $\Delta < 20$ nm were analyzed for each independent experiment n according to Eqs. (2.5)–(2.6) to determine E_s . Calculated values of E_s are reported as averages and standard deviations, where $n \geq 40$ for each sample, each a unique spatial location on the sample surface. As the above approach measures the elastic modulus of the material under mutiaxial (rather than uniaxial) loading and neglects realistic polymer deformation characteristics including nonlinear elasticity and viscoelasticity, we use the term E_s to represent the nominal indentation elastic modulus. This representation is related qualitatively to the Young's modulus E measured through uniaxial mechanical testing of bulk, linear elastic samples. Multiple batch runs of the pH assembled PAA/PAH samples were tested on different days, to identify any sample-to-sample variation and systematic experimental errors.

In later studies, the force-displacement data were processed prior to analysis using a 25 pass binomial smoothing filter to eliminate random fluctuations. Each

force-displacement curve was then visually inspected and aligned against a representative force curve from the same experiment, whereby the force and separation data were zeroed by overlaying the corresponding loading regions using a free-scale, non-rotatable coordinate system. Since accurate determination of the initial contact point is a critical issue in nanoindentation of compliant polymer films, an additional noise threshold was applied to the $\log P - \log \Delta$ representation of smoothed curves to identify this (0,0) point objectively and repeatably. Linear least-square fits of the $\log P - \log \Delta$ representation of smoothed responses were conducted and yielded intercept values from which nominal E were calculated from Eq. (2.3), as described above. Calculated values of E_s are reported as averages and standard deviations, where $n \geq 40$ for each sample, each a unique spatial location on the sample surface. Prior to using PEMs from a given assembly batch, the stiffness of a randomly selected sample from each assembly of batch of PEMs was “spot-checked” using the above procedure with $n \geq 20$, wherein each test sample was compared against a pre-calibrated PEM of similar assembly pH and known stiffness. This approach greatly facilitated rapid characterization of the mechanical stiffness of newly assembled PEM batches. A detailed discussion of the limitations of nanoindentation can be found in the published account of this technique and its application to endothelial cell adhesion (46).

2.5 Contact Angle Measurement Based Calculation of Surface Interaction Energies

Contact wetting angles may be used to determine interfacial surface energy of interaction between a cell and a given material surface, including PEMs (2, 82-84). There are three accepted methods for determining the free energy of interaction between two-component and three-component systems: the equation of state method; geometric mean; and the Van Oss acid-base approach.

All three methods rely upon measurement of surface tension components of test solvents derived from observed contact angle wetting values. The equation of state method only requires the measurement of one test solvent to determine the interaction energy between two-state systems (cell-material), before and after adhesion (2). This means that measurements must be made twice: one measurement for the free surface and one measurement with the adherent cell on the surface. Between the remaining two methods, the Van Oss approach encompasses all of the experimentally derived parameters that the geometric mean method can provide, but at the expense of requiring additional test solvents. Of the three methods, the Van Oss approach was regarded as the most developed

technique for biological applications, based upon a survey of the literature by Sharma and Rao regarding cell adhesion in over 100 species of microbes (2), and is widely cited in the literature pertaining to microbial cell adhesion (2, 84-100). For this reason, liquid contact angles were used according to the Lewis acid-Lewis base theory of Van Oss to determine thermodynamic properties of the surface-bacterial cell-liquid interface (84). Using the Van Oss approach, liquid contact angles of three or more test solvents are measured and then entered into the Van Oss-Young equations:

$$(1 + \cos\theta) \gamma^{\text{tot}}_L = 2\sqrt{(\gamma^{\text{LW}}_S \gamma^{\text{LW}}_L)} + 2\sqrt{(\gamma^+_S \gamma^-_L)} + 2\sqrt{(\gamma^-_S \gamma^+_L)} \quad (2.9)$$

and

$$\gamma^{\text{tot}}_i = \gamma^{\text{LW}}_i + \gamma^{\text{AB}}_i \quad (2.10)$$

$$\gamma^{\text{AB}}_i = 2\sqrt{(\gamma^+_i \gamma^-_i)} \quad (2.11)$$

where γ^{tot}_i is the total surface tension of a material i , γ^{LW}_i is the apolar component of the surface tension, γ^{AB}_i is the polar component, and γ^+_i , and γ^-_i are the electron acceptor (Lewis acid) and electron donor (Lewis base) properties of the material. Van Oss-Young's equation is solved simultaneously to yield the apolar, Lewis acid,

and Lewis base components of the interfacial tension. The total interaction energy between the bacterial cell and the substrata material is then given by:

$$\Delta G = (\gamma^{LW}_1 + \gamma^{LW}_2)^2 - (\gamma^{LW}_1 + \gamma^{LW}_2)^2 - (\gamma^{LW}_1 + \gamma^{LW}_2)^2 + 2[\sqrt{\gamma^-_W} (\sqrt{\gamma^+_1} + \sqrt{\gamma^+_2} - \sqrt{\gamma^+_W}) + \sqrt{\gamma^+_W} (\sqrt{\gamma^-_1} + \sqrt{\gamma^-_2} - \sqrt{\gamma^-_W}) - (\sqrt{(\gamma^+_1 \gamma^-_2)} - \sqrt{(\gamma^-_1 \gamma^+_2)})] \quad (2.12)$$

To solve this nonlinear equation, total surface tension of the cellular component is needed. A review of the various techniques for acquiring cell surface tensions can be found in Sharma and Rao (2), but the most common technique involves measurement of the contact wetting angle on a deposited bed of cells termed a "lawn". Measurement of contact angles on bacterial lawns is not completely standardized. Moreover, the differences amongst samples with respect to the physical characteristics of deposited bacterial lawns can give rise to large errors unless special care is made to control hydration, percent humidity, timing between liquid droplet deposition and contact angle measurement, and total equilibration time (2). For these reasons, it was decided that previously established values of the surface tension components would be used for the bacterial species or closely related strains (see Table A.3.1). This is a reasonable approach, since the variable tension components in these studies are not those of the bacteria, but those of the PEMs. All PEM components were determined experimentally, and care was taken not to compare energetic properties between bacterial species but only between PEMs for a given bacteria species.

2.6 Calculation of Surface Charge Density from Electrostatic Model

We attempted to assay the concentration of PEM surface free carboxylic acid groups ($\text{COOH}_{\text{surface}}$), as a means of assessing net negative charge at the fluid-PEM interface. The PEM samples were stained with the common cationic aqueous dye, methylene blue (MB). In PAA-based PEMs, MB incorporation occurs due to interaction with negatively charged carboxylate residues along the PAA polymer chain that are readily accessible to soluble MB (69). Incorporation of MB was characterized by visible-range absorbance. PEMs assembled at pH 2.0/2.0 with a terminal layer of PAA show the most MB absorbance (~ 0.6 absorbance units a.u.), nearly three-fold greater than the next most-negatively charged PEM, pH 3.5/7.5 with a terminal layer of PAH (~ 0.2 a.u.) In contrast, pH 6.5/6.5 and pH 3.5/8.6 absorbance spectra are indistinguishable from background, which suggested very few unbound free acid groups. Hence, MB incorporation was thought to be an indication of the extent to which microbes were able to interact with local negative charges near the PEM surface. However, MB has been shown to bind as an aggregate at concentrations above $1 \mu\text{M}$ (101, 102), a threshold below which was insufficient to visualize $\text{COOH}_{\text{surface}}$ on any of the PEM samples. Thus, it was not possible to either accurately calibrate the binding ratio of MB dye to free COOH , nor correlate the relationship between a given absorbance value

and $[\text{COOH}]_{\text{surface}}$. Additionally, we could not rule out the possibility that MB carboxylate binding might occur by exchange with cationic PAH amine residues, and therefore may not assess net negative charge at all. That is to say, if MB adsorption on these PEMs occurs via cation exchange arising from differential affinity that favors MB binding to the oppositely charge PEM polyion, then the assumption of net PEM negativity becomes questionable. Moreover, MB absorbance for surfaces with low concentrations of unbound or freely-exchanging negative charge groups and surfaces with excess positively charged functional groups will be similarly low, making it impossible to discriminate between neutral and net positive interfaces. Finally, incubation in 0.15 mM NaCl PBS solution in excess of 30 seconds reduced the absorption spectra of all PAA/PAH PEMs to baseline, in stark contrast to some PEM absorption spectra incubated in Milli-Q water (e.g., PAA/PAH 2.0/2.0). SPM-enabled nanoindentation measurements were performed on PEMs incubated in Milli-Q water versus PEMs incubated in NaCl solution or PBS (Appendix A.4) to compare the mechanical stiffness of samples that demonstrated this reduction in absorption. However, no significant change in mechanical stiffness was observed for 2.0/2.0 PEMs used in this study when incubated in 0.15 mM NaCl or 0.15 mM PBS (NaCl within). Note that for assembly pH = 4.0/4.0, there was substantial batch variation in E across the samples measured (see Table A.4.1 for a complete list of stiffness measurement values). Such variation was often observed for individual indentations (i.e., local mechanical properties) within given samples of the pH = 4.0/4.0 PEMs, though the

reasons were never identified. Nevertheless, it was subsequently decided that pH 4.0/4.0 PEMs should be abandoned in favor of alternate PEM samples, pH = 3.5/7.5 and pH = 3.5/8.6, (see Chapter 5).

Comparison of the relative electrostatic repulsion at the fluid-PEM interface was carried out using a technique developed by Dean et al. to model electrostatic forces in glycosaminoglycan brush arrays (103, 104). Force-distance curves were first acquired via SPM force spectroscopy, in deionized water using a test surface comprising of mercapto-undecanoic acid (MUA) functionalized gold surface (105) with calibrated charge density (103, 104) of $Q = -18 \text{ mC/m}^2$, from which the surface charge density of the colloidal probe was calculated using models adapted from Rixman et al. (103, 104). This MUA surface was prepared by Dr. A. Jackson (105). Force-distance curves were acquired for experimental samples in deionized water (ionic strength $I = 0.0027$) or 0.1 M NaCl ($I = 0.1$) after an overnight thermal equilibration of the surface and cantilevered probe in fluid within the AFM. The maximum deflection of the cantilever on approach to the sample surface was maintained constant via the previously described closed-loop algorithm standard to the MFP 3D controller. All sample locations were measured a minimum of twenty times per approach cycle, over 5-10 locations per surface.

Curves representative of the data set were generated by alignment of the contact point, defined as the beginning of the region of constant compliance, followed by statistical averaging of the respective force and separation curves for a given approach cycle. The resultant curve for each surface location was the

average force detected by the average approach vector normal to the sample surface. Measurements that did not possess a region of constant compliance were zeroed by examining for either a jump-to-contact region, followed immediately by cantilever deflection; or, for data acquired in $I = 0.1$ M solvent, comparisons to data acquired in Milli-Q water at the same distance from the surface to determine where physical deflection occurred. Representative curves were then used for modeling the electrostatic surface charge density to a distance within 5 nm of the calculated contact point, and surface charge density calculated from a least squares fit of the model to the data (103, 104). Further discussion of this technique and its relevance to the PEM-bacterial adhesion event is discussed in Chapter 5.

2.7 Summary

This chapter describes the motivation for using polyelectrolyte multilayers and some of the characterizations relevant to the studies that follow in Chapter 3-5.

SPM-enabled nanoindentation was used to quantify the mechanical stiffness of PEM substrata, and the results of this quantification are described in each cell study. This characterization was the first demonstration of a mechanically tunable thin film that did not use covalent chemical modification or result in significant alteration of the chemical composition, to achieve a wide range of stiffnesses.

In subsequent chapters, the notation for assembled PEMs was chosen to simplify the presentation of the critical results of the experiments in regard to specific features of the PEM/-cell interaction. To that end, each chapter in this thesis utilizes PEM nomenclature adopted to place emphasis on the net mechanical or chemical properties highlighted in the material-cell interaction, rather than on the specific assembled PEM system. Furthermore, the nomenclature remains consistent with its use in each corresponding publication. This allows the reader to directly relate the PEM nomenclature in each chapter to that of the corresponding publication.

Additionally, as the technique for analysis of the PEM film characterization evolved over time, it should be noted that such evolution of the analysis techniques never resulted in contradictory measurements of mechanical stiffness. Rather, later studies reinforced previous findings and assisted in reducing statistical error among data replicates and between different PEM samples.

Establishing a robust material system to probe cell anchorage behavior as a function was a critical step in the development of this body of work. Subsequent chapters present the results of our exploration of the PEM interactions for both eukaryotic and prokaryotic cell types. In the next chapter, the initial mechanical characterization of PAA/PAH films is described, along with eukaryotic cell studies that establish that adhesion of endothelial cells correlates with quantifiable differences in substrata stiffness E .

CHAPTER 3 PHYSICOCHEMICAL CONTROL OF HMVEC ADHESION TO POLYELECTROLYTE MULTILAYERS

Note: The contents of this chapter were previously published in Biomaterials. Dec 2005;26(34):6836-6845, and includes the work of co-authors M.C. Berg, I.S. Tobias, M.F. Rubner , and K.J. Van Vliet.

3.1 Background and Motivation

3.1.1 Endothelial Cell Structures and Mechanoselective Behavior

The living, eukaryotic cell is an intricate sensor and actuator, responding dramatically to minute changes in external mechanical and biochemical environments. Though one may model the extracellular environment *in vitro* using experimental tools mechanical, chemical, and physical resolution and characterization, the extent to which such factors influence cell behavior and cellular group dynamics is not fully understood. Eukaryotic cell growth *in vivo* occurs under complex mechanical and chemical extracellular conditions. The types of physiologic stresses and strains eukaryotic cells experience depend upon factors such as cell type and associated organ; the physical location of the cell with respect to other tissue types of distinct mechanical properties; and possible

mechanical functions of the parent tissue or surrounding structures. For reasons described in Section 1.3, our model system for the mechanosensitive eukaryotic cell is the endothelial cell (or, EC; also called the vascular endothelial cell, or VEC, and used interchangeably throughout). Unlike the physiological support cells, such as vascular smooth muscle cells (VSMCs), endothelial cells do not regulate surrounding tissue tone directly through contraction, and this has a direct effect on the makeup of actin-myosin cytoskeletal networks found inside the EC (106, 107). Despite the fact that ECs do not exhibit muscle cell contractility, ECs nevertheless express many of the same regulatory and structural protein elements found in traditional muscle cells, such as tropomyosin and α -actinin (106, 107). Furthermore, the actin and myosin levels within ECs are intermediate to that of cardiac and skeletal muscle cell expression levels (106, 107). However, this is thought to be related to the diverse functional requirements of ECs: they must actively resist mechanical deformation from changes in vasomotor tone, shear stress from blood flow, mediate cell transmigration in leukocyte infiltration, migrate during angiogenesis and wound repair, and they must be able to rapidly reorganize intercellular contacts to regulate vascular-tissue permeability (106-111).

It is widely recognized that chemical and mechanical cues from the extracellular milieu are necessary for the maintenance of cellular homeostasis and the appropriate response to normal cell stimuli (3, 4). Vascular endothelial cells represent one important cell type which responds to both fluid flow-induced monotonic shear stress (12, 15, 16) and substrate-mediated cyclic radial

stress (17) through morphological reorganization and, ultimately, changes in phenotype or function. Additional stresses applied to or by ECs under physiological conditions include cyclic strain from stretching/contraction processes; fluid or semi-fluid shear stress from flow based processes; stress from cell migratory processes, which involve a careful balance of forces derived from cell protrusions with those derived from opposing and cooperative adhesive interactions (5); and, in non-motile ECs, anchorage dependent stress arising from the cell-cell adhesion that occurs between neighboring partners.

Epithelial-class cells experience lateral tension from cell-cell adhesion at specially configured intercellular (IC) junctions. This tension differs from that associated with another class of macromolecular structures called focal adhesions and focal contacts, the contacts between membrane embedded structures and the basement membrane (BM) (see Section 3.1.2). IC junctions consist of extracellular contacts between special Ca^{++} -dependent adhesion molecules called cadherins present on each cell surface (107). Additional adhesion molecules, platelet-endothelial cell adhesion molecules (PECAMs), form a second network of contacts and are specific to ECs and platelet cells. The cadherins are membrane spanning adhesion molecules anchored via a trimeric complex of α , β , and γ -catenin to α -actin and special junctional actin fibers. Junctional actin fibers arrange in hoop-like structure around the periphery of the cell, in-plane with the EC monolayer and approximately parallel to the basement membrane (107). This ring-like actin network serves as a mechanically supportive (MS) contact with adjacent cells, in

that it resists the deformation by forces from the neighbor cells and general mechanical forces that occur during normal vascular function (106, 109, 112). A similar type of MS contact called a hemidesmosome is found at the interface of the cell and the basement membrane, but is anchored via glycoproteins called integrins through a different network of actin filament structures called stress fibers (Section 3.1.2) (106, 109, 112). The junctional network is also distinct from the cortical actin web, comprised of thin actin filaments that blanket the cytoplasmic side of the cell membrane and form intracellular membrane anchorage points via association with the protein fodrin (107, 110).

In addition to cytoskeletal mediated mechanical behavior, ion channels embedded within the endothelial cell membrane respond to mechanical force. Lateral tension related to cell-cell connections and that which arises during times of hypo- or hyper-osmotic challenge result in opening of the central channel pore, thereby allowing the influx of channel specific ions (13, 107, 113). Additionally, shear stress from fluid flow is a potent regulator of separate, mechanically active Ca^{++} ion channels located on the luminal side of the endothelial cell. Ion channels activated in this manner have been shown to participate in initiating the MAPK signal transduction cascade, in addition to other molecular signalling systems derived from mechanical perturbation of contacts on the basolateral side of the cell (13, 107, 113, 114).

3.1.2 Integrins as Mechanosensitive Mediators of Eukaryotic Cell Interactions in the Extracellular Environment

Eukaryotic cells form adhesive contacts with the extracellular environment via specific and non-specific molecular interactions with neighboring cells, and interactions with protein and proteoglycan molecules embedded in the extracellular matrix surrounding the cell. Polarized epithelial-type cells, which include the family of endothelial cell variants, interact with the matrix on the basolateral side of the cell, forming adhesive contacts with a collection of proteins and sugars collectively designated as the basement membrane (BM). This cell-BM interaction forms the basis for cellular adhesion in the direction orthogonal to luminal or extra-luminal tissue structures. As described in Section 3.1.1, lateral connectivity is achieved via cell-cell contacts.

Specific cell receptors, termed integrins, are embedded in the EC membrane within distinct lipid domains and mediate the adhesion of cells to the BM (115). Integrins have been shown to participate in intracellular and extracellular signaling processes in addition to their role in adhesion, thus establishing them as important molecules in the overall homeostasis of the cell (8, 9, 115). In this regard, integrins are responsible for the integration of signals outside traveling into the cell, and conversely inward signals being communicated to the exterior of the cell. This is sometimes referred to as “inside-out, outside-in” signaling (111, 116).

Integrins are a class of membrane embedded tyrosine kinases, proteins that utilize tyrosine isomers to transfer or accept inorganic phosphate as part of the mechanism of cellular signal transduction. Comprised of an alpha unit and a beta unit that combine non-covalently to form heterodimeric protein complexes, integrins span the cellular membrane, thereby creating a direct link from the inside of the cell to the outside environment. Certain bacterial cells have similar molecular-scale structures linking the cytoplasmic region to the ectoplasmic region, but it is not generally the case that they mimic integrin function (Section 5.1). Integrins are modular structures, in that each alpha and beta subunit has molecular variants with variable affinity of interaction in the dimer, and differing specificity with the proteins present in the extracellular milieu. There are 18 known alpha subunits and 8 beta subunits, each capable of pairing with a member of the opposite heterodimeric partner to form an integrin with distinct ligand specificity (115). This results in a broad range of molecular ligands capable of binding with specificity to integrin receptors. For example, variants of both the alpha and beta subunit combine to interact with the extracellular protein fibronectin (integrin $\alpha_v\beta_3$) during early stages of wound repair, and are replaced in late stages by yet another variant complex (integrin $\alpha_2\beta_1$) as collagen levels increase in fresh tissue deposits (117-119). When one considers that co-receptors may further modify binding for integrin mediated ligand-receptor interaction the diverse profile of molecular interactions becomes exceedingly high.

The cytoplasmic integrin tail associates with a number of proteins, many of which are bound directly to the actin-myosin cytoskeletal structures known as stress fibers (8, 107, 110, 115). Integrins form direct linkages with a vast number of cytoskeletal associated proteins such as paxillin; filamin; α -actinin; and the linkage pair vinculin and talin, which are crosslinked to actin filaments by the vinculin-binding protein tensin (110, 115).

Focal adhesion kinase (FAK) also associates with the tail end of the integrin β -chain. Together with paxillin and the protein Src (oncogenic tyrosine kinase, sarcoma), a trimeric complex is established representing the major interacting partner of integrins located in the macromolecular ECM anchoring structure known as a focal adhesion (FA) (110, 115). Focal adhesions are found across the basolateral side of the EC, and are linked in the cytoplasm by stress fibers of composed of filamentous actin complexed with myosin light chains. As with junctional actin rings, the protein α -actinin anchors the stress fiber to the endoplasmic side via crosslinking with the trimeric vinculin-tensin-talin complex. The complexation of Src and FAK with integrins represents a significant aspect of the phenotypic changes observed with EC mechanical stimulation. FAK and Src interact via SRC-homology (SH) domains found in the cytoplasmic tail (SH₂ and SH₃), and are sensitive to acute changes in the phosphorylation state of the integrin tail (SH₂) or twists in the proline-rich regions of the SH₃ domain (8, 9, 110,

115). Both FAK and Src feed interact with the Rho-Gtpase protein Rac, a key regulator of cytoskeletal actin organization.

A variety of stimuli are capable of activating integrins, but unlike traditional receptor tyrosine kinases the molecular recognition event is not as important as the physical and mechanical aspect of the binding partners. Each integrin is capable of binding an extracellular molecular partner, with the molecular binding site preferentially binding peptides containing the amino acid trimeric leader sequences Arg-Gly-Asp, or RGD (8, 115, 120). It is widely known that most extracellular mechanical forces or in-plane membrane forces that cause a deformation or translocation of integrins results in phenotypic change. Integrins activated signaling cascades are known to initiate from physical deformation (32, 121-123), translocation within membrane domains, or crosslinking by biological or chemical means (e.g., mitogens, phorbol ester crosslinking) (8, 9, 115, 124). The associations with members of the Rho-GTPase protein family described above are integral in the activation of signaling cascades (MAPK, ERK, MEK) leading to whole cell reorganization or cell migration. The RGD-mediated attachment of eukaryotic fibroblast cells is explored in more detail in Ch. 4.

3.1.3 Cellular Response to Substrata Stiffness

A distinct but important approach to the mechanical modulation of cell function is through manipulation of the mechanical properties of the underlying substrate, as

is critical in the development of tissue engineering scaffolds. The mechanical compliance of cell substrata affects acquisition of specific cell functions *in vivo* and *in vitro*. For example, *in vivo* studies have shown that cardiac trauma concurrent with significant local decreases in cardiac tissue compliance can cause smooth muscle cells to secrete bone minerals typically produced by osteoblasts (125). Additionally, *in vitro* studies have shown that the motility of and contractile forces generated by fibroblasts, the chief cellular components of scar tissue, can be directed by varying the nominal mechanical compliance of the underlying poly(acrylamide)-based bulk hydrogel substrata (36). However, as it is well known that soluble and substrata-bound biochemicals also strongly affect cell function, it has been difficult to decouple the mechanical and chemical cues of cell response within a single experimental system. This complexity is due chiefly to two factors: (1) There are few materials which can be assembled to vary mechanical properties over a significant range without significant modulation of the polymer chemistry, e.g., addition of chemical crosslinking agents; (2) There exist few approaches to quantify the mechanical properties of such materials within aqueous environments that parallel *in vitro* conditions. Indeed, our limited capacity to deconvolute effects of mechanical and biochemical stimuli on cell phenotype is underscored by the introduction of combinatorial chemistry approaches whereby hundreds of distinct biopolymer compositions are rapidly screened to identify suitable substrates for directed stem cell differentiation (41).

In this study, we utilize weak PAA/PAH polyelectrolyte multilayers, and show that the PEM mechanical properties can be controlled directly through modulation of the component solution pH during PEM assembly. Polyelectrolyte multilayers are named as such due to the layer-by-layer (LbL) method of assembly described in Section 2.2, and are in fact interpenetrating networks rather than mesoscopic/macrosopic layers. These materials naturally form ionic crosslinks between polyanions and polycations during PEM assembly. The degree of ionic crosslinking for a given polyanion/polycation pair increases as assembly pH approaches neutrality. Thus, the extent to which the PEM swells in aqueous environments decreases as assembly pH approaches neutrality. Nanoscale poly(acrylic acid)/poly(allyl amine hydrochloride) PAA/PAH PEM films (thickness $h < 50$ nm) have been reported previously to affect fibroblast and hepatocyte adhesion as a function of assembly pH and in proportion to PEM swellability (40, 41, 47, 70, 71, 75). Although the extent to which PEMs swell would be expected intuitively to scale with the mechanical compliance of the polymer, systematic mechanical characterization of adhered, hydrated PEM films of thickness < 1 μm has not been reported and thus cannot be correlated with mechanical properties of biological cell substrata. Thus, our objectives herein were to (1) characterize systematically the nominal elastic moduli E_s of thin ($h \leq 200$ nm) PEM substrata in aqueous environments; and (2) to correlate E_s with the adhesion and proliferation of human microvascular endothelial cells (MVECs) through independent variation of E_s and PEM surface chemistry. The capacity to quantify local deformation of

polymeric films in aqueous environments through adaptations of nanoindentation in scanning probe microscopes, or SPMs, (42, 47, 49, 50, 52, 55, 56) is a promising approach to such quantification, provided that the complexity of multiaxial contact deformation in viscoelastoplastic substrata is considered carefully. Although SPM-enabled nanoindentation has been recently applied to estimate E_s of several hydrated PEM systems of μm -scale film thickness (42, 47, 49, 50, 52, 126) and of hydrated PEM microcapsules of nm-scale wall thickness (57, 127-130), this study quantifies the nanoindentation-measured E_s of hydrated, nm-scale PEMs in relation to adherent cell response.

3.2 Materials and Methods

3.2.1 PEM Assembly and Materials

Poly(acrylic acid) (PAA, Polysciences), poly(acrylamide) (PAAm, Polysciences), and poly(allylamine hydrochloride) (PAH, Sigma-Aldrich), were used to assemble PAA/PAH and PAA/PAAm polyelectrolyte multilayers (PEMs) as described previously (40, 41, 47, 70-72, 75). Briefly, dilute solutions of polyelectrolytes (0.01 M) were prepared in deionized water (Milli-Q, 18 M Ω /cm), and adjusted to pH = 2.0, 4.0, or 6.5 using HCl or NaOH. A layer-by-layer (LbL) dipping technique was employed to coat 35 mm-diameter and 60 mm-diameter tissue culture-treated polystyrene Petri dishes (TCPS, Becton Dickinson, Franklin Lakes, NJ) with alternating layers of PAA and PAH adjusted to the same pH, resulting in ionically

crosslinked PEMs. PEM samples are typically described in the literature by the cation/anion pair and assembly pH for each polyelectrolyte, e.g., PAA/PAH 2.0/2.0. To be consistent with such notation and further indicate the identity of polyelectrolyte added last, we denote the terminal polyion in bold type. Thus, a PAA/PAH PEM assembled at pH = 2.0 for both polyelectrolytes with a final layer of PAA is designated as **PAA**/PAH 2.0/2.0. The number of layers was varied to obtain a uniform dry (unhydrated) thickness $h = 40$ nm for PAA/PAH PEMs assembled at pH = 2.0 (20 layers or 10 bilayers), pH = 4.0 (16 layers), and pH = 6.5 (100 layers), with one additional layer thickness for PAH-terminated PEMs (69). Unmodified TCPS and PAA/PAAm PEM (6 layers at pH = 3.0, thermally covalently crosslinked at 95°C for 8 h) served as established, positive and negative controls for cell attachment, respectively (47, 72). Hydrated PEM thickness ranged from ~60 nm (pH = 6.5) to ~200 nm (pH = 2.0), as confirmed previously through in situ ellipsometry and atomic force microscopy (40, 47, 69-71).

3.2.2 Mechanical Testing and Data Analysis of PAA/PAH Multilayers

Nanoindentation on all PEM samples was performed as described in chapter 2 (Ch. 2.4-2.5). Force-displacement ($P-\Delta$) responses were recorded in fluid (filtered 150 mM NaCl phosphate buffered saline; 275 mOsm, pH = 7.4) at a velocity of 2 $\mu\text{m}/\text{sec}$ to a maximum cantilever deflection δ of <50 nm. Upon thermal equilibration of the experimental system, $P-\Delta$ responses were recorded at distinct positions on

the substrate surface, such that each response was generated at a different location. Mechanical output was analyzed offline using the scientific computing software IGOR (Wavemetrics, Lake Oswego, OR) as described in Chapter 2.

3.2.3 Cell Culture, Attachment and Proliferation Assays

Human dermal microvascular endothelial cells (MVEC, Cambrex Bioscience) were maintained at 37°C under 5% CO₂ in vented T75 flasks containing endothelial basal medium (EBM-2, Clonetics) supplemented by 2% fetal bovine serum as well as growth factors and antibiotics (EGM-2, Clonetics). The osmolality and pH of this media (275 mOsm; pH 7.6) is quantitatively similar to that of 150 mM PBS (276 mOsm; pH 7.4) used in nanomechanical characterization of the substrata discussed in Section 2.3 (131). Cells were passaged every seven days, with total media exchange every 48 hours. Cells used in experiments were harvested at passages 3 - 5.

Cell assays were carried out in 35 mm-diameter tissue culture-treated polystyrene Petri dishes (Becton Dickinson) coated with either PAA- or PAH-topped PEMS (for clarity, denoted in this Chapter by **PAA/PAH** or **PAA/PAH**, respectively) at assembly pH = 2.0, 4.0, or 6.5 as indicated. Prior to cell seeding, all surfaces were sterilized with 70% ethanol (EtOH) in a sterile field for 1 hour; UV sterilization was avoided to prevent any photo-crosslinking that might alter the mechanical compliance of the substrata.

Cells were freshly cleaved from T75 flasks through trypsinization, and directly seeded in triplicate at a cell density of 84,000 cells/35 mm-diameter dish. Total media exchange was conducted every 48 hours, and digital images were acquired daily to monitor attachment and growth within a single $2\ \mu\text{m} \times 2\ \mu\text{m}$ region of each sample. Cells were harvested from the PEMs at day 7 post-seeding. Each sample group was cleaved individually to ensure approximately equal duration of exposure to the trypsin/EDTA cleaving agent. Cells were stained (1 neutralized cell suspension: 1 trypan blue) prior to hemacytometric counting to assess total cell number at day 7. In order to assess the effects of mechanical compliance and terminal polyelectrolyte layer on initial cell attachment and subsequent cell proliferation, we determined cell density as a function of days in culture through inverted optical light microscopy (OM200, Leica) digital image acquisition and analysis of the same $6.25\ \text{mm}^2$ section of the PEM samples every 24 h up to day 6.

3.3 Results and Discussion

3.3.1 Effect of Multilayer Assembly pH on Mechanical Compliance

Nanoindentation of fully hydrated PAA/PAH and PAA/PAAm multilayers was conducted to quantify the mechanical compliance of these PEMs in terms of E_s . Figure 3.1 shows that E_s varied significantly as a function of assembly pH, but does not vary to a statistically significant extent as a function of the last polyelectrolyte layer added (PAA or PAH). E_s increased by several orders of magnitude in direct

correlation to the increase of PEM assembly pH, consistent with a model of increased interchain ionic crosslinking (69, 132). Although large deviations occurred in E_s values for PAA/PAH 4.0/4.0, these were indicative of the effect of thermal fluctuations during mechanical testing of hydrated polymers in fluid, and the differences among PEMs assembled at varying pH were significantly greater than this deviation. Thus, the nominal indentation elastic modulus E_s of the hydrated PAA/PAH system of nm-scale thickness can be

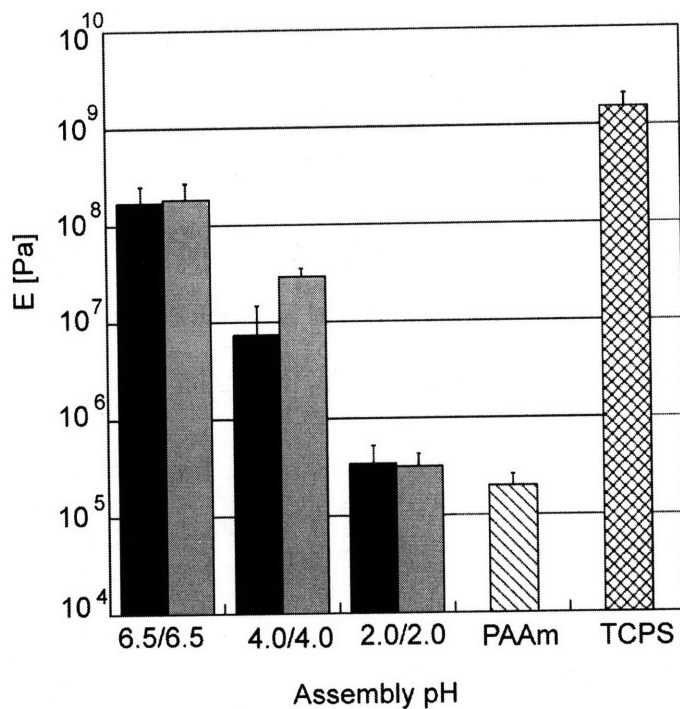


Figure 3.1 Indentation elastic modulus E_s as a function of assembly pH of polyanion and polycation solutions, pH = 6.5, 4.0, and 2.0 The terminal or top layer of the PEM is indicated as polyanion PAA (solid black) or polycation PAH (solid gray). Polyacrylamide multilayers (PAAm, striped) and polystyrene (TCPS, cross-hatched) are shown for reference, and used as negative and positive controls, respectively. Standard deviation is shown for each sample ($n = 15$).

modulated significantly via the solution pH at which the multilayer is assembled, and the resulting mechanical compliance of the PEM is independent of the outermost (PAA or PAH) layer.

These PEMs were assembled under salt-free conditions in aqueous solutions (see Section 2.2), and can then be used in the hydrated state (with water or buffered salt solutions) or

dried and then rehydrated for later use. Although mechanical characterization was conducted in PBS and cell assays were conducted in cell culture media, the close correspondence of osmolality and pH in these two solutions indicates that PEM compliance will not differ with respect to solution choice. In separate studies, it has been found that no quantitative difference in compliance of these PEMs in PBS or cell culture media over several days in solution.

3.3.2 Effect of Substrate Compliance and Assembly pH on Cell Attachment and Proliferation

Human microvascular endothelial cells (MVECs) were cultured over a seven day period on PAA/PAH multilayers to elucidate whether attachment and proliferation of MVECs correlated with the observed differences in mechanical compliance of the substrates. Cell density (viable cells/mm² of available substrate) at day 7 is shown in Fig. 3.2. A clear correlation between the cell density and E_s can be observed: Cell density at day 7 post-seeding increases as the compliance of the multilayer decreases. Clearly, PEMs assembled at pH = 6.5 were the least compliant PEMs ($E_s = 153 \pm 70$ MPa) and exhibited cell densities consistent with or exceeding that of tissue culture treated polystyrene (TCPS), regardless of the terminal polyion. These data indicated slightly more than a single population doubling for PAH-terminal PEMs at assembly pH = 6.5; less than one population doubling for PAH-terminal PEMs at assembly pH = 4.0 (78% increase in total cell

number) and TCPS (55% increase in total cell number); and a 40% decrease with respect to seeded cell number for PAH-terminal PEMs at assembly pH = 2.0. Consistent with previous reports (40, 47, 70, 71), PAA/PAAm multilayers showed zero cells attached at day 7 post-seeding and were considered a negative control for cell-substratum adhesion. The difference in cell density between PAH-terminal and PAA-terminal multilayers was quantitatively repeatable.

Although the mechanical compliance is not strongly affected by the terminal PEM layer, in general the chemical interface is altered modestly to exhibit either excess carboxylate (PAA) or excess amine (PAH) functionality of the terminal layer at near-neutral pH. That is, PAA-terminal PEMs should generally exhibit uncompensated negative surface charges at pH ~ 7, whereas PAH-terminal PEMs should generally exhibit uncompensated positive surface charges. However, this is an oversimplification, as the amount of uncompensated surface charge is also related to the pH-dependent degree of ionic crosslinking and is less pronounced for lower assembly pH. Furthermore, previous studies of these particular PEMs by Mendelsohn et al., demonstrated that protein adsorption of cell adhesion promoting and cell-adhesion neutral proteins to these PEMs could not account for differences observed in cell-multilayer interactions (40). Therefore, it can reasonably be concluded that the observed adhesion trends are not due to differential adsorption of cell adhesive proteins or a conditioning film that promoting adhesion to the stiff 6.5/6.5 films relative to the compliant 2.0/2.0 films.

Therefore, assembly pH of PAA/PAH PEMs modulates both mechanical compliance and cell density over extended *in vitro* timescales, while the terminal polyelectrolyte layer modestly affects cell initial cell attachment independently of substrata mechanical compliance. In order to assess whether the inverse correlation between substratum compliance and cells harvested via trypsination at day 7 was

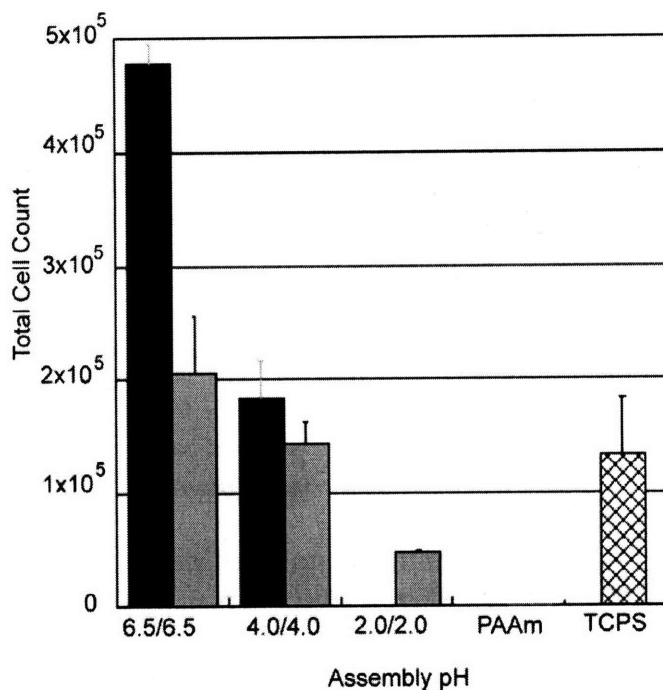


Figure 3.2 Total number of cells harvested from 60 mm-diameter Petri dishes at seven days post-seeding, as a function of PEM assembly pH The terminal or top layer of the PEM indicated as polyanion PAA (solid black) or polycation (solid gray). Polyacrylamide multilayers (PAAm) and polystyrene (TCPS) are negative and positive controls of cell attachment, respectively. Standard deviation is indicated for each sample ($n = 3$).

attributable to differences in cell attachment, cell proliferation, or both, a single region of each sample was observed via optical microscopy over each day in culture. Figure 3.3 shows MVEC density (number of cells /mm² substratum) as a function of time *in vitro* for a single 6.25 mm² area ($n = 3$ for each condition) for PAH-terminated PEMs. These data represented cells that appeared to be well-

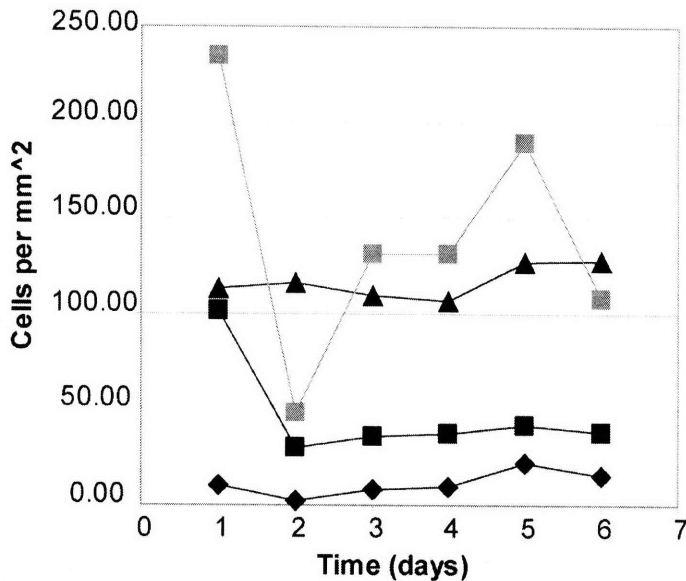


Figure 3.3 Spatial density of cells attached as a function of days in culture Cell density measured through optical imaging analysis of a specific area of 6.25 mm^2 for each sample. Cells seeded at $84,000 \text{ cells/sample}$ or $\sim 30 \text{ cells/mm}^2$ if uniform density assumed. Sample legend: PAA/PAH 2.0/2.0 (black diamond); 4.0/4.0 (black square); 6.5/6.5 (black triangle); and tissue culture polystyrene (gray square).

extended time periods. At 1 day post-seeding, MVEC density was inversely related to PEM compliance, indicating that initial cell adhesion to the substratum was directly related to E_s . MVEC density decreased for most samples upon full media exchange at day 2 (via vacuum aspiration), due presumably to poor adhesion between the nominally attached cells and substrata (and, to a lesser extent, normal detachment during cell division) in this specific region of the sample. Note that MVEC density on PAA/PAH 6.5/6.5 did not decrease upon media exchange, indicating strong cell attachment in the observed region of the sample. The

attached to the substrate and distinct from rounded or fully detached cells, as assessed via optical microscopy. Admittedly, this quantification of cell adhesion is less rigorous than trypsinization and counting of an entire sample after a fixed number of hours in vitro, but enabled observation of the same specific region of the sample over

increase in MVEC density over days *in vitro* was not a strong function of E_s . That is, the number of cells observed within the same specific area of the substratum over time correlated closely with that observed upon the first full media exchange, indicating essentially no proliferation of the cells in the observed region, regardless of assembly pH. Therefore, one cannot conclude that E modulates proliferation under these conditions. Although the observed region in Fig. 3.3 represents <1% of the total substratum area in each sample and thus may not correlate quantitatively with population doublings demonstrated in Fig. 3.2, this observation is consistent with the mild increase in total cells harvested at day 7 with respect to seeded cell number. Similar trends regarding the number of cells per unit area over days *in vitro* were observed for PAA-terminated PEMs, which showed greater cell attachment over the course of the seven-day observation than PAH-terminated PEMs for pH > 2.0. However, it should be noted that a true proliferation assay was not performed in this series of experiments. Performing a proliferation assay may provide a more detailed and quantitative assessment of the affect that E has on the population expansion of MVECs.

As noted above, we did not quantify nor control the extent of amine and carboxyl functional groups on the PEM surfaces as a function of terminal layers and assembly pH. Thus, these data demonstrate only that MVEC growth on these PEM substrata depends both on mechanical compliance and surface chemistry, and do not clarify how general amine/carboxyl functionality affects cell attachment for a given substratum compliance.

The direct measurement of mechanical compliance for hydrated polyelectrolyte multilayers of nanoscale thickness in fluid allows us to correlate qualitative concepts of macromolecular structure with quantitative mechanical properties that can be compared, modulated, and correlated with cell response. For example, it is well established that the percent swelling of PAA/PAH PEMs increases as assembly pH departs from neutrality (40, 47, 70, 71), yet it is difficult to characterize and design materials based upon percent swelling. However, current models hold that changes in percent swelling are a consequence of increasing or decreasing the number of ionic interchain PEM crosslinks, and it is generally known that modulation of crosslinking is a determinant of substrata mechanical properties. Although the effect of these different PEM materials on cell attachment has been demonstrated previously for both fibroblasts (40, 47, 70, 71) and hepatocytes (70), the approach presented herein facilitates quantitative comparison of the mechanical environment to which the cells are subjected, independently of the biochemical environment and in direct relation to other potential substratum materials such as TCPS.

3.3.3 Limits of Nanoindentation Experiments and Analysis

Although few alternatives exist for experimentally measuring mechanical properties of hydrated polymeric substrata of nm-scale thickness, it is important to note several limitations of this method. These limitations include idealizations of the

mechanical contact problem, the finite thickness of the PEM, and the mechanical behavior of polymers.

Hertzian contact mechanics analysis is typically invoked to estimate Young's elastic modulus E_s from the spherical nanoindentation response. Hertzian contact includes several assumptions regarding dimensions of the indenter and the indented material; the technical limitations of this analysis in the context of scanning probe microscope-enabled indentation are summarized in Section 2.3. In the present experiments, we applied this analysis by (1) idealizing the nominally sharp probe as spherical at its apex; and (2) restricting our analysis to indentation depths $\Delta < 20$ nm, the depth to which this spherical approximation would hold and to which the finite thickness of the PEM could be reasonably neglected. Alternatively, commercially available spherical beads for which micron-scale radii are well-known can be attached to the cantilevered probe, thus reducing the nominal stress σ and strain ε for a given P while concurrently reducing the spatial resolution of the tested area (55). Agreement between (film thickness-corrected) Hertzian analysis of cones and spheres result in similar magnitudes of E_s for micron-scale hydrogels (42, 49, 50, 52).

An equally important limitation of Hertzian analysis in the present context is that hydrated PEMs are likely best considered as viscoelastic materials over timescales relevant to cell processes, whereas we have neglected rate effects in our characterization of PEM mechanical compliance. We have confirmed that, for a

fixed displacement rate of 2 $\mu\text{m/s}$ and for $\Delta < \Delta_c$, neither the P - Δ response nor the calculated E_s are a function of maximum load P . This indicates that these PEMs are linearly elastic at this loading rate and range of applied strain, but does not rule out the possibility that they are viscoelastic. We did not explore the effects of displacement rate (nominal strain rate) on the mechanical response of these PEMs. However, it is reasonable to assume that time-dependent deformation does not significantly affect cell attachment and proliferation processes that occur over a timescale of days.

Despite these constraints, it is instructive and encouraging to note that the calculated average value of E_s obtained for tissue culture polystyrene, obtained without curve fitting or selective analysis of specific data sets, was ~ 8 GPa, which corresponds reasonably well with literature values of E that range from 2.3 - 3.4 GPa for bulk (mm-scale thickness) polystyrene under uniaxial loading (133). Further, Pavor et al. have reported E_s for a similar PEM system (PAA/PAH 7.5/3.5 with hydrated thickness $h = 500$ nm), as determined by instrumented nanoindentation with a sharp diamond probe (134). Although the technical limitations of instrumented nanoindentation preclude analysis of significantly thinner, hydrated PEM films, these authors found $E_s = 70$ MPa, in reasonable agreement with our results for PAA/PAH 6.5/6.5 ($E_s = 150$ MPa).

Furthermore, reports that estimate elastic moduli for a different PEM of nm-scale thickness (sulfonated poly(styrene) SPS/PAH, $h = 20$ nm) through continuum

analysis of PEM microcapsule swelling indicate $E = 130 - 170$ MPa (127-130), although AFM indentation of hydrated microcapsules indicate $E = 1.3 - 1.9$ GPa (57). As both SPS and PAH are fully charged upon assembly of the SPS/PAH multilayer, this PEM is most similar to the PAA/PAH 6.5/6.5 system discussed herein. Although the microcapsule experiments differ in that the PEM microcapsule is not adhered to a rigid substrate and is deformed under osmotic pressure, these results are also consistent with our findings for PAA/PAH 6.5/6.5, and suggests that the nominal elastic properties of these nanoscale PEMs can approach those of elastomers.

In addition to the above mechanical characterization of nm-scale PEMs, others have employed SPM-enabled nanoindentation to characterize PEMs of μm -scale thickness. Although variations among PEM thickness, constituents, and assembly pH complicate direct comparison of results, μm -scale PEMs characterized in this manner over the same displacement rates appear to exhibit E_s ranging 10^3 to 10^7 Pa, or at least two orders of magnitude more compliant than the nm-scale PAA/PAH PEMs considered in the present study. For PAH/azobenzene-containing polyelectrolyte PEMs ($h = 1.1 \mu\text{m}$, pH = 5.0 to 10.5), Mermut et al. have reported that E_s ranges 100 kPa to 10 MPa, with E_s decreasing with increasing assembly pH for this polyion pairing (for pH > 5.0). Although Mermut et al. demonstrated a nonlinear decrease in E_s with increasing assembly pH, E_s for this PEM at pH = 6.5 can be interpolated as ~ 4 MPa, whereas we find $E_s \sim 150$ MPa for nm-scale

PAA/PAH PEMs assembled at pH = 6.5. For PAH/hyaluronic acid PEMs of thickness ranging 4 to 14 μm , Engler et al. have found that $E_s < 1 \text{ MPa}$ (ranging 40 to 300 kPa, with and without addition of a chemical crosslinker, respectively) (42, 47, 49, 50, 52).

In summary, the literature includes SPM-enabled nanoindentation measurements of chemically distinct, μm -scale PEMs that are considerably more compliant than the nm-scale weak PEMs considered here. Although it is plausible that the molecular configurations and thus mechanical properties measured at PEM surfaces may be altered over orders-of-magnitude changes in sample thickness, positive correlation with alternative measurements of E in chemically similar PEMs indicates that the nature of the weak polyions and assembly conditions – not the significantly decreased sample thickness – are chiefly responsible for the observed values of E_s in the PAA/PAH PEMs. In this regard, our results are in good agreement with similar studies in which SPM-enabled nanoindentation was used to quantify substrata stiffness (51, 55, 57, 116, 135, 136)(53).

3.3.4 Effects of E_s on Cell Attachment and Proliferation

Together, Figs. 3.2 and 3.3 indicate that MVECs attach preferentially (and, as a population, proliferate mildly but more rapidly over 7 days *in vitro*) on PEMs of $E_s \sim$

150 MPa as compared to more and less compliant substrata. Thus, our observations are consistent with the concept that the mechanical compliance of substrata is at least as important as surface chemistry in determining whether and how cells will adhere and with subsequent proliferation *in vitro*. It should be noted that previous reports on other cell types and among various polyion combinations has demonstrated clearly that differences in cell attachment depend much more strongly on the swellability, here quantified as mechanical compliance in terms of E_s , than on details of PEM surface chemistry (40, 41, 47, 71, 75).

As E_s of the PEM system herein can be modulated from 10^5 to 10^8 Pa for a given PEM chemistry, it is possible to consider the unique effects of substrate compliance and interfacial chemistry on MVEC attachment and proliferation. Although our results indicate that the substrata terminal layers modestly affects the initial attachment and growth of MVECs, explanation of this intriguing result based on amine/carboxyl surface functionality is not straightforward due to the nature of the ionic crosslinking in these PEMs. However, it is clear that mechanical compliance of the substrata affects initial cell attachment more strongly than does the ionic character of the terminal layer, in that no MVECs remained attached to the PEM substrate over seven days for compliant **PAA/PAH 2.0/2.0** ($E_s \sim 400$ kPa) for which E_s was lower than that of **PAA/PAH 6.5/6.5** ($E_s \sim 150$ MPa) by several orders of magnitude. The nominal cell growth on **PAA/PAH 2.0/2.0** is consistent with that observed for hepatocytes (75, 137), and reflects the coupling between mechanical and biochemical environments in mammalian cell development.

3.5 Summary

The work described in this chapter demonstrates that it is possible to both measure and modulate the mechanical compliance of hydrated PEM substrata of nm-scale thickness, and to independently modulate the chemical functionality at the cell-substrate interface to regulate cell attachment and growth. Clearly, the mechanical compliance of the substrata strongly and independently affects the attachment of MVECs *in vitro*. These results are consistent with previous reports by Rubner et al., for cells grown on a suite of PEMs that included those described herein. Additionally, others have reported similar correlations between cell phenotype and mechanical compliance, also using PEMs characterized by nanoindentation (42, 49-51, 53).

Such nanoscale substrata are particularly relevant to cell studies for two reasons. First, the thickness and optical properties of these PEMs are amenable to advanced optical imaging approaches including epi-fluorescence. Secondly, this optical imaging capability is coupled with the mechanical tunability of the thin substrata, thereby facilitating quantitative correlation between mechanical environment and cell substructures critical to cell processes. Such processes include focal adhesion complex formation, characterization of cytoskeletal tension against the substrata, cell motility, and phenotypic differentiation. Thus, quantitative correlation of tunable substrata mechanical compliance with cell

response in these optically transparent, nm-thick materials enables future investigations of subcellular responses to mechanical cues, as well as of mechanically directed development of cell phenotypes for applications including tissue engineering.

It has long been held that changes in the chemical presentation of a cell adhesive surface can alter the relative cytophilic or cytophobic nature of a material interface (138). The results outlined in this chapter suggest the possibility that cytophobic or cytophilic properties of materials proposed to be mediated via chemical variation might also be strongly correlated with differences in underlying substrata mechanical features. The next chapter addresses the role that chemical functionalization of PEM surfaces plays in cell adhesion as the mechanical compliance of the underlying cell adhesive substrata is varied. Specifically, two different techniques for the alteration of PEM surface functionality are employed with differing effects on PEM mechanical compliance, and those modified thin films are used to probe chemical and mechanical effects on eukaryotic cell adhesion as orthogonal parameters.

CHAPTER 4 CHEMICAL AND MECHANICAL PROPERTIES AS INDEPENDENT MODULATORS OF CELL ADHESION

Note: The contents of this chapter were previously published in Biomacromolecules Jun 2006;7(6):1990-1995, and includes the work of co-authors M.C. Berg, I.S. Tobias, J.A. Lichter, M.F. Rubner, and K.J. Van Vliet.

4.1 Background and Motivation

4.1.1 Chemically and Mechanically Guided Cell Behavior

Surface functionalization to promote cellular adhesion to biomaterials used as cellular growth substrata is an important component of many biological research efforts and engineering applications. High resolution imaging of cytoskeletal substructure and dynamics is critically dependent on the ability to successfully immobilize cells through formation of tight adhesive contacts (139). In addition, *in vitro* culture of adherent cell types, whether for tissue engineering or cell biology studies, also depends on the quality and strength of adhesion events (3, 46, 140). In the field of medical implants, precise control of cellular attachment is necessary to prevent microbiological contamination and promote proper graft response, and this a topic of particular interest in the area of osteogenic implantable devices (141-143).

Indeed, interfacial biology is a well-developed and rich field, and many types of biointerfacial modifications exist to promote the attachment and proliferation of cells on given synthetic or biomacromolecular growth substrates (140). Techniques to induce phenotypic change and control spatial distribution in various cell types include alteration of surface topology (144) and/or degree of interchain crosslinking in a polymeric gel (36); creation of phase separated amphiphilic surfaces (145), and functionalization with cell resistant materials that restrict cell growth and enforce patterning (146). With increasing frequency, cytophilic surface modifications are employed via adsorption of extracellular matrix proteins or related derivatives onto a rigid or semi-rigid support to reconstitute aspects of the *in vivo* extracellular environment. One widely used approach involves the conjugation of proteins or peptides containing the sequence Arg-Gly-Asp (RGD), which recruits and binds to integrin receptors on the surfaces of eukaryotic cells (75, 118, 140, 147-150). This is particularly significant because differential integrin binding alters specific cellular behaviors such as differentiation in human umbilical vascular endothelial cells (141). Conversely, differential integrin expression is known to be an important marker of endothelial cell state during angiogenesis and capillary invasion during wound healing (117, 119).

4.1.2 Biomaterial Fabrication for Decoupling Chemistry and Mechanics in the Extracellular Space

Increasingly, polyelectrolyte multilayers (PEMs) are used as bioactive substrata for the study of cell adhesion or phenotype (40, 42, 49, 50, 52, 71, 75, 151-153). PEMs are polyelectrolyte complexes fabricated via a layer-by-layer (LbL) assembly process with dilute solutions of positively and negatively charged polymers, or by the LbL assembly of weakly interacting hydrogen bond acceptors/donors with polyelectrolyte polymers of complementary polarity. Because the physical properties and film thickness of weak (pH-sensitive) PEMs can be controlled with high precision through assembly conditions such as solution pH, these materials find utility in a range of applications including but not limited to cytophilic substrata and cytophobic coatings. Importantly, these materials effectively modulate cell behavior when assembled to only nanoscale thicknesses (46), and are thus amenable to high resolution optical imaging approaches desirable for a range of in vitro cell experiments. Berg et al. have demonstrated that the cytophobic properties of a PEM comprising polyacrylic acid (PAA) and polyacrylamide (PAAm) can be reversed via surface functionalization with RGD (75). The mechanism of such attachment is believed to be mediated by integrins, as described in Ch. 3.1.2. In such studies, it is assumed but not demonstrated that biochemical functionalization of such surfaces does not alter the mechanical properties of that surface, such that the mechanical and chemical characteristics of substrata can be modulated independently to evaluate cell response. That is, if surface modifications

such as RGD incorporation alter only the biochemical interface between the substrata and adhered cells, then cellular processes such as adhesion, spreading, proliferation, and differentiation on those surfaces could be attributed unambiguously to biochemical rather than mechanical characteristics of the substrata.

Chapter 3 demonstrated that mechanical compliance of nanoscale PEM films can be modulated directly via assembly conditions (46). For weak PEMs comprising PAA and poly(allylamine hydrochloride) or PAH, nominal elastic modulus E varies by orders of magnitude for mod-2 changes in assembly pH, due to the pH-dependent degree of ionic crosslinking that correlates inversely with the capacity to swell in aqueous solutions. Further, we showed that this mechanical compliance correlated directly with the capacity of mammalian (microvascular endothelial) cells to attach to and proliferate on unfunctionalized PEMs under *in vitro* culture (46), and others have demonstrated similar effects of mechanical compliance for other PEM or hydrogel systems on different adherent mammalian cell types (42, 49, 50, 52, 154). Additionally, Picart et al. demonstrated that surface functionalization of different PEMs with RGD, with or without intentional chemical crosslinking of the multilayers, could significantly affect the cellular attachment and proliferation of osteoblasts; mechanical compliance was not characterized for any of those PEMs (48, 155).

In light of these previous findings on biochemical and mechanical modulation of cell-substrate adhesion, here we sought to confirm that the mechanical properties of PEMs were unaffected by a particular biochemical surface functionalization process. To that end, we employed scanning probe microscope-enabled nanoindentation to measure the nominal elastic modulus E of PEMs functionalized through various processing routes with a synthetic peptide containing the integrin binding sequence RGD.

4.2 Materials and Methods

4.2.1 PEM Assembly and Materials

Films were assembled as previously described (Section 2.2)(40, 71, 72, 75). Briefly, dilute solutions (0.01 M) of PAA, PAAm, and PAH were prepared in deionized water and the solution pH adjusted to 3.0 using HCl. The multilayers were assembled on standard glass slides, silicon wafers, and in 60 mm-diameter polystyrene Petri dishes using an automated layer-by-layer dipping method. Each sample was assembled with one layer of PAH to promote strong adhesion of the PAA/PAAm PEM, followed by 5.5 bilayers of PAA/PAAm. Note that PAA/PAAm multilayers are formed via hydrogen bonding, not ionic crosslinking, at this pH. Thus, the PEMs were then covalently crosslinked, as required for stability at

neutral pH conditions required for cell culture, via elevated temperature in a vacuum oven (180°C, 2 h for glass and silicon, 90°C, overnight for polystyrene).

Surface-modified samples were assembled and prepared according as described in Section 2.2. Poly(acrylic acid) (PAA) (MW = 90 000; 25% aqueous solution) and polyacrylamide (PAAm) (MW = 5,000,000; 1% aqueous solution) were purchased from Polysciences. Poly(allylamine hydrochloride) (PAH) (MW = 70,000) was purchased from Sigma-Aldrich. Peptides GRGDSPC and GRGESPC were provided by the MIT Biopolymers Lab. Sulfosuccinimidyl 6-[3'-(2-pyridyldithio)-propionamido] hexanoate (Sulfo-LC-SPDP) was purchased from Pierce Biotechnology. Poly(dimethylsiloxane) (PDMS) stamps were made by M.C. Berg according to the previously described protocol (75).

4.2.2 Mechanical Testing and Data Analysis of PAA/PAA_m Multilayers

Scanning probe-enabled nanoindentation and offline analysis was performed as described in Section 2.3-2.4 using the 3D Molecular Force Probe (Asylum Research, Santa Barbara, CA) and IGOR (Wavemetrics), respectively. To ensure that indentation occurred at sites of PAH patterning in PMDS-stamped samples, the sample surface was first imaged in contact mode using the 3DMFP (90 μm x 90 μm), but force-displacement data were not acquired in the same region that was imaged; surface modulation due to contact imaging could thus be neglected in the

interpretation of mechanical experiments. Furthermore, multiple regions were tested over a sample area that spanned ~50% the total stamped region of the PEM. Finally, multiple samples of the PAH-stamped samples were tested on different days, to identify any sample-to-sample variations and systematic experimental errors.

4.2.3 PEM Film Thickness Measurement

In order to determine whether any experimentally observed differences in PEM mechanical compliance could be attributed to differences in hydrated film thickness t , separate hydrated samples were assembled on glass substrates and imaged via scanning probe microscopy (SPM) over regions including scratches through the complete sample thickness. Unmodified PAA/PAAm, PAA/PAAm/adsorbed PAH, PAA/PAAm/stamped PAH, and PAA/PAAm/stamped PAH/RGE PEMs of nanoscale thickness were prepared on glass slides as described above. Sample slides were cleaned by dipping in sterile 0.2 μm filtered PBS, rehydrated in PBS, and scratched with a standard razor blade. PEMs were imaged in contact mode (3DMFP) using a Si_3N_4 probe of $k = 0.06 \text{ N/m}$ over regions including the scratch site at both 0° and 90° scan angles. Height measurements were calculated by measuring ΔZ at six different randomly selected regions where,

$$\Delta Z = Z_{\text{PEM surface}} - Z_{\text{trough}} \quad (4.1)$$

Standard deviation of the mean sample height was significantly smaller than the associated error in the surface roughness across the trough in individual image cross-sections, which can be attributed to slight damage of the underlying glass substrate and/or limited residual PEM within the scratch trough. Root mean square (RMS) surface roughness was determined directly from contact images via 3DMFP IGOR subroutines. Average +/- standard deviation RMS roughness among six cross-sections within a given sample image is reported. In addition, in situ ellipsometry (ISE) was employed to validate SPM measurements of water-hydrated film thickness t for the same PEMs assembled on silicon substrates. ISE determines t as a function of changes in indices of refraction n measured via light reflected from the material surface, and samples mm²-scale surface areas (40).

4.2.4 Cell Attachment to Modified PEM Substrata

Murine NIH 3T3 fibroblasts were seeded at 40,000 cells/mL onto the following PAA/PAAm (6 bilayer) substrata in triplicate 3.5 cm-diameter wells of tissue culture polystyrene six-well plates (Corning): no further modification (null); 30 sec adsorption of PAH (PAH, adsorbed) or 30 sec stamp of PAH (PAH, stamped); 30 sec adsorption of PAH followed by conjugation of RGD (RGD, PAH adsorbed) or

dummy peptide RGE (RGE, PAH adsorbed). Cells were maintained at 37°C, 5%CO₂, then trypsinized and counted via hemacytometer as well as calibrated Alamar blue (Biosource) metabolic dye reduction at day 3.

4.3 Results and Discussion

4.3.1 Biochemical Functionalization of Polymeric Cell Substrata Can Alter Mechanical Compliance

Previous studies have demonstrated that, in the absence of surface functionalization with RGD, this PEM substrate is completely cytophobic to both hepatocytes and human microvascular endothelial cells (46, 75). However, using a patterned polymer-on-polymer stamping technique, Berg et al. demonstrated that PAH-stamping followed by covalent conjugation of RGD-containing peptides at the multilayer surface could switch the cytophobicity of PAA/PAAm to that of a cytophilic substrate in a RGD concentration-dependent manner (see Fig. 4.1). This response was not reproduced via conjugation of the dummy peptide sequence RGE or by stamping of PAH in the absence of any peptide sequence, and thus attributed to specific chemical interactions between this particular adhesive ligand and the mammalian cell surfaces (75).

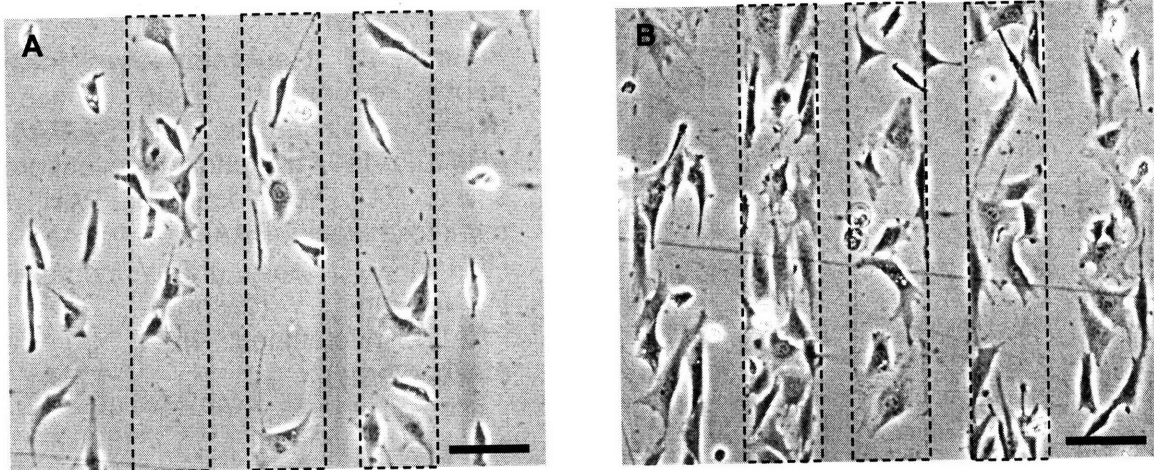


Figure 4.1 Wild-type NR6 fibroblast attachment as a function of RGD concentration PAA/PAH PEMs at 48 h post-seeding, where the PEM surface was modified via polymer-on-polymer stamping of PAH in a vertical line pattern (dashed rectangles show three representative linewidths) followed by RGD conjugation via a heterobifunctional crosslinker. Cells do not adhere as readily on PAA/PAAm PEM lines functionalized with low RGD concentrations of $\sim 53,000$ molecules/ μm^2 (A), but do adhere readily to the same PAA/PAAm lines functionalized with a higher RGD concentration of $152,000$ molecules/ μm^2 (B). Scalebars = $50 \mu\text{m}$. These materials, cell culture methods, and cell adhesion results are detailed in Ref. (75).

4.3.2 Effect of Surface Functionalization on Mechanical Compliance

To ascertain any changes in mechanical properties of these PEMs that such surface engineering may engender, instrumented nanoindentation was performed on samples representing each processing step during surface modification of PAA/PAAm with RGD or RGE. Representative $P - \Delta$ responses for each PEM sample are shown in Fig. 4.2, and nominal elastic moduli E calculated from such

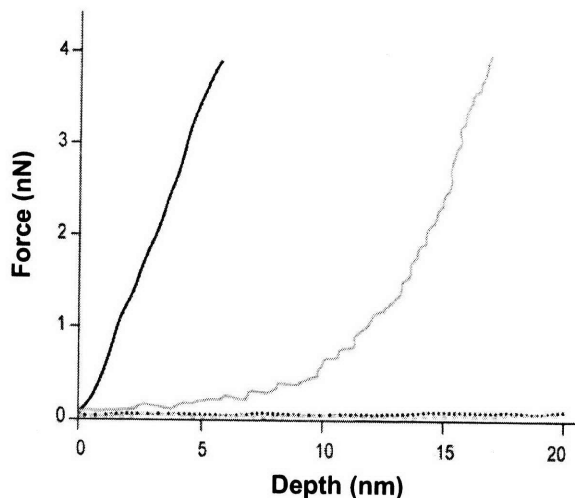


Figure 4.2 Representative force-depth responses Traces acquired during nanoindentation of PAA/PAAm PEMs in 150 mM phosphate buffered saline. PAA/PAAm/adsorbed PAH, 15 min (solid black); PAA/PAAm/adsorbed PAH + RGD (solid gray); unmodified PAA/PAAm (dashed black); PAA/PAAm/stamped PAH, 30 sec (dashed gray).

data are shown as a function of surface modification in Fig. 4.3. The unmodified PEM exhibits the lowest nominal E (2.4×10^5 Pa), consistent with the high swelling capacity and low crosslinking density of this PEM, as well as with previous mechanical analysis of this polymer film (46, 70, 71, 75). The second step in the process of surface engineering involves the addition of PAH as a base for conjugation of RGD. This can be readily accomplished by adsorption of the polymer chain from a dilute solution of PAH, or by polymer-on-polymer stamping as described by Berg et al.(75) Samples prepared with PAH according to this stamping protocol exhibited a slightly lower mean E with respect to the unmodified PEM (1.6×10^5 Pa); this difference was found to be within the margin of error of the nanoindentation approach. Although it is possible that subsequent conjugation of stamped PAH could unintentionally alter mechanical stiffness, it is unlikely that E would substantially increase. Indeed, *adsorbed* PAH samples that were subsequently conjugated with RGD/RGE showed a decrease in elastic modulus

relative to samples for which PAH was adsorbed without subsequent conjugation (Fig. 4.3). Therefore, one may reasonably conclude that PAA/PAAm multilayers modified via *stamped PAH* and RGD conjugation reverse the reported cytophobicity of this multilayer (46) due chiefly to changes in RGD ligand concentration, and not to unintended changes in mechanical compliance of the polymer substrata.

In contrast, PEMs modified by *adsorbed PAH* (15 min) exhibited $E = 4.16 \times 10^7$ Pa, an increase in mechanical stiffness by more than two orders of magnitude. PEMs modified via adsorbed PAH followed by either RGD or RGE peptide conjugation showed similar, dramatic increases in stiffness ($E = 1.67 \times 10^7$ Pa and 6.74×10^6 Pa, respectively) with respect to the unmodified PEM or the stamped PAH modification. Therefore, it is demonstrated that the transition from a mechanically compliant PEM to a mechanically stiff PEM occurs at the point of PAH adsorption, and not through the addition of the Sulfo-LC-SPDP heterobifunctional crosslinker or the RGD/RGE heptamers. Reducing the PAH incubation time to 30 sec, the time scale of PDMS stamping, showed only a modest reduction in the stiffness ($E = 6.15 \times 10^6$ Pa), suggesting that this material modification occurs rapidly.

4.3.3 Consideration of PEM Film Thickness

It is not immediately apparent why the compliance of PAA/PAAm/adsorbed PAH PEMs is so dramatically affected by adsorption of the PAH polycation. One

possible explanation is that the sample thickness decreases significantly after adsorption of PAH (e.g., by increased interchain hydrated crosslinking), such that mechanical probing of all samples to the same depth ($\Delta \sim 20$ nm) induces artifacts associated with proximity to the rigid polystyrene substrate on which the PEMs were assembled. To address this possibility, PEM film thickness was determined via scanning probe microscopy contact-mode imaging for all samples. As shown in Table 4.1, surface modifications did not significantly decrease PEM thickness. In fact, the nanoscale thickness and RMS surface roughness of PAA/PAAm with an adsorbed layer of PAH is slightly greater than that of unmodified PAA/PAAm (null), which is consistent with the increased deposition of more material in the modified film.

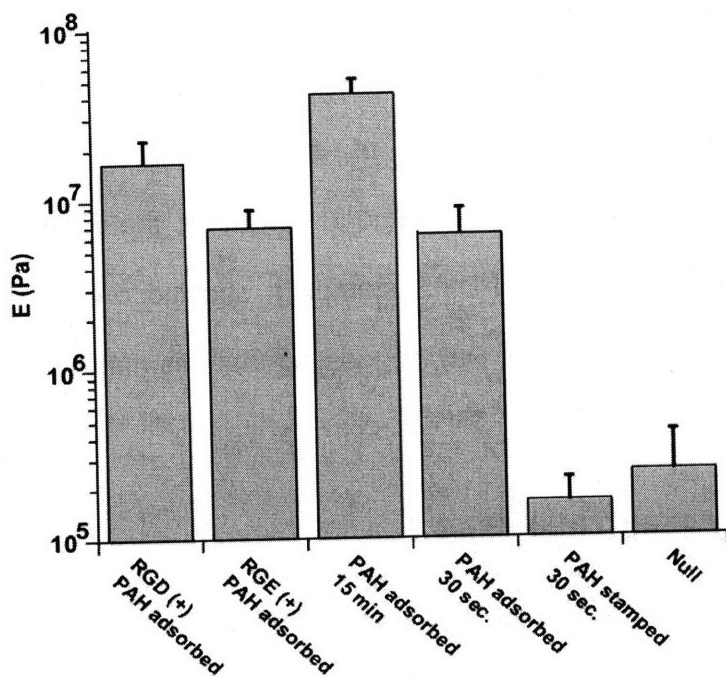


Figure 4.3 Nominal elastic moduli E of surface modified PAA/PAAm PEMs PEMs were indented to a depth of 20 nm using a scanning probe microscope in fluid (150 mM PBS, pH = 7.4) at room temperature. Error bars represent standard deviation among at least 50 measurements on a single sample. All samples except * were statistically significantly different from the unmodified PAA/PAAm PEM termed the null sample ($p < 0.0001$, ANOVA and ad hoc Fischer PLSD).

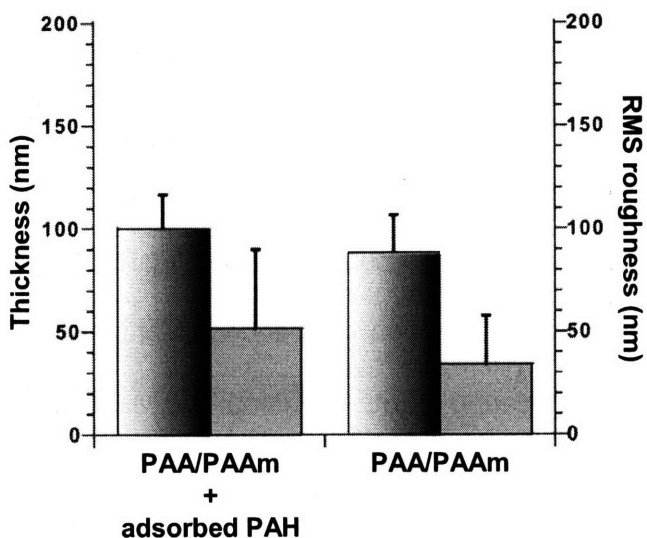


Fig. 4.4 PEM sample thickness and RMS surface roughness +/- adsorbed PAH
 Changes in mechanical stiffness in PAH adsorbed, PAA/PAAm PEMs is not due to differences in sample nm-scale thickness relative to as-deposited PAA/PAAm multilayers (grey, left axis), or to differences in RMS surface roughness (green, right axis).

Similarly, PAA/PAAm with an adsorbed layer of PAH conjugated with a hetero-bifunctional crosslinker and capped with RGE-peptide shows an increase in thickness and RMS surface roughness consistent with greater material deposition. PAA/PAAm samples modified by polymer-on-polymer stamping of PAH alone exhibit

a thickness comparable to the RGE-modified surfaces with similar increases in the RMS surface roughness. This is possibly due to the inhomogeneous nature of the polymer-on-polymer stamping technique, and also because PAH deposited in this localized fashion is not free to distribute uniformly and reorient optimally across the PEM surface over the time scale of the stamping procedure. *In situ* ellipsometry (ISE) results for the same PEMs assembled on silicon and hydrated with water were consistent with these SPM measurements of hydrated film thickness t , and are representative of a much larger surface area than considered via SPM (73).

Hydrated t of unmodified and adsorbed PAH PEMs measured via ISE was ~ 100 nm, and that of stamped PAH PEMs with and without RGE heptamer was ~ 230 nm.

Thus, the observed change in E between unmodified PAA/PAAm and the associated PAH adsorbed derivative cannot be attributed to a significant decrease in sample thickness upon PAH adsorption. Although differences in apparent t as measured via AFM are noted when comparing PEMs functionalized via adsorbed PAH (15 min) to stamped PAH, the effective strain expressed as the ratio of indentation depth ($\Delta = 20$ nm) to film thickness t was less than 20% in both cases, and thus artifacts due to contributions of the underlying (polystyrene) substrate are minimal (80). In addition, adsorbed PAH/RGE conjugated PEMs of thickness nearly identical to that of the stamped PAH PEMs show significantly decreased compliance that cannot be attributed to differences in PEM thickness (Fig. 4.4).

Neither the amount of total PAH adsorbed onto the surface nor the amount of PAH transferred via stamping were quantified rigorously. Therefore, it remains possible that observed increases in the E upon PAH adsorption are related to differences in the amount of PAH integrated within the PEM surface in each deposition protocol, even for constant duration of PAH exposure (30 s).

TABLE 4.1 Properties of PAA/PAAm polymer multilayer derivatives*

Sample	PAA/PAAm bilayers	Hydrated thickness [nm]	Surface roughness [nm]	<i>E</i> [10 ⁵ Pa]
PAA/PAAm, RGD modified‡	5.5	--	--	167.0 ± 60.0
PAA/PAAm, RGE modified ‡	5.5	214.2 ± 48.0	94.5 ± 69.6	67.4 ± 19.9
PAA/PAAm, PAH adsorbed†	5.5	99.8 ± 16.6	52.0 ± 37.8	416.0 ± 89.2
PAA/PAAm, PAH stamped*	5.5	213.1 ± 59.5	130.2 ± 95.7	15.9 ± 0.6
PAA/PAAm (Null; no PAH)	5.0	87.8 ± 19.3	34.1 ± 23.5	2.4 ± 1.7

*Young's moduli *E* were measured via nanoindentation. Hydrated thickness and surface roughness were acquired separately through scanning probe microscopy imaging of a surface area including a scratch through the complete sample thickness.

‡ PAH adsorbed for 15 min, followed by Sulfo-LC-SPDP and RGD or RGE heptamer, as indicated. RGD modified samples were not analyzed for hydrated thickness and surface roughness to conserve peptide, but the difference of only one amino acid between the RGD and RGE samples would not be predictive of any differences between these samples.

† PAH adsorbed for 15 min. Fig. 2 demonstrates no significant effect of shorter (30 sec) adsorption duration on *E*.

* PAH stamped for 30 sec.

As the PAH was added at a basic pH (pH = 9.0), it is possible that the single bilayer of PAA/PAH assembled at this pH creates a mechanically stiff surface layer. However, the depth of indentation chosen herein (20 nm) exceeds that of a hydrated bilayer by more than an order of magnitude, so such a surface-confined effect would not be expected to illicit the dramatic changes in E observed in Fig. 4.3 Therefore, even if the effective concentration of PAH available to react with the underlying PAA/PAAm PEM was greater under adsorption conditions than under stamped conditions, the increase in stiffness of the PAA/PAAm PEMs modified by adsorbed PAH cannot be easily explained by the formation of a mechanically stiff PAA/PAH layer at the PEM surface.

Some groups have reported that multilayers are capable of complete exchange of either the polycation or polyanion with soluble polyelectrolytes of like charge introduced post-assembly under certain conditions (156-158). Moreover, it has been shown that a liquid-like state exists where PEMs dissolve and either equilibrate to new, more stable configurations or disassemble entirely (159, 160). Taken together, such results might suggest that the polymer multilayer is undergoing a reconstitution during the adsorptive addition of PAH. However, the PAA/PAAm films in this study are covalently crosslinked via elevated temperature post-assembly, so it is unlikely that there is dissolution or complete exchange of PAAm with PAH during the 15 minute incubation time. Additionally, a 30 sec incubation time for PAH adsorption still produces a dramatic change in the modulus relative to the unmodified PEM ($E = 6.15 \times 10^6$ Pa and 1.6×10^5 Pa,

respectively), which is more rapid than the exchange processes reported thus far. Also, the PAH adsorption steps were performed under relatively mild conditions with respect to temperature and pH, whereas previous studies required modulation of pH, temperature, or ionic strength to achieve exchange and/or dissolution of PEMs (156-160). However, it is possible that this adsorption step induced potential phase transitions/separations, which would be consistent with the observed, slight increase in opacity of the PEM upon PAH adsorption, and this possible phase transition is currently under investigation. The central finding remains clear: Mechanical properties of weak PEMs can be significantly and unintentionally altered via certain biochemical surface modification routes, and these effects are independent of PEM thickness.

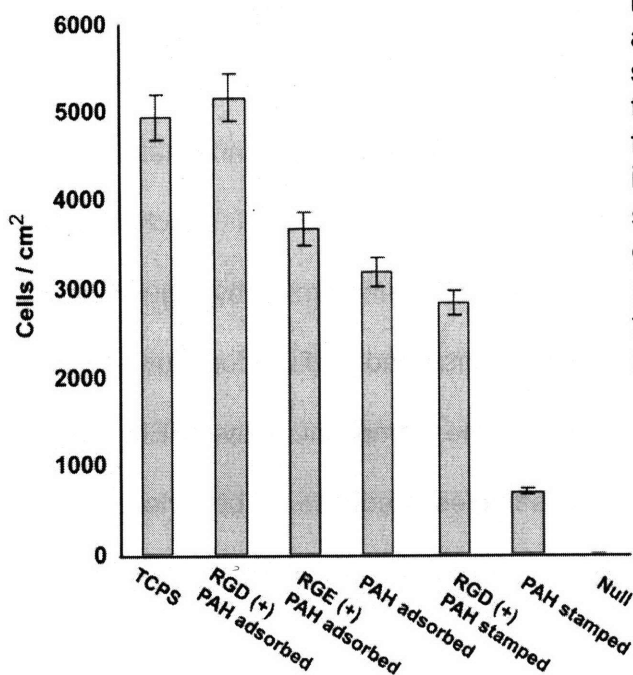


Figure 4.5 Murine NIH 3T3 fibroblast attachment at day 3 as a function of surface functionalization TCPS is tissue culture polystyrene; surface functionalization of PAA/PAAm (null) as indicated in Table 4.1. Growth area for stamped samples is 0.25 μm^2 , whereas growth area for all other samples is 9.6 μm^2 . Area is expressed in units of functionalized surface area (mean \pm standard deviation).

4.3.4 Effect of Surface Functionalization on Cell Attachment

Previous results in several substrata material systems have indicated that the mechanical stiffness of a polymeric substrate can affect cell attachment, spreading, and proliferation. As we observed decreased mechanical compliance in these PEMs upon the adsorption of PAH, we explored whether cell attachment correlated more strongly with compliance or with adhesive peptide functionalization (Fig. 4.5). In triplicate, murine NIH 3T3 fibroblasts were seeded onto PEM substrata to which PAH had been either adsorbed for 30 sec or stamped for 30 sec, with or without subsequent addition of the adhesive ligand RGD or the dummy (anti-adhesive) peptide RGE; total cell number at day 3 was measured upon trypsinization. RGD-functionalized, stiff substrata (RGD, PAH adsorbed) showed significantly greater cell attachment than RGD-functionalized, compliant substrata (RGD, PAH stamped). However, the RGD-functionalized, compliant substrata (RGD, PAH stamped) showed nearly the same cells/cm² attached as the unfunctionalized, stiff substrata (PAH, adsorbed); and the anti-adhesive peptide RGE-functionalized, stiff substrata (RGE, PAH adsorbed) showed nearly the same cell attachment as unfunctionalized, stiff substrata (PAH adsorbed). As summarized by Fig. 4.6, cells attached as a function of both substrata compliance and surface functionalization. For all samples with increased *E* relative to the compliant native PEM show marked increases in adhered cells, while samples predicted to be cytophilic via presentation of adhesion peptides also show good cell adhesion despite the magnitude of the sample compliance.

Finally, cells show increased adherence to substrata that chemically disfavor adhesion as sample stiffness is increased relative to the native PEM. Taken together, these results suggest that the mechanical compliance of the underlying cell substrata can be at least as important as ligand functionalization in dictating efficient cell attachment and proliferation.

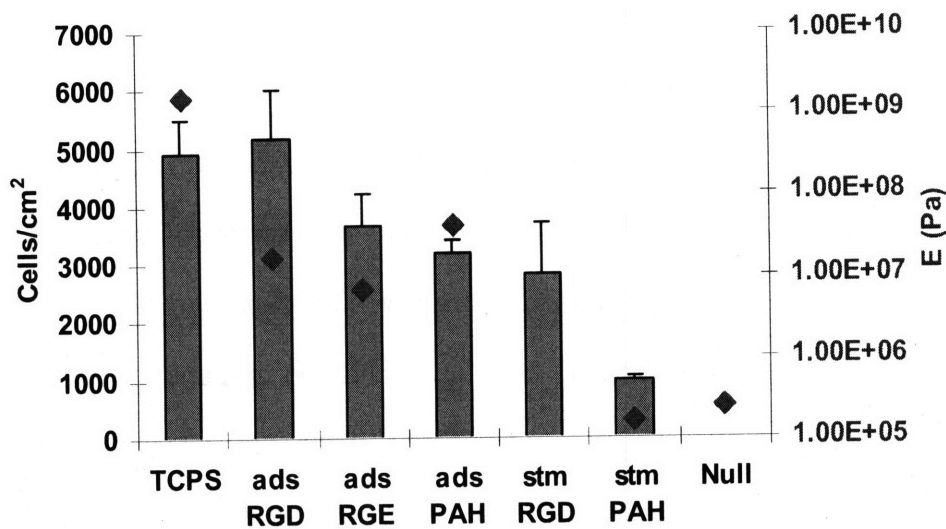


Figure 4.6 Chemical and mechanical properties orthogonally modulate cell adhesion to PEMs For all samples with increased E (red diamonds) relative to the compliant native PEM show marked increases in adhered cells, while samples predicted to be cytophilic via presentation of adhesion peptides also show good cell adhesion despite the magnitude of the sample compliance. Finally, cells show increased adherence to substrates that are chemically disfavor adhesion as sample stiffness is increased relative to the native PEM. E (red diamonds), cells/cm² (grey bars).

Our results regarding the importance of substrata chemical signaling in the process of cell adhesion to a cell exposed material interface are in agreement with the previous findings by Rubner et al. (72, 75), as well a number of reports in the literature on molecularly specific, RGD-mediated cell adhesion to substrata (49, 108, 116, 120, 124, 138, 147, 161-163); Ruoslahti presents a comprehensive review on RGD mediated cell adhesion and the use of RGD containing peptides as probes of cell adhesion mechanisms (120). The clear demonstration that mechanical stiffness can independently modulate cell adhesion, without any obvious interference with RGD mediated adhesion, represents a significant advance in the cell biology of cell contact formation. Previous reports demonstrated that thresholds of RGD density exist such that migratory cells will preferentially localize and adhere within the zone of corresponding critical RGD density (36, 37, 49, 155); and that RGD thresholds on patterned surfaces could be used to overcome cytophobicity in a concentration dependent manner with exquisite control over the chemical conjugation, patterning geometry, and RGD presentation (72, 75). Our results generalize those findings, in that we recapitulate the chemically based adhesion phenomenon in our PEM system without respect to ligand thresholds and further demonstrate that such density does not control cell adhesion when substrata stiffness is sufficiently stiff. Furthermore, we have established a narrow range of PEM stiffness whereby mechanoselective cell adhesion is favored in the presence and absence of RGD-containing peptides ($E \sim 10$ -100 MPa for these PEMs). It remains a standing challenge to 1) probe the

threshold substrata stiffness favoring pure mechanoselective adhesion on PEMs, and 2) determine whether these observations extend to other polymer or material systems.

4.4 Summary

This chapter explored the effect of adhesion peptide incorporation on the mechanical compliance of a specific polymer multilayer system comprising poly(acrylic acid) and poly(acrylamide). Systematic characterization of the PEM samples revealed significant processing dependent changes in nominal elastic modulus E : for the weak PEM considered herein, surface functionalization with RGD via polymer-on-polymer stamping of dilute PAH does not alter mechanical compliance, whereas functionalization via adsorption of dilute PAH over the same duration dramatically increases E . Thus, for weak polymer multilayers of nanoscale thickness such as PAA/PAAm, the method by which the cellular interface is modified can have unintended and profound consequences on mechanical compliance of the substrata and thereby alter the mechanical environment of attached cells. Furthermore, the changes in substratum mechanical compliance demonstrated herein cannot be attributed to changes in sample thickness or surface roughness. It is an open and important question whether these results are generally true for other polyelectrolyte multilayer systems and/or polymeric hydrogels. Nevertheless, these observations represent an

important contribution to the field with respect to the design, processing, and characterization of cell-adhesive/cell-repellent interfaces.

Biochemical surface modification of polymeric growth substrates to enhance or inhibit cellular attachment is important for a wide range of biological and bioengineering problems. Typically, it is tacitly assumed that these modifications – including incorporation of adhesion proteins and peptides such as RGD – alter only the local chemical environment and leave the mechanical properties of the surface unaffected. These findings serve both as a caution in the design of surfaces and experiments for which only chemical modification is desired, and as an opportunity to choose surface modification routes that alter mechanical and biochemical interfaces independently.

The work presented thus far has demonstrated that substrata mechanical compliance and surface functional chemistry both contribute to the cell adhesion process in eukaryotic cells. In the literature, chemomechanically dependent adhesion has been linked to processes involving the eukaryotic cytoskeleton and integrin mediated signaling (6). Prokaryotes such as bacteria are known to possess structures analogous to the eukaryotic cytoskeleton (termed the proto-cytoskeleton, or bacterial cytoskeleton). This raises the interesting question of whether bacterial adhesion can be modulated via extracellular mechanical force. However, unlike eukaryotes, not all bacteria possess the full complement of proto-cytoskeletal proteins and the functionality of these structures is highly variable

among different bacterial species. In the next chapter, chemical and mechanical properties of PEMs are used to probe factors that control adhesion of bacterial prokaryotes to material surfaces. Furthermore, the question is addressed whether the prokaryotic adhesion response is mediated via soluble factors, such as solution ionic strength; differences in cell wall composition, or proto-cytoskeletal processes, such as expression of actin protein homologs.

CHAPTER 5 EXTRACELLULAR PHYSICOCHEMICAL AND MECHANICAL FACTORS IN BACTERIAL ADHESION TO PEMS

Note: The contents of this chapter were previously published in Biomacromolecules Jun 2008;9(6):1571-1578, and includes the work of co-authors J.A. Lichter, M. Delgadillo, T. Nishikawa, M.F. Rubner, and K.J. Van Vliet.

5.1 Background and Motivation

5.1.1 Controlling Microbial Adhesion: a Critical Unmet Need

Hospital acquired infections (HAIs) represent an estimated \$4.5 billion cost (93) with an associated annual mortality of 100,000 persons in the US alone (66). Similar studies in the UK estimate that HAIs cost nearly three times that of care for patients with no infection and result in an average of 11 extra days of hospital care (93). Of the nearly 2 million infections per year, the Centers for Disease Control estimates that between 54-68% are associated with sites commonly linked to surgical wounds or medical assistive devices and implants. The commensal bacterial species *S. epidermidis* is the most common agent of infection (93, 164), with virulence attributed to initial attachment of a viable bacterial population to the surface (165) of a medical device and subsequent formation of a mature biofilm. As at least 64% of infections worldwide occur at sites of medical assistive devices

and implants (66), it is widely recognized that identification of the synthetic surface properties that inhibit bacterial attachment is critical to the general design of simple and versatile biofilm prevention strategies.

Approaches to limit bacterial colonization have focused on chemical degradation of stably adhered bacteria, including surface functionalization with microbicidal agents (89, 166, 167); surface impregnation with slow releasing biocides such as gold or silver (168-171) and antibiotics (89, 172); or surface functionalization of specific antimicrobial peptides and polymers (166, 173, 174). All of these methods rely on limiting the bacterial growth subsequent to colonization, primarily through the action of bactericidal agents. However, the utility of such materials in biomedical applications is limited by certain properties inherent in their design. For example, surface functionalization of chemicals and peptides may render the antimicrobial agents ineffective, masking active regions of the compound through conjugation or improper orientation (138); or the coupling may chemically inactivate the compound altogether (138, 175). Additionally, the fabrication protocols for such materials will be limited by the molecular stability of the antimicrobial agent(s) used. Biocide-releasing materials risk depletion of the active agent over time. A related issue is whether one can graft the antimicrobial ligand with sufficient density to effect the desired cell response (138). Implantable surfaces that incorporate metal compounds must resist corrosion; possess biological compatibility; and may need to be flexible or moldable so as to operate under mechanically dynamic conditions, thus limiting the versatility of such

materials. Finally, the development of bacterial resistance to antimicrobial agents is a major factor in any material design that limits microbial infections by incorporation of antimicrobial compounds.

Bacterial resistance to the standard suite of antibiotic drugs is an established medical dilemma, and the continued emergence of new bacterial strains with antibiotic resistance has added an additional urgency to the development of microbial resistant materials. Previously isolated chiefly to the clinical setting, reported cases of community acquired methicillin-resistant *S. aureus* (MRSA) infections have steadily increased over the decades (67), and more recently in the United States been linked to deaths in communal settings as diverse as athletic teams, pediatric environments, and amongst injection drug users (20, 65, 67). A recent study by Klevens et al. of nine geographically separate U.S. communities established that 72% of reported methicillin-resistant *S. aureus* (MRSA) infections arose in the community. Of those infections, over 58% were associated with exposure to clinical factors, such as recent surgery or medical device implantation (66).

Some clinicians have posited that injudicious use of antibiotics, poor patient compliance to drug regimens, and the combined ability of many bacterial strains to freely exchange genetic content created a selection pressure favoring multi-drug resistance via rapid mutation and cross-strain plasmid exchange (176, 177). Antibiotic resistance acquired by this means cannot be easily reversed by the development of new pharmaceuticals, as this is part of the mechanism for

development of multi-drug resistance. In this regard, non-microbicidal materials that resist primary colonization may prove exceptionally effective in preventing infections in both the community and the clinic because the selection pressure is no longer dictated only by survival of the bacterial cell, but instead by the efficacy of adhesion of that bacterium to a given material.

5.1.2 Properties of Gram (+) and Gram (-) Bacteria: Cell Envelope Shape, Chemical Composition, and Elasticity

Gross classification of bacteria can be ascribed according to cell shape. These include spheres, or cocci; cylindrical rods, termed bacilli; and spiral cylinders termed spirochetes. In the absence of shape inducing proteins, the default bacterial shape is spherical (61, 63). Cell shape determination is controlled by a diverse set of cytoplasmic proteins classified as the bacterial cytoskeleton. The number of distinct cytoskeletal proteins varies between species of bacteria in addition to variation within genotype variants of the same species (i.e., strains), and the presence of specific cytoskeletal proteins is highly strain dependent. Many bacterial cytoskeletal proteins have low sequence homology with their eukaryotic counterparts, and some bacterial proteins with high sequence similarity to bacterial cytoskeletal proteins are not known to form filamentous structures *in vivo* (61, 63). Therefore, homology to eukaryotic cytoskeletal proteins is typically established by the structural fold, ability to form filaments, or the cellular function of a given protein.

One of the most common cytoskeletal proteins found in bacteria is filamentous temperature sensitive protein Z (ftsZ), responsible for establishing the bacterial division plane during cellular replication (61-63, 178-180). FtsZ is found in nearly all bacteria, including the coccal species, and is analogous in structure and function to the eukaryotic cytoskeletal protein tubulin. FtsZ is responsible for recruiting cell cycle proteins during division, but does not confer shape to the cell. Specifically, ftsZ controls cell wall synthesis during the replication/division cycle interacting with penicillin-binding proteins (PBPs), a class of proteins critical for the proper formation of the cellular envelope (62). Note that interaction with PBPs occurs in a fundamentally different way than that described for the actin-like protein homologs described below, since ftsZ-PBP interactions occur during cellular division.

In both Gram (+) and (-) rods, the actin-analogue protein murein cluster B (mreB) forms helical filamentous structures along the cell membrane or cell wall. MreB regulates cell width and length in *E. coli*, forms a membrane complex that interacts with PBPs, and participates in chromosomal separation and compartmentalization in the resting state (61, 62, 180). MreB filaments extend across the length of the greater axis of the cell, interacting with the inner cell membrane. MreB is part of the *mreBCD* operon, a gene cluster that is associated with genetic structures responsible for the synthesis of the PG sacculus (63). The downstream gene products mreC and mreD penetrate the cell membrane and interact directly with the PBPs responsible for membrane stabilization (63).

Specifically, mreC and mreB form a complex bridged and activated by mreD, where mreC facilitates the interaction of mreB with the PG synthetic proteins present in the periplasmic space (63). When mreB is depleted from the cell or chemically blocked, the resultant cells are spherical and have increased radius (~2-fold increase in *E. coli*) (61-63, 180-182). Some species, such as *Bacillus subtilis* (*B. subtilis*), have several filamentous proteins that give rise to the rod phenotype (MreB, MreBH, and Mbl). Despite such redundancy, mreB is essential for survival in *B. subtilis* (61, 62, 180), and complete ablation of the *mreBCD* operon in *E. coli* results in 10,000-fold reduction in viability and loss of rod-shape phenotype (181, 182). Viability is recovered in cells capable of over expression of *ftsZ*, the cytoskeletal protein associated with cell division (63, 181, 182).

The protein crescentin, found in *Caulobacter crescentus*, is the sole member of a third class of bacterial cytoskeletal proteins functionally and structurally analogous to eukaryotic cell elements, intermediate filaments (61-63). Crescentin localizes to the cell wall, inducing curvature along the one side of the long axis of the cell, giving it a crescent shape (61, 62). Spiral cells for which shape induction is understood have no known pro-spiral cytoskeletal elements; instead, the spiral form is induced through elements in the cytoplasm or flagellar structures (61-63). Shih and Rothfield have argued that complex cell forms are not well understood (63), and a standing problem in cell biology is related to the connection between whole-cell shape determinants and cellular function. This makes cell shape an

interesting parameter in any investigation involving cell adhesion among different bacterial species.

Bacterial species are further classified according to their reaction to the so-called Gram staining procedure. Gram staining involves retention of the cationic dye crystal violet after treatment with iodine and ethanol. Gram staining is a simple yet powerful way to qualitatively distinguish extracellular properties among bacterial species via chemical and physical properties. A positive Gram stain (G(+)) indicates that a bacterial cell has a multi-layered (murein) peptidoglycan (PG) cell coat, or sacculus (61, 64, 183). A Gram negative stain (G(-)) indicates the presence of a thinner sacculus comprised of a single PG layer, in addition to an inner cell membrane. Certain microbes lack cell walls or possess cell membranes enriched with mycolic lipids that resist Gram staining (members of the Gram-variable branch), but most bacterial cells can be divided into either G(+) or G(-) classes.

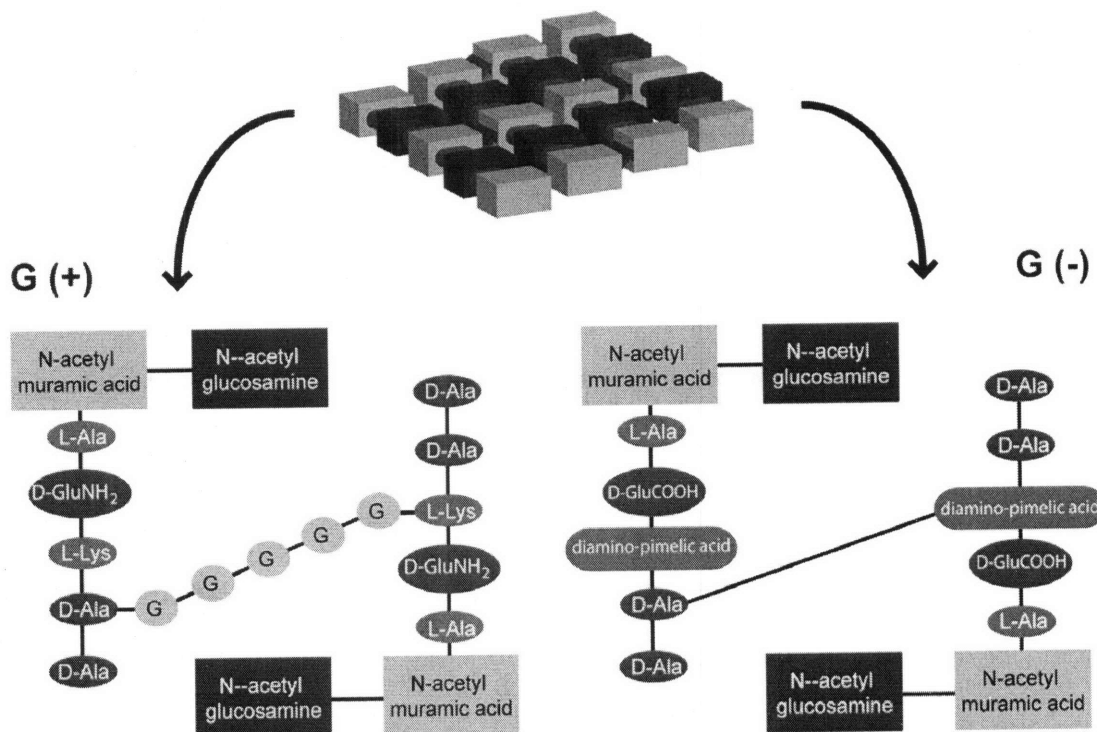


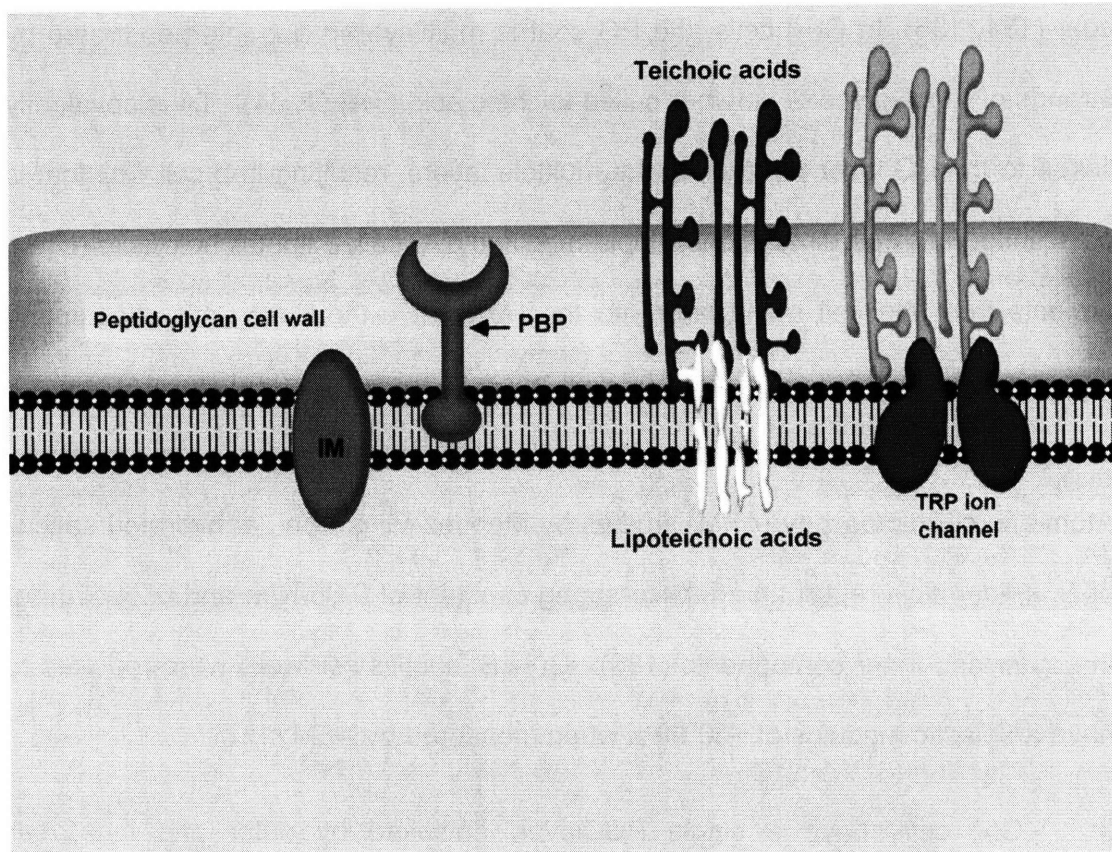
Figure 5.1 Chemical crosslinking in the bacterial cell wall Carbohydrate polymers composed of dimers of NAG and NAM are crosslinked throughout the cell wall via peptide bridges. In many Gram (+) cells the peptide bridge has a highly flexible, pentaglycine linker sequence. In *E. coli*, a Gram (-) rod, there is no pentapeptide linker; carbohydrate polymers are directly linked through the transpeptide side chains. NAG, N-acetyl glucosamine; NAM, N-acetyl muramic acid; G, glycine; D-GluNH₂, D-glutamine; D-GluCOOH; D-glutamic acid; D-Ala; D-alanine; L-Lys; L-lysine (1).

The PG coat is primarily composed of a carbohydrate dimer, N-acetyl muramic acid (NAM) and N-acetyl glucosamine (NAG), assembled into linear chains (1, 64). This carbohydrate framework is crosslinked through a transpeptide side chain stemming from the 3-hydroxy position of NAM. The type of transpeptide linkage in the PG wall, the PG wall architecture, and the constituents molecules embedded in the PG structure vary considerably between G(+) and G(-) species.

For example, in many G(+) cells, crosslinking occurs via a glycine pentapeptide linking D-alanine (D-ala) residue to L-lysine (L-lys) on the opposite strand; whereas, in cells such as *E. coli*, crosslinking occurs directly from one transpeptide to the other, with substitution of L-lysine with meso-diaminopimelic acid (*m*-A₂pm) (64, 184). It is important to note that no crosslinking substitution pattern in the PG coat is absolute; variations occur across different species and strains of bacteria as well as within the PG coat of an individual cell. This affords some protection against host defenses and natural biocides that degrade the cell wall, and prevents the cell coat from assuming a semi-regular crystalline structure thereby conferring some flexibility to the otherwise stiff cell wall (64, 184). Some cells secrete a complex mixture of external PG elements in addition to the cell wall that subsequently form an ordered structure referred to as a capsule, that aid in evasion of phagocytosis and decrease bacterial adhesion by masking specific adhesion molecules; *E. coli* approximates capsular secretion with thin appendages termed curli that are discussed in more detail below (64). Cells such as *S. epidermidis* secrete a disorganized, loosely bound carbohydrate rich structure, called a slime layer (e.g., glycocalyx), which aids in cell adhesion (64, 183). Taken together, there is tremendous potential for variation in cell wall chemical composition, architecture, and structure among differing bacterial species. Just as with cell shape, this makes comparison between differing cell envelope composition a critical feature of any study related to bacterial adhesion. coat (184, 185).

The chemical structure of the cell wall directly affects the elasticity of the PG coat (184, 185). In G(+) cells, the PG coat is multilayered and interpenetrated by strands of a polyglycerol polymer called teichoic acid (TA) (1, 64). TA is covalently linked to the PG layer throughout the multiple layers, resulting in a cell wall that is crosslinked in three dimensions. Lipid-modified TA, called lipoteichoic acid (LTA), projects from the cell membrane into the PG coat without covalent attachment, stabilizing the interaction of the cell wall and cell membrane. However, proteins can project through the PG coat, the cell membrane, or span both structures. Atomic force microscopy (AFM) studies by Mendez-Vilas et al. of hydrated sacculi of *S. epidermidis* report an effective spring constant of 0.08 N/m and 0.24 N/m for the outer and inner components (186). G(+) *B. subtilis* cell walls were reported to have an elastic modulus of ~30 MPa when measured by AFM (187).

G(-) cells have a single PG layer, enclosed by outer and inner cell membranes (1, 64). The periplasmic space resides between the outer-membrane/PG coat and the inner-membrane. The outer cell membrane is a dual leaflet: the outer leaflet is composed of lipid A, an endotoxin; and lipopolysaccharide (LPS, O-antigen), which is the predominant constituent of the outer leaflet (1, 64). Phospholipids are the major component of the inner leaflet of the membrane. LPS is highly antigenic, and useful for serologic identification of bacterial strains (1, 64, 183). LPS can project ~ 120 nm above the cell surface (187), but does not usually promote bacterial adhesion except by non-specific interaction with cell surface receptors such as lectins (1).

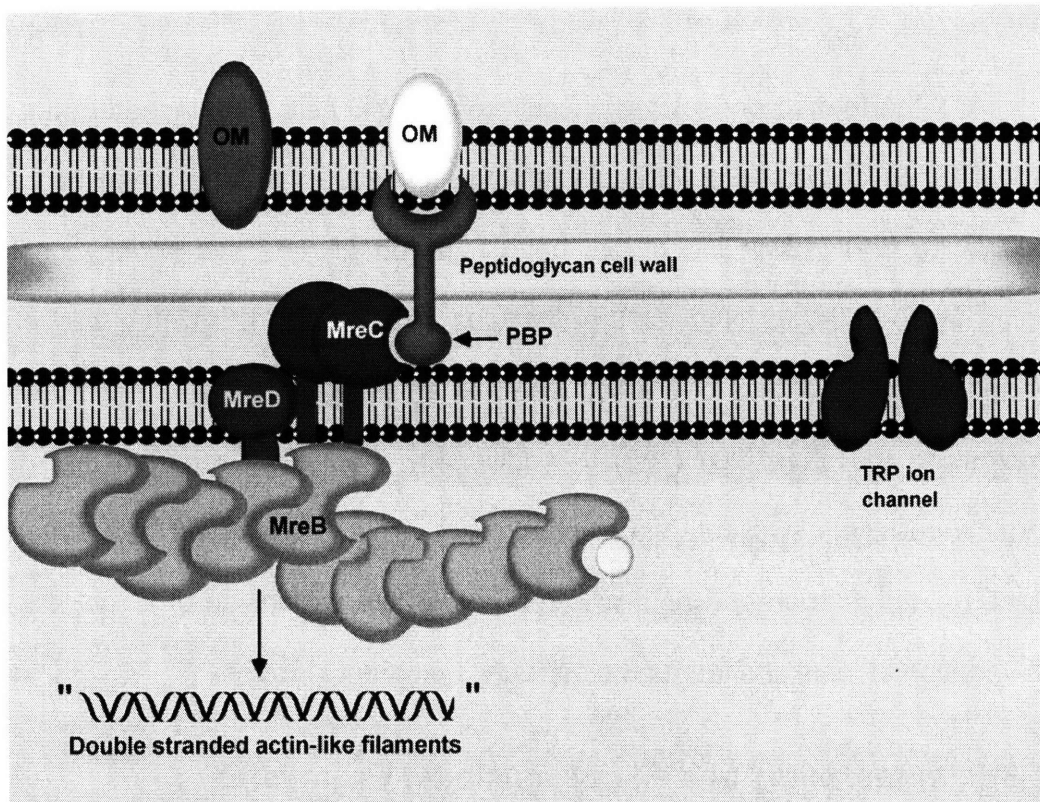


Schematic 5.1 Architecture of the Gram-positive cell coat The cell sheath consists of a thick peptidoglycan cell wall with embedded teichoic acid polymers (red, orange modular structures). Lipoteichoic acid polymers are embedded in the inner cell membrane and assist in anchoring the cell wall to the membrane. Penicillin-binding proteins anchored in the peptidoglycan cell wall (PBP, blue receptor). Ion channels of the transient receptor potential protein superfamily are embedded in the inner membrane, and open in response to hypo-osmotic shock induced lateral cell membrane tension. A wide variety of additional proteins are also embedded in the inner membrane (green, IM.) (*rendered in Paracel Pathworks*).

AFM performed on isolated sacculi from *E. coli* cells demonstrated that the cell wall is an elastically deformable structure with $E \sim 25$ MPa when hydrated (~ 300 MPa, dry) (188), and others have reported an effective spring constant ranging from 0.03-0.05 N/m for the sacculus of *E. coli* K-12 (187). Yao et al. reported that the stiffness of the cell wall was anisotropic, ~ 2 - 3 -fold stiffer when compressing the short axis (188). Additionally, Yao et al. reported that dried sacculi were highly swellable upon rehydration. This is consistent with structural studies by others such as Koch, who reported 300% expansion of *E. coli* sacculi with variation of ionic strength of the surrounding media (185).

5.1.3 *S. epidermidis* and *E. coli* as Model Organisms

S. epidermidis is a Gram (+) spherical cell belonging to the coagulase-negative family of *staphylococci*. Cell division in all *staphylococci* occurs along any of the three spatial dimensions, unlike other common Gram (+) spherical species, such as *streptococci*, that divide uniaxially and form long chain-like structures (64). The resultant morphology for rapidly dividing *S. epidermidis* cells is an aggregate cluster of cell groups, though one can easily observe isolated *staphylococcal* cells via optical microscopy. In the simplest approximation, *S. epidermidis* is a passively diffusing, spherical particle of approximate radius $r = 0.5 \mu\text{m}$ (1). *S. epidermidis* is non-motile, thereby eliminating concerns that active cellular translocation might convolute observations when testing physical and chemomechanical effects on cell



Schematic 5.2 Architecture of the Gram-negative cell coat The cell sheath consist of an outer membrane with embedded proteins (green, white ovals), some of which interact with the so-called penicillin-binding proteins (PBP, blue receptor). PBPs are anchored in the peptidoglycan cell wall, and interact with the MreC, a member of the trimeric protein complex comprised of gene products from the MreBCD operon. MreC and MreD are anchored in the inner cell membrane. MreB is associated on the cytoplasmic side of the inner membrane and forms helical filamentous structures with ATPase activity (yellow sphere, ATP/GTP). Ion channels of the transient receptor potential protein superfamily are also embedded in the inner membrane, and open in response to hypo-osmotic shock induced lateral cell membrane tension. (*rendered in Paracel Pathworks*).

adhesion. Chemotaxis, the movement of a cell along a chemical gradient, is also not a factor when evaluating *S. epidermidis* adhesion. However, the presence of long cylindrical structures extruding from the inner cell to the outer cell, termed pili or fimbriae, and shorter tuft-like structures anchored at the extracellular surface (189, 190) add some hydrodynamic volume to the cell and may passively retard free diffusion (84). Nevertheless, the relative simplicity of the cellular architecture of *S. epidermidis* compared to that of other bacterial species, coupled with the absence of active processes that might compete with free diffusion, make this cell an ideal model for studying chemomechanical effects on microbial adhesion.

The Gram (-) rod *E. coli* is more complicated than *S. epidermidis* in almost every aspect. Structurally, *E. coli* cells possess more diverse and complex fimbrial structures that can be classified into four distinct groups. Type I pili, similar to the pili structures found in Gram (+) cells, are ~ 7 nm wide shaft-like appendages that narrow at the tip to ~2-3 nm (1). The pili structure is typically built from multimeric protein complexes as a structural support shaft (pilus) with an adhesive tip specific for a class of molecular targets, for a given set of multimers. For example, the *fim* class of fimbrial proteins assembles as a column comprised of the protein FimA; the adhesive tip is a combination of three proteins FimG, FimF, and FimH and is specific for mannose-conjugated proteins (1, 14, 22, 23, 191). Interestingly, *fimH* mediates shear-force induced anchorage of *E. coli* to mannosylated surfaces under flow conditions (14, 19, 22, 23, 191). P-fimbriae are similar to type I pili in diameter, tend to be lengthier along the shaft and have a longer adhesive tip (1,

192). They are expressed in virulent *E. coli*, although they are not necessarily isolated to pathogenic strains. Along the pilus, P-fimbriae are comprised of subunits termed PapA. Two adaptor proteins PapK and PapF, link PapA to the adhesin PapG that is specific for, a kidney cell surface protein called globoside receptor (192). A critical feature of P-fimbriae is its participation in the adhesion dependent signalling pathway termed CpX, which has been shown to regulate stable adhesion to abiotic surfaces after initial cell adhesion is established (192, 193). Type II fimbriae are ~2-3 nm in width, and radiate from the cell wall similar to Type I and P-pili (1). Structures named curli are found on the extracellular side of in *E. coli* as small tuft-like structures < 3nm in width and aggregate closer to the cell coat, forming an extremely dense surface envelope resembling a capsule (1).

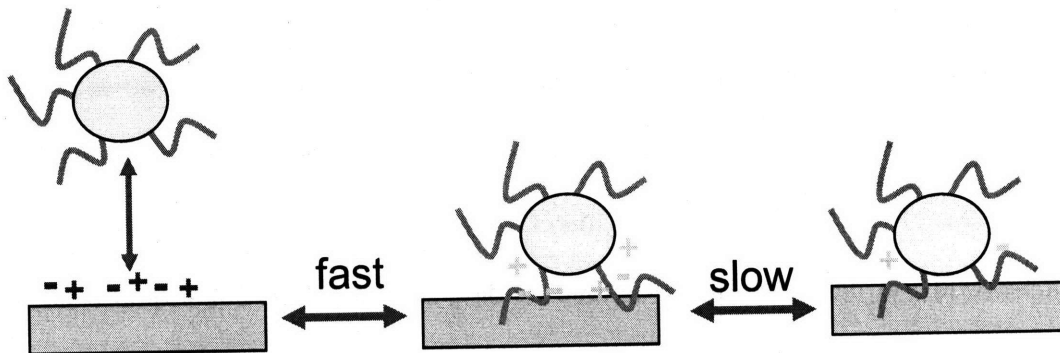
As detailed in section 5.1.2, *E. coli* has a more complex cytoskeletal architecture than *S. epidermidis*, which gives the cell its shape and allows limited communication between the periplasm and the cytoplasm via the *mreBCD* proteins (63, 180). In addition to the division-ring protein *ftsZ* that is present in *S. epidermidis* and *E. coli*, between the two bacterial species only *E. coli* expresses the cytoskeletal proteins *mreB*, *mreC*, and *mreD*; a group of proteins forming a putative trimeric complex that spans the inner cell membrane, projects into the periplasm, and establishes intimate connections to the cell wall synthetic machinery (63). *MreB* is an ATPase located on the cytoplasmic side of the inner cell membrane, and is activated by its association with *MreD* embedded in the membrane (61-63). The ATPase functionality of *mreB* is required for

polymerization into filamentous structures, but has also been suggested to play a role on overall cell regulatory processes associated with cell wall stress (62). Embedded within the *E. coli* cell membrane are two distinct classes of mechanically sensitive (MS) ion channels that control ion flux during conditions of hypoosmotic shock (7, 18, 194-196). The MS ion channels respond to lateral tension in the inner cell membrane, opening at pressure levels just under those sufficient to cause cell lysis (7, 195). The MS channel of large conductance (MScL) and MS channel of small conductance (MScS) are both expressed in *E. coli*, and are members of the protein superfamily known as transient receptor potential (TRP) ion channels (see Ch. 3) (7, 18, 113, 194-196). TRP ion channels are also found in Gram (+) cells, and MScL has been identified and sequenced in *S. aureus*, a close relative of *S. epidermidis* (195).

5.1.4 Coupled Interactions of Cell-Material Properties In Bacterial Adhesion

Biofilms, structured communities of bacteria protected by a polysaccharide matrix, require the initial attachment of a viable bacteria population on a surface (165). Bacteria adhere to surfaces according to the so-called two-stage, kinetic binding model. The first stage of binding is rapid and easily reversible. During this initial kinetic stage, bacteria first sense the interface at either long (> 50 nm), mid-(10-20 nm), or short range (<10 nm, avg. 1-5 nm) (1). Long range forces are

primarily van der Waal's attractive forces, which direct bacterial movement towards the material interface. Mid-range forces combine van der Waals attraction with Coulombic forces, and depend strongly on the physical and chemical properties of both the bacterial-material interface and the medium across which the bacteria and the material interact. For example, the electrical double layer (i.e., the distance over which the force from electrical charge decays in a given medium) is significant over a range of ~ 20-30 nm in deionized water for net charged surfaces, and assists diffusion of the cell towards the surface. This can also be thought of as a physical length scale over which charge interactions are screened from one another, and thus do not contribute to the physical interaction between solubilized particles. However, for solutions with physiologic ionic strength the double layer is reduced to a distance of < 1 nm, so nearly all charge interactions are rapidly and effectively screened out by ion shielding over a small length scale except those in near molecular contact or charge groups that are sequestered in molecular recesses (84). Short range interactions consist of hydrophobic attractive forces, hydrophylic repulsion, steric interactions, hydrogen bonding, and interactions between charge transfer sites on the bacterium and material interface (1, 84, 138). The second stage of bacterial adhesion is slower than stage one, and involves more specific interactions between proteins in the fimbrial



Schematic 5.3 The two-step kinetic binding mechanism Bacteria adhere to surface according to a two step kinetic process. The first stage of binding is governed by mid-long range forces on approach, such as van der Waals attraction, and hydrophylic repulsion and electrostatic repulsion. Fimbriae play a role in overcoming the repulsive interactions in this region, as the force acting on the fimbrial tip is small because of the very small tip radius ($r = 1-5 \text{ nm}$). Adhesion in this phase is fast, reversible, and weak; cells eventually adhere as the number of fimbrial-material interactions grow. In the second phase, specific molecular interactions take place between ligands and their cognate receptors on both the bacterial and host-material surfaces. For abiotic surfaces, the second step is restricted to molecular recognition of specific chemical moieties, or pre-patterned molecular agents (1).

structure and binding partners on host cells (1, 84, 86, 93). Fimbrial proteins that aid in cell adhesion to specific molecular targets are termed adhesins, although some non-specific adhesion molecules are included in the class of adhesins. Most notable is lipoteichoic acid (LTA) and lipopolysaccharide (LPS), major virulence factors in Gram(+) and Gram(-) bacterial species, respectively (1). The second adhesion step is slowly reversible, requiring release of all adhesin-material binding interactions. This has led some to refer to the second kinetic step as the irreversible binding step, although this is technically inaccurate. A third stage in bacterial adhesion, termed colonization, occurs when the bacteria have formed stable contacts with an interface, retained viability, and can truly be considered

permanently resident on the material interface (1, 164). It should be noted that colonization is not synonymous with infection, which is usually associated with the presence of a virulence agent, or pathogen (183). When one considers bacterial adhesion to non-biological surfaces, it may be tempting to disregard the events that occur beyond the first step of the kinetic binding model, since subsequent steps often involve binding between adhesins with their specific cell surface markers (1, 64, 183, 197). However, bacterial attachment to polymeric materials *in vivo* is enhanced by presence of extracellular matrix elements, in addition to proteins secreted or shed by host cells (1, 197). Francois et al. note that surface wetting properties of a given polymer implant material correlate with this protein adsorption (197), and similar surface wetting properties have been proposed to positively correlate with bacterial adhesion (84).

Prevention of bacterial adhesion to material substrata prior to colonization has been limited by incomplete understanding of the quantitative effects of physicochemical forces that regulate this process. Physical characteristics such as surface roughness do not appear to impact bacterial adhesion consistently. Teixeira et al. reported reduced adhesion of *S. epidermidis* to both smooth and rough chemically modified urethane surfaces (97). Other studies have reported a small influence of increased surface roughness promoting bacterial adhesion, but were unable to quantify this effect or to conclusively correlate roughness with adhesion of statistical significance (86, 87, 93, 94, 97, 198). This notwithstanding, there are many reports correlating increased surface roughness with increased

bacterial adhesion (93, 199, 200). The proposed mechanism involves increased material surface area with which the bacterium may interact, increasing the likelihood of cell adhesion (93). However, among some such reports it has been noted that this roughness-induced promotion response is non-linear, and depends on the experimental definition of roughness in addition to the range over which the roughness is varied (93, 201). Consequently, no quantitative scale or upper/lower thresholds have been established indicating how a given surface roughness affects bacterial adhesion.

Material surface charge and/or hydrophobicity have been reported to be crucial during the primary, kinetic step of adhesion (1, 98, 202, 203). However, several studies have reported no correlation between microbial adhesion and hydrophobicity (87, 198), and claimed the presentation of surface functional groups capable of charge transfer (the so-called Lewis acid/base character of the surface) as the critical factor governing bacterial adhesion (85, 96, 98). There are several reports on antimicrobial effects of cationic polymers (166, 167, 204, 205). This has been theorized to occur either through membrane disruption by long chain, quaternary ammonium salts (QAS)(166, 167); or by cation induced ion exchange of divalent ions essential for membrane stabilization, from the microbe to the surrounding media (204, 206). It is important to note that the cationic cytotoxicity does not translate to reduced bacterial adhesion. Murata et al. specifically note that antimicrobial surfaces designed according to the ion exchange mechanism can become fouled (204), thus leaving open the question of how adhesion to such

surfaces is affected by cationic groups. Tang et al. demonstrated that hyaluronic acid coated surfaces were resistant to *S. epidermidis* growth and postulated that this was due to high net negative charge from surface exposed carboxylates (198). Another significant factor influencing adhesivity are the physical and chemical properties of the bacterial strain itself (14, 19, 93, 134, 203).

When one considers that adhesion to synthetic surfaces can be dependent on highly variable properties such as physical traits of the individual bacterial strains; factors such as material surface roughness, variable over nm- μ m scale with non-linear effects on adhesion; and interactions over networks of charge and hydrogen bonding, the complexity of the adhesion step becomes clear. In an attempt to reduce this complexity to a single parameter, some have examined total interaction energy between the microbe, material, and liquid media, usually expressed as the work of adhesion (82, 95, 98). However, the surface energy is a property that incorporates physical and chemical features of the bacteria and the material at the interface including hydrophobic attractive and hydrophylic repulsive forces; surface roughness; and charge transfer and hydrogen bonding capacity (2, 84, 85, 95). The contradictory reports regarding significant factors for bacterial adhesion are evidence that no one material or cellular feature can completely explain how microbial attachment is controlled. Additionally, such contradictory results may also indicate unrecognized interactions that modulate bacterial attachment.

Here, we consider whether the mechanical compliance of the surface, now widely appreciated to modulate the adhesion and function of eukaryotic cells (42, 46, 47, 116), may also regulate adhesion of viable *S. epidermidis* and *E. coli* to underlying substrata. To vary the physicochemical and mechanical properties of the substrata, we employed a class of synthetic polymer thin films termed weak polyelectrolyte multilayers (PEMs). The chemical functionality and mechanical compliance of such films can be adjusted by simple variations of the layer-by-layer assembly conditions such as choice of polyanion/polycation or assembly pH (46). The effective elastic modulus E or stiffness of such hydrated films under in vitro culture conditions can be varied over several orders of magnitude. We and others have shown that this substrata stiffness modulates tissue cell adhesion independently of physicochemical characteristics such as adhesive ligand density (42, 45, 47). Recent advances in high resolution imaging, analysis, and simulation of bacteria subcellular structures suggest cytoskeletal and adhesive receptor molecule analogues in prokaryotic cells such as bacteria may enable mechanoselective adhesion (14, 19, 191, 198). Through extensive characterization of these tunable polymeric substrata, we demonstrate that both *S. epidermidis* and *E. coli* exhibit mechanoselective adhesion. As a result, bacterial colonization can be significantly reduced by modulating substrata compliance independently of short and long-range physicochemical properties of the cell-material interface

5.2 Materials and Methods

5.2.1 PEM Assembly and Materials

PEMs were assembled as previously described in Chapter 2. In this series study, multilayers were assembled PAA layer first on aminoalkylsilane coated glass slides (Sigma-Aldrich) or, for Fig. 5.2 only, on medical grade titanium (ASTM F67, President Titanium, Hanson, MA). The PEMs used in testing adhesion to medical grade titanium were subject to thermal treatment (80° C, 30 min). Sample notation refers to the assembly conditions with the pH of the PAA followed by the pH of the PAH, i.e., a 3.5/8.6 PEM was assembled using PAA at a pH 3.5 and PAH at a pH 8.6. All PEMs were prepared to a final dry thickness of ~50 nm. The sample set included 2.0/2.0 (9.5 bilayers), 4.0/4.0 (7.5 bilayers), 6.5/6.5 (49.5 bilayers), 3.5/7.5 (5.5 bilayers) and 3.5/8.6 (5.5 bilayers). The following samples were used to study the effect of masking underlying PEM substrata in Fig. 4: 6.5/6.5 (50 bilayers; PAH topped) plus 0.5 bilayer of pH 2.0 PAA; 6.5/6.5 (49.5 bilayers) plus one bilayer of 2.0/2.0; and 2.0/2.0 (9.5 bilayers) plus pH 6.5 PAH. Self-assembled monolayers used in charge variation assays were provided by Dr. A. Jackson and Prof. F. Stellaci, and are discussed in Section 5.3.1.3.

5.2.2 Mechanical Testing and Data Analysis of PAA/PAH Multilayers

Mechanical stiffness was quantified as the effective elastic moduli E , as determined from SPM-enabled nanoindentation force-displacement responses acquired from an atomic force microscope (3D Molecular Force Probe, Asylum Research, Santa Barbara, CA), as previously described (Section 2.3-2.4) (46). Silicon nitride cantilevers (MLCT-AUHW, Veeco Metrology Group, Sunnyvale, CA) were used to indent PEMs to maximum depths of <20 nm with a threshold filter to maintain equal loads for each indentation. The probe radius of curvature R_p was ~50 nm; cantilever spring constant k was nominally 0.1 N/m and was experimentally determined for each cantilever (45, 46, 207). Nanoindentation was performed in an acoustic isolation enclosure (Herzan, Inc.) at room temperature in 0.2 μ m-filtered PBS or Milli-Q water. Nanoindentation force-depth data were analyzed in IGOR (Wavemetrics, Lake Oswego, OR) and E was determined according to the previously described modified Hertzian contact model (see Chapter 2) (46).

5.2.3 Substrata Surface Energy and Interaction Energy

To determine the total interaction energy and surface tension components of the substrata, liquid contact angles were measured for the polar solvents water and ethylene glycol; and the apolar solvents hexadecane and diiodomethane. Each

measurement for a given solvent was performed using the sessile drop technique, and contact angles recorded for static, advancing, and receding drop forms (73). Contact angles were measured using a camera-equipped Advanced Surface Systems machine, and each sample was measured 5-10 times. Liquid contact angles were used to determine thermodynamic properties of the surface-bacterial cell-liquid interface according to the Lewis acid-Lewis base theory of Van Oss (98). Using the Van Oss approach, liquid contact angles of three or more test solvents are measured and then the nonlinear Van Oss-Young equations solved simultaneously, as described in section 2.6. The numerical values for each for each liquid component were obtained by solution of the simultaneous equations using the solver tool found in Microsoft Excel 2003. The surface tension parameters of each bacterial surface were assumed to correlate with published values of closely related strains or bacterial strains with similar phenotype. In the case of *S. epidermidis*, values were used from a representative slime producing strain of *S. epidermidis* (RP62A/ATCC 35894); and or *E. coli* the values for the strain W3300 were used. It should be noted that the bacterial components of this equation act as constants, and therefore do not affect interpretation of trends. However, surface tension properties of additional clinically relevant strains were examined using the same technique and were qualitatively similar (data not shown), further indicating that interfacial energetics as described by the current formulation of Young's theory do not adequately address the observed effects.

5.2.4 Substrata Surface Charge Density

Surface charge density Q was analyzed for PEMs 2.0/2.0 and 6.5/6.5 via AFM force spectroscopy (3DMFP, Asylum Research), using cantilevered carboxylic acid-functionalized polystyrene spheres of approximately 3 μm radius (BioForce Nanosciences, Ames, IA; nominal $k \sim 0.1$ N/m) Force-distance curves were first acquired in deionized water using a test surface comprised of mercapto-undecanoic acid (MUA) functionalized gold surface with calibrated Q (103, 104) of $Q = -18$ mC/m², from which the Q of the colloidal probe was calculated using models adapted from Rixman et al. (103, 104). Force-distance curves were acquired for experimental samples in deionized water (ionic strength $I = 0.0027$) or 0.1 M NaCl ($I = 0.1$) after an overnight thermal equilibration of the surface and cantilevered probe within the AFM. The maximum deflection of the cantilever on approach to the sample surface was maintained constant via a closed-loop algorithm supplied by Asylum Research. All sample locations were measured a minimum of twenty times per approach cycle, over 5-10 locations per surface. Curves representative of the data set were generated by alignment of the contact point, defined as the beginning of the region of constant compliance, followed by statistical averaging of the respective force and separation curves for a given approach cycle. The resultant curve for each surface location was the average force detected by the average approach vector normal to the sample surface. Measurements that did not possess a region of constant compliance were zeroed by examining for either a jump-to-contact region, followed immediately by

cantilever deflection; data acquired in $I = 0.1$ M solvent were compared to data acquired in Milli-Q water at the same distance from the surface to determine where physical deflection occurred. Representative curves were then used for modeling the electrostatic surface charge density to a distance within 5 nm of the calculated contact point, and surface charge density calculated from a least squares fit of the model to the data (103, 104). The Igor programs used to prepare the data for analysis is detailed in Appendices A.1 and A.2. Analysis of the Data was performed using previously published MATLAB code provided by Kaungshin Tai and Prof. Christine Ortiz (103, 104).

5.2.5 Determination of Relative Free Carboxylic Acid Presence at the PEM Surface

Methylene blue staining of freshly rehydrated PEMs for the determination of relative free carboxylate presence at the PEM surface was performed as described in Section 2.2.7. Briefly, prepared PEMs were immersed for 15 min in 0.005 M solutions of methylene blue in deionized water (pH 7). The PEMs were then rinsed in two clean water baths for 2 min each and dried with an air gun. Incorporation of methylene blue into the PEMs was measured by UV-Vis spectroscopy ($\lambda = 450 - 700$ nm) with peak intensities at $\lambda \sim 580$ nm (69).

5.2.6 Bacterial Attachment Assays

Bacterial strains used in this study were *S. epidermidis* (ATCC # 14990), and the standard *E. coli* K-12 strains W3100 (ATCC # 14948) and MC1000 Δ *mreB* (from ATCC # 39531, with permission of Prof. K. Gerdes and provided by Prof. M. Goldberg). Waterborne bacterial attachment assays were adapted from the protocol of Tiller, et al. (167). Briefly, Miller Luria-Bertani or LB-Miller broth (VWR) was inoculated with a monoclonal strain of the indicated bacterial strain using a sterile plastic loop and incubated overnight at 37°C with shaking agitation. Two 50 mL aliquots of the primary culture were centrifuged at 2700 RPM for 10 min at 4°C, the LB broth decanted, and the remaining bacterial cell pellets resuspended in 150 mM NaCl PBS (VWR). Following resuspension in PBS, the cells were centrifuged twice (5 min, 2700 RPM) to ensure complete removal of LB broth, with a final resuspension in 18M Ω Millipore water. The optical density (OD) of the bacterial suspension was measured using a spectrophotometer at $\lambda = 540$ nm, and adjusted to OD = 1.0, which corresponds to 10^9 cells/mL for *S. epidermidis* and between 10^8 - 10^9 cells/mL for *E. coli*. The resuspension was serially diluted with water from 10^9 cells/mL (measured via optical density) to create suspensions of 10^3 - 10^8 cells/mL. Studies in water were conducted at 10^7 cells/mL. Samples (in triplicate for each condition) were placed in the bacterial solutions for 2 h at room temperature and then rinsed in three water baths. Samples were incubated under 1% LB agar (VWR) gel overnight, and the number of colonies counted to determine the ability of viable bacteria to attach to each sample. Adhesion assays in PBS

were identical, except that the final resuspension occurred in PBS and the incubation period occurred at 37°C with shaking. For all experiments, samples with few colonies were counted by hand. For more densely populated slides, at least 10 digital images per sample were acquired with a 4x objective using an inverted optical microscope (Leica).

5.2.7 Colony Image Analysis

To determine colony size and density (#colonies/cm² of substrata), image analysis was conducted using ImageJ (Rasband, W.S., ImageJ, National Institutes of Health, Bethesda, Maryland, USA, <http://rsb.info.nih.gov/ij/>, 1997-2004) as bundled and distributed free of charge by the Wright Cell Imaging Facility (<http://www.uhnresearch.ca/facilities/wcif/download.php>). Images were converted to 8-bit binary format and flattened using a pseudo-flatfield filter to normalize the luminescence across the image field. When necessary, the ImageJ standard watershed algorithm was applied to separate intersecting colonies, thus facilitating more accurate colony counts. Colony densities were determined by normalizing the mean colony number per image by the calibrated total image area.

5.3 Results and Discussion

5.3.1 Substrata Mechanical Stiffness Can Regulate Adhesion of Viable *S. epidermidis* Bacteria

5.3.1.1 Bacterial Colonization can be Reduced by Material Substrata Modifications

Although the competing mechanisms remain unclear, a large body of data suggests that both physical and chemical modifications of a material surface can be engineered to limit bacterial colonization (86, 89, 166-168, 170, 172-174, 198). For example, as shown in Fig. 5.2, coating surgical-grade titanium alloy with a synthetic polymer film reduced the density of waterborne *S. epidermidis* bacteria colonies by orders of magnitude after immersion in 10^7 bacteria/mL. Reduced colonization over both 2 h and 4 h incubation timescales is relevant to medical procedure durations such as cardiac assist and orthopedic implant devices (208). This polymer film comprised a PEM of poly(allylamine hydrochloride) (PAH) and poly(acrylic acid) (PAA) ionically crosslinked through layer-by-layer dipping of the titanium into polycation and polyanion solutions at pH 2.0 (see Section 5.2.1) prior to full hydration and equilibration in sterile deionized, distilled water.

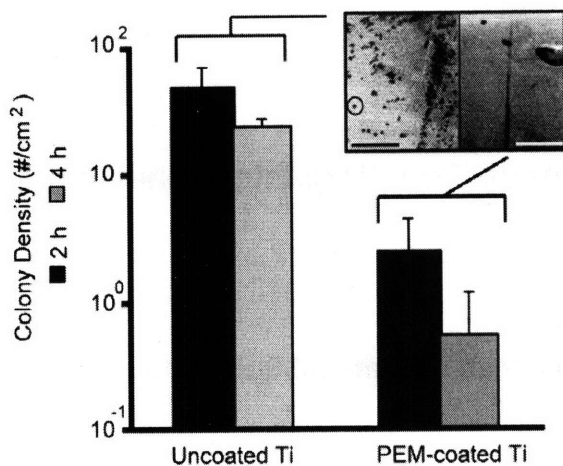


Figure 5.2 PEMs reduce bacterial adhesion on medical grade titanium Adhesion of waterborne *S. epidermidis* is reduced by coating with a pH-tunable polyelectrolyte multilayer (PEM) film of PAA and PAH assembled at pH 2.0, and is stable at both 2 h (inset; circle indicates one such colony) and 4 h incubation duration. Scale bars = 5 μ m.

5.3.1.2 Weak Polyelectrolyte Multilayers Modulate Stable Adhesion of *S. epidermidis* Bacteria

To consider how modifications of the substrata assembly conditions might affect *S. epidermidis* colonization, we then considered these substrata assembled at assembly pH extremes of 2.0 or 6.5. Assembly of these weak PEMs at pH 2.0 results in substrata of much lower stiffness (effective elastic modulus $E \sim 1$ MPa) than at pH 6.5 ($E \sim 100$ MPa) (46). As shown in Fig. 5.3A, for a 2 h incubation of substrata in seeding concentrations ranging from 10^3 to 10^8 bacteria/mL of 150 mM NaCl phosphate buffered saline, average colony density (number of colonies per unit substrata) was greater on mechanically stiffer substrata. For a given seeding concentration, the average colony size observed after 24 h culture was also much greater on the more compliant substrata; this suggests that the properties of these substrata affected bacterial adhesion and/or colony growth. Figure 5.3B indicates

that the observed differences in colony density occurred at the adhesion step: colony size depended on colony density for both substrata. In other words, the initial bacterial attachment increased with increasing substrata stiffness, but the subsequent colony growth was likely limited by available space and nutrients post-adhesion.

In order to consider the characteristics of the polymer substrata that directly affect attachment of *S. epidermidis*, we conducted a larger study in deionized water to eliminate possible charge shielding and reorganization of the ionic crosslinks

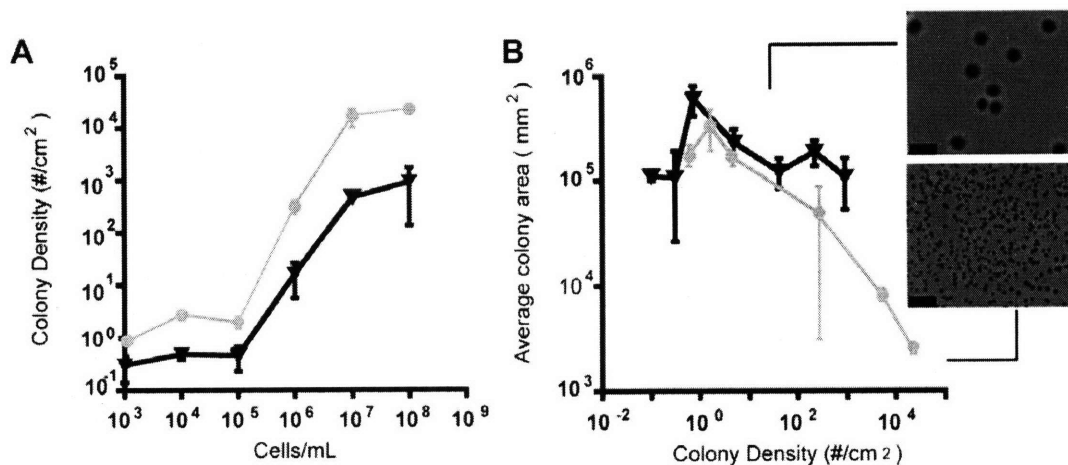


Figure 5.3 Bacterial colonies observed for $10^3 - 10^8$ *S. epidermidis*/mL in 150 mM NaCl PBS (A) Average colony number per unit substrata area increased with increasing incubation concentration for greater than 10^5 cells/mL; for all concentrations, the density of colonies observed on the PEM substrata assembled at pH 6.5 (●) was significantly greater than that observed on the substrata assembled at pH 2.0 (▼). (B) For given initial concentration, colony number was greater and colony size was smaller on stiffer substrata, supporting a model whereby bacteria attachment is modulated in part by substrata stiffness, but subsequent growth is affected predominantly by available space and nutrients. Scalebars = 500 μ m.

within the PEM substrata in salt solutions. For the substrata considered, we quantified the mechanical compliance and the physicochemical surface properties considered to affect microbial adhesion.

5.3.1.3 Characterization of Polymeric Substrata Properties

Table 5.1 indicates physicochemical and mechanical characteristics of substrata employed in the larger study. PAA and PAH were adjusted to the same pH (e.g., PAA/PAH 2.0/2.0) as well as to different pH (e.g., PAA/PAH 3.5/7.5) during assembly in order to increase the range of substrata properties. Atomic force microscopy (AFM) imaging of hydrated substrata in tapping mode indicated a range of root mean square (RMS) surface roughness from 3 to 30 nm. AFM-enabled nanoindentation of the PEMs hydrated in deionized water indicated an average elastic modulus E ranging over two orders of magnitude from the stiffest PEMs assembled at pH 6.5 ($E = 80.4$ MPa) to the most compliant PEMs assembled at pH 2.0 ($E = 0.8$ MPa), consistent with our previously reported mechanical characterization of these PEMs in 150 mM NaCl phosphate buffered saline (46).

Surface energies of interaction were calculated according to Van Oss' adaptation of Young's theory (98), which correlates the interfacial tension and surface energy of interaction between materials in a solvent. Four solvents of disparate surface tension and polarity were used (Section 5.2.3). The apolar and polar components of this surface tension relate to the Lifshitz-van der Waals and

Lewis acid-Lewis base (charge transfer) character of each sample, respectively; both interactions are thought to influence bacterial adhesion (98). Thermodynamic properties at the PEM-liquid interface have been characterized using the Van Oss approach to describe the assembly process, but to our knowledge have not been applied in the context of microbe-water-PEM (MWP) interactions (83). The surface interaction energy ΔG_{MWP} for all PEM substrata considered narrowly ranged from 26-29 mJ/m² and were statistically indistinguishable for the case of *S. epidermidis* (see Chapter 2.6 for more thorough discussion of the Van-Oss method and parameter variation. A complete list of the energy component values for all solvents used in this thesis, including supplemental parameters used in the calculation of ΔG_{MWP} , is detailed in Appendix A.3)

To avoid the previously described problems associated with MB dye incorporation (Section 2.7), dye based assays were abandoned in favor of techniques that might afford molecular control over the polymer charge density. Bacterial adhesion was assayed on surfaces comprised of self-assembled monolayers (SAMs) synthesized from mixtures of 11-mercapto-undecanoic acid (MUA), and either decane thiol (DT) or octane thiol (OT) attached to Cr/Au coated glass slides (105). We reasoned that charge density control would occur via adjustment of the MUA: DT ratio at the assembly step, and further control would be afforded by pH adjustment at the time of bacterial challenge, if necessary. We assayed a suite of SAMs with MUA compositions ranging from 0-100% (0, 10, 25, 50, and 100%, plus a non-coated Au-control). However, after three separate

adhesion tests, *S. epidermidis* showed no discernible positive or negative pattern of adhesion to the SAMs.

Assembly pH (PAA/PAH)	Symbol	ΔG_{MWP} (mJ/m ²)	ΔG_{MWP} (mJ/m ²)	[RMS] (nm)	<i>E</i> (MPa)
		<i>S. epidermidis</i>	<i>E. coli</i>		
2.0/2.0	▼	29.0 ± 7.5	36.6 ± 7.4	30.2 ± 29.5	0.75 ± 0.05
6.5/6.5	●	27.2 ± 8.95	35.6 ± 8.9	2.7 ± 1.6	80.4 ± 38.0
3.5/7.5	◆	27.2 ± 8.0	35.9 ± 7.98	12.2 ± 9.0	36.6 ± 5.7
3.5/8.6	■	27.0 ± 6.9	35.8 ± 6.93	18.5 ± 16.6	73.2 ± 16.6

Table 5.1 PEMs used to test physicochemical and mechanical properties affecting bacterial attachment Assembly pH of polyanion and polycation indicated, respectively, for PEMs assembled to ~50 nm dry thickness (≥ 57 nm hydrated thickness) with PAA as the last layer. All properties measured in deionized water. Total interaction energy ΔG_{MWP} of the microbe-water-polymer system, interaction energy for *microbe*-water-PEM are listed as indicated; root mean square (RMS) surface roughness; and nominal elastic moduli *E*. Data expressed as average \pm standard deviation. Symbols used throughout to indicate the corresponding PEM in all figures.

Due to the inconclusive results, this approach was abandoned. An alternative approach to controlling surface charge density involving chemical quenching of COOH groups through EDC assisted esterification was attempted. Several reaction conditions were effective in chemically blocking the COOH groups, but in all cases nanomechanical indentation showed significant stiffening of the films by a factors ranging from ~10-100 fold.

Our focus shifted to direct measurement of electrostatic properties of hydrated PEMs. To assess net surface charge density Q present at the fluid-PEM interfaces, the substrata assembled at pH extremes of 2.0 and 6.5 were probed in deionized water using a carboxylated colloidal sphere approximately the size of a few bacteria (3 μm radius; particle size from BioForce Nanosciences, Ames, IA). As PEM assembly relies on charge over-compensation to increase substrata thickness, one might expect the observed net-negative Q because the anionic polymer, PAA, was layered last. However, it is important to note that although these polymeric substrata are termed multilayers due to the layer-by-layer assembly process, the structure is not striated and the polyanion and polycation macromolecular chains are highly entangled. As shown in Fig. 4D, charge densities of PEMs assembled at pH 2.0 and 6.5 were well within one standard deviation ($Q = -2.29 \pm 0.1 \text{ mC/m}^2$ and $-3.18 \pm 1.4 \text{ mC/m}^2$, respectively). Q was unchanged in solutions of higher ionic strength such as 150 mM NaCl PBS, although charge is effectively screened in such ionic solutions.

In summary, the nominal elastic moduli of these substrata varied over nearly two orders of magnitude, while the other reported physicochemical characteristics regulating bacterial adhesion varied to a known or statistically indistinguishable extent. We confirmed that these surface properties were unchanged when the substrata were hydrated over the timescales of the bacterial incubation assays discussed below.

5.3.1.4 *S. epidermidis* Adhesion Modulated Chiefly by Substrata Mechanical Compliance

We employed the above ensemble of substrata in a 2 h incubation of 10^7 cells/mL in deionized water and observed the average colony density following 24 h culture under 1% agar. *S. epidermidis* remained viable in ion-free suspensions well in excess of the duration of the attachment assays. Figure 5.4A demonstrates strong positive correlation between the substrata elastic moduli and colony density, with an approximately 100-fold increase in colony density for a 100-fold increase in substrata stiffness.

Since substrata stiffness may be correlative with physicochemical surface interactions that more strongly or more directly affect this initial bacterial adhesion, we also considered correlations with surface roughness, total interaction energy, and charge density. The RMS surface roughness varied among the substrata from 3 to 30 nm, yet Fig. 5.4B indicates no discernable effect on bacterial attachment over this range and distribution of surface roughness. Figure 4C shows that the

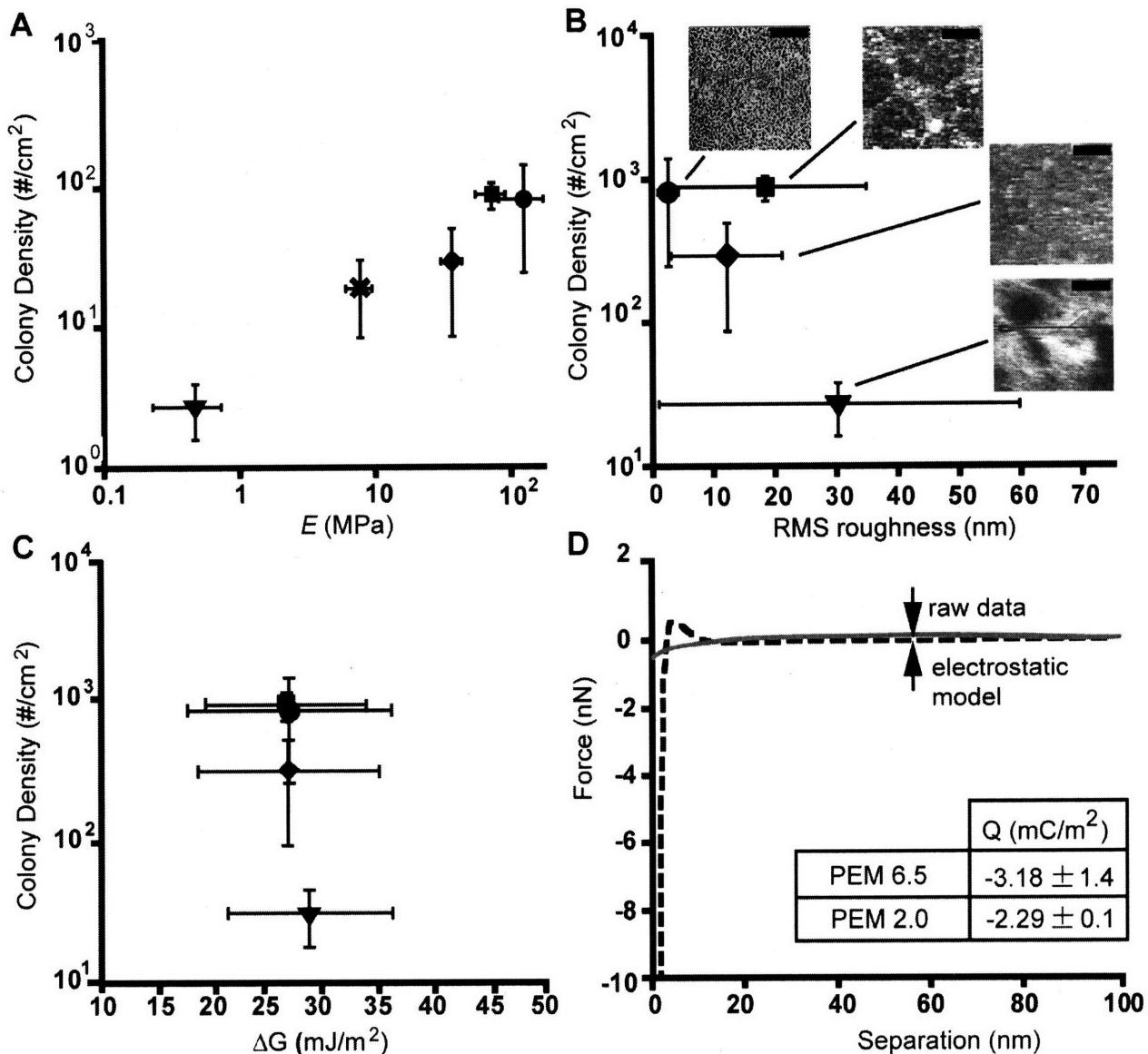


Figure 5.4 Colony density as a function of various surface parameters (A) Colony density varies directly with substrata elastic moduli E . All sample differences statistically significant (1-way ANOVA, $\alpha = 0.05$, $P = 0.0059$). (B) Colony density is independent of RMS surface roughness of the substrata. Scale bar = $5 \mu\text{m}$. (C) Total interaction energy ΔG_{MWP} for the microbe-water-PEM system is statistically indistinguishable among all substrata considered (1-way ANOVA, $\alpha = 0.05$, $P = 0.987$). (D) Surface charge density Q , as measured via electrostatic repulsion of a carboxylated spherical probe in Milli-Q water (see Methods), is within standard deviation for PEMs assembled at pH 2.0 (compliant) and pH 6.5 (stiff). Representative charge repulsion curve (solid) and constant-surface-charge model fit (dashed) are shown. Symbols refer to the following PEMs: PAA/PAH 2.0/2.0 (∇), 4.0/4.0 (\times) in A to consider intermediate substrata stiffness, 6.5/6.5 (\bullet), 3.5/7.5 (\blacklozenge), and 3.5/8.6 (\blacksquare).

surface interaction energy of the *S. epidermidis*-water-PEM system ΔG_{MWP} was statistically indistinguishable (1-way ANOVA, $\alpha = 0.05$, $P=0.987$) among these mechanically dissimilar substrata. Finally, we found net surface charge density to

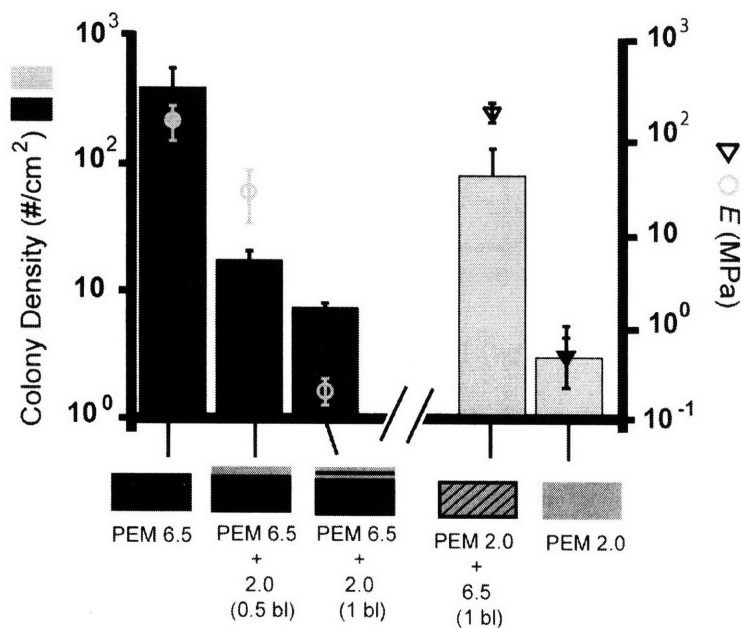


Figure 5.5 Multilayer addition to modulate composite substrata stiffness Addition of 0.5 and 1 bilayer of PAA/PAH at pH 2.0 onto a stiff PEM (pH 6.5) decreases the effective mechanical stiffness of the substrata (grey circles) and decreases the bacterial colony density (black columns). Addition of one bilayer of pH 6.5 PAA/PAH to a compliant PEM (pH 2.0) increases effective stiffness (black triangles) and bacterial colony density (grey columns). Substrata were incubated with bacteria at concentrations of 10^7 cells/mL for 1 hr. We observed statistically significant differences in the colony densities among the masked PEM 6.5 substrata and among the masked PEM 2.0 substrata, respectively. The stiffness of substrata in this graph are specific to this batch and differ from those reported in the table. (1-way ANOVA, $\alpha = 0.05$ with $P = 0.00027$ and 0.0031 , respectively).

be quite similar for the two substrata that differed most in both surface roughness and mechanical compliance (PEMs assembled at pH 2.0 and 6.5). In fact, Fig. 4D shows that the slight interfacial electrostatic repulsion of these PEMs in deionized water (~ -3 mC/m²) extends less than 20 nm from the PEM surface. This interaction distance is small compared to the projected length of

bacteria fimbriae or pili that extend 500 to 1000 nm from the bacterial cell surface (1, 189, 190), suggesting one mechanism by which bacteria overcome such electrostatic repulsion. Thus, at least for substrata of comparable surface interaction energies and charge density, it appears that adhesion of viable *S. epidermidis* can be modulated by the mechanical stiffness of the substrata. For the physicochemical properties quantified here, *S. epidermidis* colony density increases with increasing substrata stiffness over the range of $1 \text{ MPa} < E < 100 \text{ MPa}$.

To further test this hypothesis, we leveraged the tunability of layer-by-layer assembly to gradually alter effective compliance of the PEM surface. After

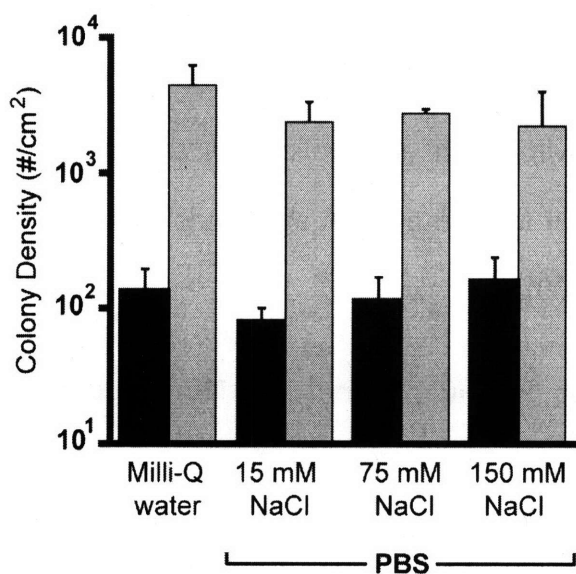


Figure 5.6 Bacterial colony density on compliant substrata (black, $E \sim 1 \text{ MPa}$) is lower than that on stiff substrata (gray, $E \sim 100 \text{ MPa}$), regardless of solution monovalent ion concentration in which 10^7 cells/mL incubated with substrata.

assembling stiff substrata at pH 6.5, we then added 0.5 and 1 bilayer of the compliant PEM at pH 2.0; after assembling compliant substrata at pH 2.0, we added 0.5 bilayer of the stiff PEM at pH 6.5. As expected, E of the stiff PEM surface decreased upon addition of compliant layers from the extrema of $E \sim 100 \text{ MPa}$ (pH 6.5) to $\sim 30 \text{ MPa}$ (pH 2.0, 0.5 bilayer),

and ~ 1 MPa (pH 2.0, 1 bilayer). Effective E of the compliant PEM increased to $E \sim 100$ MPa when topped with PAH 6.5, due ostensibly to polycation interpenetration and crosslinking (136). Figure 5.5 demonstrates that by changing the effective substrata compliance through this approach, *S. epidermidis* colony density progressively decreased with increasing PEM compliance. The assembly of such composite films has the potential to alter other surface characteristics within this substrata set, but the strong correlation between effective substrata stiffness and colony density is retained. This gradual masking of mechanoselective adhesion is consistent with previous studies on eukaryotic cells (47), but is observed here after addition of just a single compliant polyelectrolyte layer; decreased adhesion of fibroblasts is not observed until addition of at least five bilayers of the compliant PEM to the stiff PEM. This may be attributed in part to the increased forces and distances over which eukaryotic cells can strain the underlying substrata through actomyosin traction at focal adhesions of diameters comparable to a single bacterium (81, 209).

5.3.1.5 Mechanoselective Adhesion is Independent of Monovalent Ion Concentration.

To consider whether the presence of the monovalent ions in 150 mM NaCl phosphate buffered saline (PBS) strongly affected the observed trends, bacterial attachment to the most mechanically distinct PEMs (assembled at pH 2.0 and 6.5) was monitored over a titration of salt concentrations. Solution molarity of 150 mM

approximates physiological ionic strength, and the absence of Ca^{2+} and Mg^{2+} ions approximates low extracellular calcium levels predominantly complexed with serum albumin or negative ions (210). Figure 5.6 shows that there is no major change in colony density with increased solution ionic strength (pure water to 150 mM NaCl PBS). More generally, this suggests that the molecular agents involved in this mechanosensation are not sensitive to monovalent ionic strength changes over this broad spectrum. Additionally, the Debye screening length, the distance from the substrata surface over which electrostatic effects extend through the aqueous media, is a function of the ionic strength and is ~ 100 nm in water and < 1 nm at the highest ionic strength assayed (98). One may reasonably conclude that the effect of surface charge density and its associated free energy on bacterial adhesion are negligible under all solution molarities in this system, since there is no significant change in the adhesion response as the screening length is modulated across different length scales. This titration result is particularly interesting in light of recent hypotheses that bacterial sensing of mechanical stimuli may occur through stretch-induced activation of transient receptor potential (TRP) ion channels (18-20). Our results suggest that TRP channels are not required.

Alternatively, it is possible that bacterial fimbriae/pili mediate a mechanoselective process similar to the so-called catch-bond mechanism posited to explain effects of shear flow stress on cell adhesion dynamics: lifetime of noncovalent interactions can be increased under external mechanical force (14, 19, 22). As bacterial pili collide with and sample substrata during incubation, the

mechanical resistance of the material to pili retraction would increase with increasing substrata stiffness; this stabilization on stiffer substrata could increase the lifetime of pili-substrata interactions during the fast step of bacterial two-stage binding kinetics (1). *S. epidermidis* possesses several glycosylated substructures at both the pili and extracellular capsule (189, 190) known to form attachments to materials and capable of complex interactions similar to those observed in other bacterial species that form pili catch-bonds. Together, these results do not invalidate the physicochemical effects reported to influence microbial adhesion. Clearly, several competing surface features affect bacterial adhesion, viability, and subsequent colonization. Rather, the current study demonstrates that mechanical compliance of the substrata presents an important additional factor.

5.3.2 Substrata Mechanical Stiffness can Regulate Adhesion of Viable Wild-type *Escherichia coli* K-12 Bacteria and a $\Delta mreB$ Spherical Mutant

5.3.2.1 *E. coli* Adhesion Modulated Chiefly by Substrata Mechanical Compliance

Our previous experiments demonstrated that adhesion of the Gram (+) bacterial species *S. epidermidis* to weak PAA/PAH PEMs of varying assembly pH scaled predominantly with increasing elastic modulus (E) of the PEM thin film, while moderate effects on adhesion due to PEM surface chemical properties were

also observed. The pH tunable control of adhesion in *S. epidermidis* raises the possibility that other bacterial species may respond in a similar way when challenged with materials of differing stiffness. The physical and chemical makeup of the bacterial cell surface is a critical determinant for adhesion to a given material in most bacterial species (86, 93).

To determine whether our results could be extended to other species of bacteria, the adhesion profile of the Gram (-) rod *E. coli* species K-12 was assayed using the same suite of PEMs used to test adhesion of *S. epidermidis*. PEMs with variable stiffness were incubated in the presence of *E. coli* according to the bacterial attachment protocol described above. The *E. coli* strain designated w3100 was chosen because it represents a common lab standard with a well documented lineage (211).

Cells were incubated for 2 h in deionized water with a seeding concentration 0.5×10^7 cells/mL, and following 24 h culture under 1% agar the average colony density was recorded. Representative morphology for colonies grown on the two extreme PEM samples is shown in Figure 5.7A-B, as observed with a 4x objective microscope. Final colony density of *E. coli* is significantly lower on compliant PEMs (5.7B) than that of stiffer substrata (Fig. 5.7A), and scales directly with E for all PEMs tested. For the two extreme PEM samples, PEM 2.0/2.0 and 6.5/6.5, there is ~ 1000 fold decrease in final colony density for a ~ 100-fold reduction in E (Fig. 5.7C). Surface RMS roughness does not show any clear correlation to final colony density (Fig. 5.7D); and surface interaction energy for the *E. coli*-water-PEM

system ΔG_{MWP} (Fig. 5.7E), was also not an attributable factor to this adhesion

response

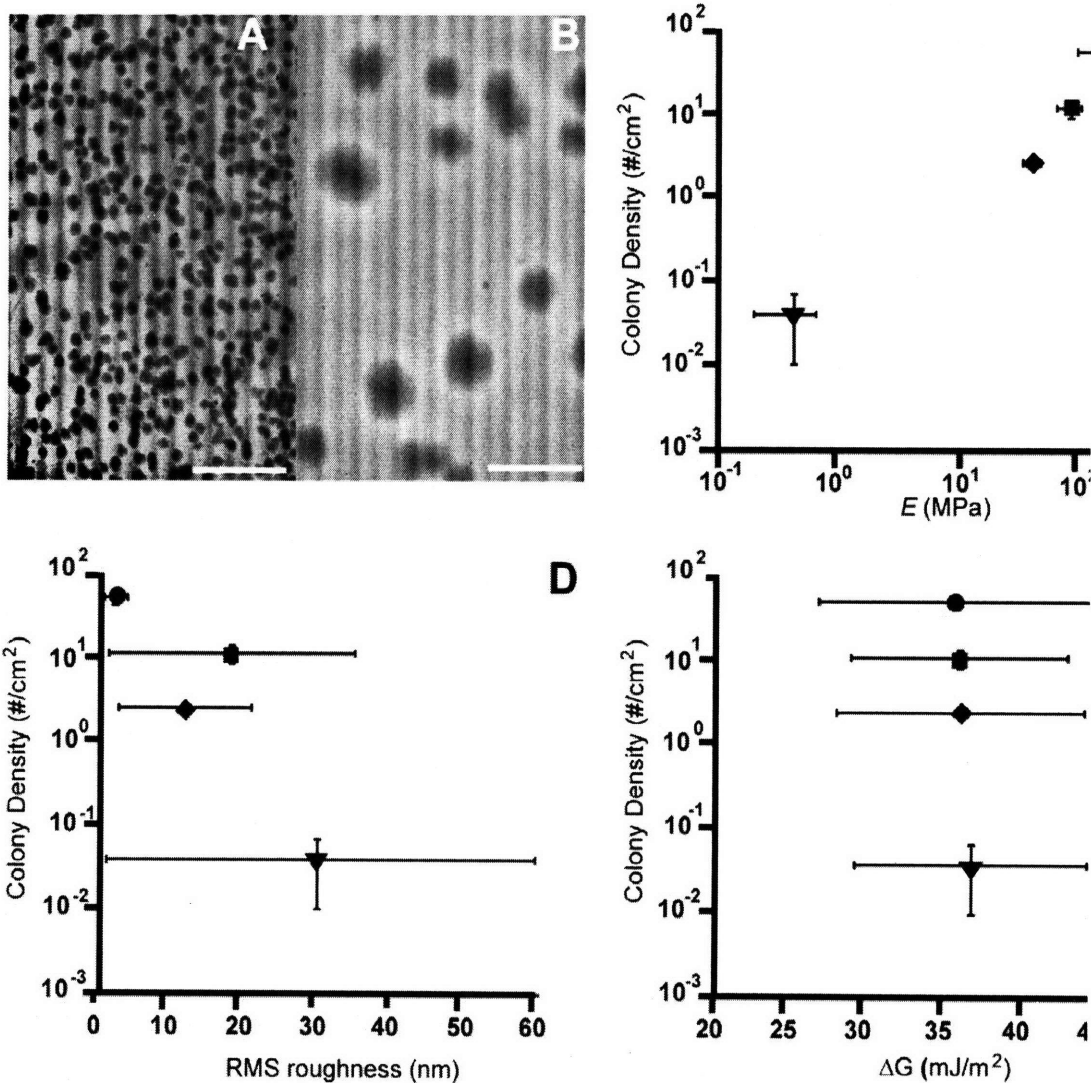


Figure 5.7 Colony density as a function of various surface parameters

Fig. (A-B) Representative colonies for wild-type *E. coli* K-12 on PEM 6.5 (stiff) and PEM 2.0 (compliant), respectively. Scale bar = 1 mm. (C) Colony density varies directly with substrata elastic moduli E . (D) Colony density is independent of RMS surface roughness of the substrata. (E) Total interaction energy ΔG_{MWP} for the microbe-water-PEM system. Symbols refer to the following PEMs: PAA/PAH 2.0/2.0 (▼), 6.5/6.5 (●), 3.5/7.5 (■), and 3.5/8.6 (◆).

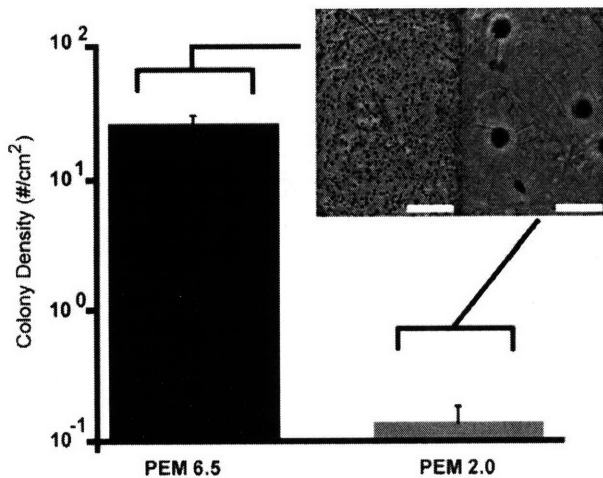


Figure 5.8 Adhesion of $\Delta mreB$ *E. coli*
 Final colony density for spherical mutant $\Delta mreB$ *E. coli* cells grown on PEM 6.5 (black, stiff) versus PEM 2.0 (gray, compliant.) Inset: Representative photos of colonies grown on PEM 6.5 (left), and PEM 2.0 (right). Scalebar = 1 mm.

While *E. coli* adhesion is proportionally more sensitive to changes in the substrata mechanical stiffness than the adhesion observed for *S. epidermidis*, it should be noted that the overall final colony density for *E. coli* is higher than that of *S. epidermidis* for all PEMs tested. Chemical and physical properties of the

bacterial cell surface are reported to play a role in adhesion, and these results do not rule the possibility that such properties have a weak effect on adhesion. The differences in chemical composition between *S. epidermidis* and *E. coli* both inside and outside of the cell are extensive (see Section 5.1.2).

There is also a clear difference in shape between *S. epidermidis*, a spherical cell and *E. coli*, a rod-shaped cell. It is interesting to note that rod-shaped *E. coli* has a surface area ranging from 2-8 fold that of *S. epidermidis* (assuming a spherical *S. epidermidis* cell, average radius ~ 0.5 μm) (185, 212). One possible explanation for increased adhesion of rod-shaped *E. coli* versus spherical *S. epidermidis* shaped may be that increased surface area assists formation of

adhesive interactions with material surfaces. Clearly, studies were needed to address either the cell shape or the exterior cell composition before attributing this relative increased sensitivity solely to mechanoselective adhesion.

One approach would be to culture G(+) rods, such as *Bacillus subtilis* using the same suite of PEMs and comparing the adhesion of *Bacillus* to that of *E. coli*. However, *Bacillus subtilis* exhibits even more complicated cell behavior than *E. coli*, in that it exists in several morphological states under normal culture conditions; undergoes sporulation at high cell density or under cell stress; and it grows fibril-like colony structures that would complicate determination of final colony density because colonies could grow normal to the PEM surface (183). The approach described below involves using a spherical mutant of *E. coli*, one lacking the actin homolog *mreB*. Using *mreB*-depleted cells, one can test whether the physical difference in cell shape between the two species have any relationship to the differing adhesion profiles, while preserving many of the cell surface chemical differences between the two cell types.

5.3.2.1 Adhesion of a Spherical *E. coli* Mutant Lacking Actin-like MreB is Modulated Chiefly by Substrata Mechanical Compliance

As described above, the actin homologue *mreB*, a genomic element from the *mreBCD* operon essential for *E. coli* survival (181, 182), is responsible for the rod-like shape in wild type (wt) *E. coli* (39, 181, 182). When this operon is knocked

out in *E. coli* cells with concomitant overproduction of the tubulin analogue *ftsZ*, the resultant cell population survives with total loss of their rod-like shape and adopt a spherical morphology (schema 3) similar to *S. epidermidis* (181, 182). Thus, *mreB* knockout *E. coli* ($\Delta mreB$) can be used to directly test the effect of cell shape on cell adhesion on tunable PEMs.

Final colony density for PEM 6.5/6.5 and PEM 2.0/2.0 challenged with $\Delta mreB$ assay is shown in Figure 5.8. The insets depict the representative colony morphology under 4x objective magnification, and show no marked difference in size or morphology between $\Delta mreB$ colonies plated on PEMs and those of *S. epidermidis* or wt *E. coli*. These results demonstrate ~100 fold reduction in adhesion with ~ 100 fold decreases in *E*, a trend similar to *S. epidermidis* adhesion to the same class of PEMs. Thus, the relative sensitivity to changes in substrata *E* is similar for both spherical cell types used in this study, regardless of species and despite tremendous differences in extracellular envelope composition. However, it has been established that stable *mreB* mutants have ~ 2-fold reduced range of viability; and can swell to a radius of 1 μm (181). Therefore it is reasonable that a reduction in final colony density could arise as a consequence of reduced viability of adherent bacteria. However, the quantitative effect of such a reduction is unknown. Additionally, *mreB* mutants with the swollen phenotype will have comparable surface area to wild type *E. coli*. As yet, it is not clear how such a state affects other physical and chemical properties of the cell, particularly factors influential for cell adhesion. Thus, while spherical *E. coli* cells demonstrate a

quantitatively similar shift in adhesion to PEMs upon changes in substrata stiffness E as that seen in *S. epidermidis*, without further study one cannot rule out the possibility this apparent shape effect is coincidental. Moreover, the adhesion profiles for both strains of *E. coli* are quantitatively greater than that observed for *S. epidermidis* exposed to PEMs. Nevertheless, it is clear from the adhesion assays that the trend in bacterial adhesion in both wt and $\Delta mreB$ *E. coli* scales directly with increasing substrata stiffness and, consequently, that this effect cannot be attributed solely to factors in the cellular envelope or to cell shape.

5.4 Summary

The experiments described in this chapter demonstrate that mechanical compliance of material surfaces represents an additional design parameter by which colonization of both beneficial and potentially infectious bacteria can be modulated. We find that the adhesion of viable, colony forming *S. epidermidis*, *E. coli*, and spherical *E. coli* strain MC1000 $\Delta mreB$ correlates positively with increasing elastic modulus of weak polyelectrolyte multilayers, over the range $1 \text{ MPa} < E < 100 \text{ MPa}$. These observations were not attributable to differences in posited physicochemical regulators of bacterial adhesion, including RMS surface roughness, surface interaction energy, and surface charge density of the PEM thin films.

Similar trends in bacterial adhesion were observed for Gram(+) *S. epidermidis* and Gram(-) *E. coli*, demonstrating that physical properties of the extracellular region of the sacculus cannot be solely responsible for this mechanosensory response. For the bacteria concentrations considered, neither divalent ions nor monovalent ions such as Na^+ and Cl^- are required for this mechanosensory function, suggesting that activation of TRP ion channels is not required for mechanoselective adhesion of *S. epidermidis*. Although the underlying mechanisms require further study, it is clear that the mechanical stiffness of nanoscale polymeric substrata can strongly modulate adhesion of viable bacteria in aqueous suspensions, independently of several other interactions at the cell-material interface. Moreover, resistance to bacterial adhesion occurs on PEM coated medical grade titanium over a time course relevant to many common surgical implantation procedures, a promising result that suggests a possible role for PEMs as tools in the clinical setting.

CHAPTER 6 CONCLUSIONS AND DIRECTION FOR POTENTIAL FUTURE PROJECTS

A detailed, molecularly-based understanding of how cells respond to extracellular chemomechanical cues is of great importance to the field of applied cell biology and biomedical engineering. The studies in this thesis were designed to quantify the effects of substrata-defined mechanical and chemical cues on behavior of cells adhered to those substrata. These studies were successful in demonstrating a direct relationship between PEM substrata stiffness and cell adhesion in eukaryotic cells. In the broader context of cell biology, the VEC studies clearly indicate that the concept of mechanotransduction arising from anchorage-dependent mechanical forces between the cell and extracellular environment should be considered in the analysis of cell behavior, and this phenomenon is now widely recognized within the field of cell biology.

The second major aspect of this thesis dealt with interdependency between extracellular chemical and mechanical signals in eukaryotic cell adhesion. The experimental approach taken relied upon the unexpected change in mechanical properties of PEMs upon adsorption of a cationic polymer PAH, compared to addition of the same polymer via polymer-on-polymer stamping. The most notable result was that cells were able to respond both to chemical cell-adhesion promoters and to mechanical cell adhesion signals, despite the presence of cytophobic signals (RGE peptide) or mechanically unfavorable conditions (RGD

peptide conjugated to compliant films). This result indicates that mechanical and chemical cues can be utilized independently or in tandem to control the adhesion of eukaryotic cells to polymer film-coated materials.

Finally, the first systematic study of chemomechanically modulated adhesion of prokaryotic cells is described in this thesis. The results thus described show a clear dependence of microbial adhesion on substrata stiffness E for the G(+) bacterium *S. epidermidis*. Subsequent experiments with *E. coli* demonstrated that this response can be generalized beyond the single species of *S. epidermidis*, across the two classes of G(+) and G(-) bacteria. Issues such as the effect of bacterial shape and the associated intracellular shape-inducing elements on mechanoselective adhesion; the comparison of mechanically modulated attachment as a function of differences in Gram (+) and Gram (-) bacterial cell envelopes; the role of *TRP* ion channels, which are known to be mechanically activated; and the time dependence of the adhesion response were all addressed. In each case, subsequent observations supported the initial findings that the adhesion of viable bacterial species correlates directly with quantifiable differences in stiffness of the substrata with which the bacteria were incubated. The results thus far are insufficient to make broad claims on the exact mechanism of mechanosensation in bacteria, and require further studies to detail the response element more generally. Future work should address the mechanistic process that controls the observed mechanoselective adhesion. A thorough understanding of the prokaryotic chemomechanical response element, and mapping the mode by

which bacteria are capable of detecting differences in surface material properties have strong potential to affect the way in which bioengineers approach problems in microbiology. This mechanistic and predictive understanding would influence the manner in which clinicians approach prevention and treatment of bacterial infection, and could direct subsequent design of material systems aimed at exploiting this chemomechanical response element. A complete study of the prokaryotic response to mechanical stress is a considerable undertaking, but a reasonable starting point includes verification of the generality of mechanoselective adhesion in several representative species of bacteria. The relevance of this finding in relation to the biomedical field was described herein with respect to hospital acquired infections. Future studies should also focus on other outstanding health-related issues, such as bacterial contamination, water purity and the crisis of microbial related diarrheal diseases, the latter of which cause an estimated 3-4 million deaths per year (213).

Overarching goals of this thesis research include harnessing the principles gleaned from observations made using this model system towards development of alternative therapeutic approaches or new materials suitable for use in clinical settings. Such applications could include chemically and mechanically optimized vascular tissue engineering, for example. Alternatively, one could envision using mechanical guidance for the prevention or stimulation of angiogenesis, in concert with traditional chemical inhibitors/stimulants. On a more fundamental level, the field of developmental biology will greatly benefit from a clearer understanding of

how mechanical forces influence developmental processes, and whether such forces guide cells along particular lineage fates. As previously mentioned, the molecular agents involved in active remodeling of the eukaryotic cytoskeleton are also participants in the MAPK kinase cascade. This signaling pathway is part of a phosphorylation cascade that results in the activation of effector proteins in the cytosol, and of transcription factors in the nucleus. A thorough map of the molecular pathways would provide new strategies for controlled engineering of vascular tissues, potential alternative control points during angiogenesis that are independent of small molecule approaches, and could lead to a broader understanding of eukaryotic response to mechanical stimuli.

Understanding the molecular, physical, and mechanical basis for microbial adhesion to surfaces has even broader applications. The benefit to general molecular and cellular biology is comparable to that described for eukaryotic cell mechanotransduction above. However, as described in Chapter 5, the medical field would clearly benefit from a detailed knowledge of the factors controlling surface adhesion of microbes, since it follows that technologies developed to limit bacterial adhesion may be able to decrease overall transmission of some of the most clinically dangerous bacterial species. However, in cases where microbes are of benefit, technological platforms might be developed that enhance bacterial adhesion either for capture in, say, systems of genetically engineered protein expressing microbes; or for stabilization of long-term bacterial beds, wherein the

microbes produce and possibly excrete some beneficial side product (e.g., petroleum products) or break down toxic refuse.

As understanding of mechanistic principles governing mechanoselective behavior advances, the applications for both eukaryotic and prokaryotic in the field of mechanotransduction will multiply. This thesis work was conducted with that goal in mind. The contributions described in this thesis have provided new examples of cell types that display mechanoselective behavior on well-characterized polymeric substrata. Furthermore, new insight into material processing effects on mechanical stiffness serves to inform studies in this area. Finally, the demonstration of mechanoselective adhesion in cell types evolutionarily primitive to human derived cells, such *S. epidermidis* and *E. coli*, represent a significant advance in our understanding of the breadth of mechanoselective cell adhesion.

APPENDIX A.1 SOURCE CODE FOR DATA EXTRACTION FROM MFP EXPERIMENT FILES

****Note:** Portions of this code are currently non-functional, but will be utilized in upcoming additions to the MFP operating software (MFP XOP.) The procedure file itself was fully operational at the time of data collection, but may now be obsolete due to the periodic updates to both the MFP XOP program that runs in IGOR and Asylum Research upgrades to both hardware and IGOR software versions. This is true for all IGOR code presented in this thesis. When operational the procedure file creates a graphical interface that allows the MFP user to extract any type of data file obtained from force pull experiments for use in offline analysis programs; the procedure can also be called from the command line or the “MFP & Controls” menu option. Very little commenting is including in the code itself, because the commands are basic IGOR function calls. Anyone who has completed the Wavemetrics tutorial required to learn how to use IGOR, will be able to understand and run this code with functional MFP XOP builds.

The data file architecture employed by Asylum Research combines the x-y data into a single file, and adds to that an attached record of the instrument variables at the time of file creation (termed the wave note). The presence of the wave note and the combined x-y wave data can complicate offline analysis in other programs. Consequently, this extraction procedure creates two new binary files for each native binary wave file extracted corresponding to the X- and Y-waveforms;

the wave note is preserved in all binary data files. If subsequent analysis is not performed in IGOR, then the files must first be saved using this program, loaded again as individual binary files in IGOR, and then exported in the appropriate format. This can all be done in the same packed experiment file (file extensions labeled .pxp, the file created by IGOR.exe).

File name:"SaveMyForce2007.ipf"

Menu "MFP &Controls"

"SaveMyForce",SaveMyForce("",0)

"GUI ForceSaver",GUISaver()

end

//function creates Gui file save Box

function GUISaver()

NewPanel /W=(420,80,720,200)

DoWindow/C ForceSave

ModifyPanel cbRGB=(15535,44607,42768)

SetDrawEnv fsize=15

DrawText 20, 20, "Save force curves to the disk by data type"

Button

button0,pos={85,35},size={120,25},proc=SaveButton,title="SaveForce Curve"

End

```

function TempHolder()
    NewPanel /W=(420,80,720,200)
    DoWindow/C TempHold
    ModifyPanel cbRGB=(15535,44607,42768)
    SetDrawEnv fsize=15
    DrawText 20, 20, "Function not ready yet, jerk!"
End

function SaveButton(ctrlName) : ButtonControl
    String ctrlName

    //String ofolder = GetDataFolder(1)
    //NVAR numpoints = root:packages:S_MagicBox:gSidepoints
    // sets up possibility to control Ext, Ret features by entering #'s

    SaveMyForce("",0)
End

function SaveMyForce(BaseStr,DoMod)
    String BaseStr
    Variable DoMod

    // Variable NumIn
    // DoAlert 1, "Modify Plots?"
    // variable DoMod = V_Flag
    // Print DoMOd, V_Flag
    // DoMod = V_Flag

```

```

// Print DoMOd, V_Flag
// If (NumIn < 1)

if (!Strlen(BaseStr))
    Prompt BaseStr,"BAseName:"
    DoPrompt "BaseName:",BaseStr
    if (V_Flag)
        return(0)
    endif
endif

NewPath/C/M="Save Force Plots"/O/Q SaveMePath
if ( V_Flag)
    return(0)
endif

String DataFolder = "root:ForceCurves:"
String SavedDataFolder = GetDataFolder(1)
SetDataFolder(DataFolder)
String DataList = WaveList(BaseStr,";",",")

Variable A, nop = ItemsInList(DataList,";")
String DataName
for (A=0;A<nop;A+=1)
    DataName = StringFRomList(A,DataList,";")

```

```

Wave Data = $DataName
if(domod ==1)
    Duplicate/O Data $":Temp:"+DataName
    Wave Data = $":Temp:"+DataName
    if (StringMatch(DataName,"*Defl*") == 1)
        Data *= .1
    elseif (StringMatch(DataName,"*Raw*") == 1)
        Data = 99
    endif
endif
Save/C/O/P=SaveMePath Data as DataName+".ibw"
if (DoMod == 1)
    KillWaves Data
endif
endfor
SetDataFolder(SavedDataFolder)

```

End

```

//•DeflWave[] = ph2_10000[p][1]
//•Duplicate/O/R=[0,DimSize(ph2_10000,0)][1,1] pH2_10000 DeflWave
//•Duplicate/O/R=[0,DimSize(ph2_10000,0)-1][0,0] pH2_10000 RawWave

```

//•Duplicate/O/R=[0,DimSize(ph2_10000,0)/2][1,1] pH2_10000 Defl_EXT

//•Display/K=1 Defl_Ext

//•Duplicate/O/R=[DimSize(ph2_10000,0)/2,DimSize(ph2_10000,0)-1][1,1]
pH2_10000 Defl_Ret

//•Display/K=1 Defl_Ret

APPENDIX A.2 SOURCE CODE FOR LOADING/UNLOADING CURVE EXTRACTION AND SURFACE CHARGE ANALYSIS PRE-PROCESSING

****Note:** Portions of this code related to the trigger point determination, and its use in precisely extracting the loading region were provided by Jason Beemis, Asylum Research. The expected inputs for this macro are the collective force and separation files output from the a single experiment and output from the macro in Appendix A.1. Expected outputs are force and separation files with file structures oriented and truncated for input into the MATLAB code from the Ortiz group (Chapter 2.7). The respective force and separation files can be combined in IGOR using the wave averaging utilities in the standard release to generate a single force and single separation file that represents the experimental “average approach curve”, as descried in Section 2.7.

File name: "ExtensionProc_WorkingV3.ipf"

```
#pragma rtGlobals=0           // Use modern global access method.
```

```
Menu "MFP &Controls"
```

```
    "Extension Extraction", ExtProc("", "", 0, "")
```

```
    "Group Extraction", GroupExt("", "", 0, 0)
```

```
    "Extract Subgroup", SubExt()
```

```
End
```



```

        Prompt Trigger,"Reverse indexing?: "
        DoPrompt "Reverse indexing?: ", Trigger
        if (V_Flag)
            return(0)
        endif
    endif

//*****
*****//

variable numActual = Str2num(num)
String ForceStr = BaseStr
String SepStr = ReplaceString("Force", BaseStr, "Sep")

Make /O/N =(DimSize($BaseStr,0)) Force, Sep
Duplicate /O $ForceStr Force
Duplicate /O $SepStr Sep

// this will flip the orientation of the curves to match the surface-on-right viewpoint.
// if the user does not specify to do it or if this function is called individually from the
// menu or the command line without values.
    if (Flip <1)
        Sep*=-1
    endif

// smooths the data. This could be made optional at some future point.
    smooth 25, Sep, Force

```

```
//*****  
*****//
```

```
String NoteStr = Note($ForceStr)
```

```
// this acquires the note attached to the Forcepull file
```

```
String Indexes = StringByKey("Indexes",NoteStr,":","\r")
```

```
String DirectionList = StringByKey("Direction",NoteStr,":","\r")
```

```
//would be something like:
```

```
//Indexes = "0,631.4,1263.8"
```

```
//DirectionList = "Nan,1,-1,"
```

```
//This means that from point 0 to 631.4 the tip was moving towards the surface
```

```
Variable Start, Stop, Last
```

```
Variable Direction
```

```
Start = str2num(StringFromList(0,Indexes,","))
```

```
Stop = str2num(StringFromList(1,Indexes,","))
```

```
Last = str2num(StringFromList(-1,Indexes,","))
```

```
Direction = Str2num(StringFromList(1,DirectionList,","))
```

```
//Direction tells you which way the tip was moving (1 = towards surface, 0 = dwell, -  
1 = retract)
```

```
//*****  
/
```

```
Make /O/N=(Stop-Start+1) ExtendSep, ExtendForce
```

```
Make /O/N=(Last-Stop) RetractForce, RetractSep
```

```
String ExtF = "EF" + ForceStr
```

```
String ExtS = "ES" + SepStr
```

```
String RetF = "RF" + ForceStr
```

```
String RetS = "RS" + SepStr
```

```
if(!Strlen(Folder))
```

```
    NewDataFolder /o :root:ForceCurves
```

```
endif
```

```
duplicate /O/R = [ start, stop-1] Sep ExtendSep
```

```
duplicate /O/R = [ start, stop-1] Force ExtendForce
```

```
duplicate /O/R = [ stop, ] Sep RetractSep
```

```
duplicate /O/R = [ stop, ] Force RetractForce
```

```
////////////////////////////////////  
////////////////////////////////////
```

```
// A little more processing here for later curve averaging. This just reverses the  
register for extension curves
```

```
// to make it sync with retraction curves, and zeroes all the seps at the maximum  
force for each curve.
```

```
//-----  
-----//
```

```
if(stringmatch(Trigger,"y"))
```



```
Prompt GroupStr, "BaseName:"
DoPrompt "BaseName:", GroupStr
if (V_Flag)
    return(0)
endif
endif
```

```
If( !Strlen(Reflect))
    Prompt Reflect, "Switch force curve orientation on the X-axis? :"
    DoPrompt "Switch force curve orientation on the X-axis? :", Reflect
    if (V_Flag)
        return(0)
    endif
endif
```

```
if (!Strlen(Register))
    Prompt Register, "Reverse indexing?: "
    DoPrompt "Reverse indexing?: ", Register
    if (V_Flag)
        return(0)
    endif
endif
```

```
/**
/
```

```
String MainFolder = GetDatafolder(1)
```

```

SetDataFolder root:
if(!DataFolderExists(":ForceCurves"))
    NewDataFolder /O root:ForceCurves
endif

```

```

SetDataFolder root:ForceCurves
String WorkFolder = GetDataFolder(1)
SetDataFolder root:
String ForceList = WaveList(GroupStr + "*Force", ";", "")

```

```

//*****
/

```

```

Variable A, B,C, nop = ItemsInList(ForceList, ";")
String DataName, listStr, capStr
for (A=0;A<StopSet ;A+=1)
    capStr = num2Str(Offset+A)
    if (Offset < 10)
        listStr = GrepList(ForceList, "000" + capStr)
    elseif (Offset <100)
        listStr = GrepList(ForceList, "00" + capStr)
    elseif (Offset <1000)
        listStr = GrepList(ForceList, capStr)
    endif
    B = A +Offset
    //C =WhichListItem(listStr, ForceList)
    //DataName = StringFromList(C,ForceList, ";")

```



```
variable StartCurve, StopCurve, Range
setDatafolder root:
Prompt StartCurve, "Start with curve: "
DoPrompt "Start with curve: ", StartCurve
if(V_Flag)
    return(0)
endif
```

```
Prompt StopCurve, "End with curve: "
DoPrompt "End with curve: ", StopCurve
if(V_Flag)
    return(0)
endif
```

```
Range = StopCurve - StartCurve + 1
```

```
if(Range <= 0)
GroupExt("", "", "", StartCurve, 1)
else
GroupExt("", "", "", StartCurve, Range)
endif
```

```
End
```

```
// This ends the .ipf code functional at the time of data acquisition and analysis.
```

```
// Legacy code is listed below. This was non-functional at the time of data analysis
// but kept for the sake of archiving the earlier iterations of this .ipf file.
```

```
//Function WaveCheck(waveStr)
```

```
//    string waveStr
```

```
//End
```

```
//Function AvgForce(BaseStr, num)
```

```
//    Variable num
```

```
//    String BaseStr
```

```
////*****
**/
```

```
//    if (!Strlen(BaseStr))
```

```
//        Prompt GroupStr,"BaseName:"
```

```
//        DoPrompt "BaseName:",BaseStr
```

```
//        if (V_Flag)
```

```
//            return(0)
```

```
//        endif
```

```
//    endif
```

```
////*****
**/
```

```
//    string ForceName, SepName
```

```
//    if (num == 0)
```

APPENDIX A.3 SUPPLEMENTAL DATA TABLE RELATED TO DETERMINATION OF THE MICROBE- PEM INTERACTION ENERGY

PEM Assembly pH (PAA/PAH)	Symbol	γ_{Tot} (mJ/m ²)	γ_{AB}	γ_{LW}	γ^+	γ^-
2.0/2.0	▼	48.5	25.1	23.3	48.5	25.1
6.5/6.5	•	47.3	21.5	25.8	47.3	21.5
3.5/7.5	◆	47.4	20.5	26.9	47.4	20.5
3.5/8.6	■	47.3	20.1	27.2	47.3	20.1
water		72.8	51.0	21.8	72.8	51.0
ethylene glycol		48	19	29	48	19
diiodomethane		50.8	0	50.8	50.8	0
hexadecane		27.5	0	27.5	27.5	0

Table A.3.1 Surface tension components for the microbe-water-polymer system used to test physicochemical and mechanical properties affecting bacterial attachment. Components were determined by analyzing the contact angles of several solvents according to Young's equation (see Methods); or were obtained from reported values in the literature. Data expressed as (mJ/m²) are relative to standard assumed values for water. Symbols are used to indicate PEMs corresponding to those found in table 5.1 (p. 149).

PEM Assembly pH (PAA/PAH)	Symbol	γ_{Tot} (mJ/m ²)	γ_{AB}	γ_{LW}	γ^+	γ^-
2.0/2.0	▼	48.5	25.1	23.3	48.5	25.1
6.5/6.5	●	47.3	21.5	25.8	47.3	21.5
3.5/7.5	◆	47.4	20.5	26.9	47.4	20.5
3.5/8.6	■	47.3	20.1	27.2	47.3	20.1
RP62A <i>S. epidermidis</i>		52.7	17.23	-	2.18	34.14
O157 K- <i>E. coli</i>		56.19	24.31	-	50.58	2.93

Table A.3.2 Surface tension components for the microbe-water-polymer system used to test physicochemical and mechanical properties affecting bacterial attachment. Components were determined by analyzing the contact angles of several solvents according to Young's equation (see Methods); or were obtained from reported values in the literature. Data expressed as (mJ/m²) are relative to standard assumed values for water. Symbols are used to indicate PEMs corresponding to those found in table 5.1 (p. 149). Component values for bacteria listed as they appear in Sharma and Rao (2).

APPENDIX A.4 SUPPLEMENTAL INFORMATION RELATED TO THE DIFFERENCES BETWEEN E MEASURED IN DEIONIZED WATER VERSUS SALT

Below are the results of test performed to establish parameters for the stability of PEMs in liquid media and assembled on differing adhesive platforms. We had previously observed a decrease in MB staining between PEMs incubated in water versus 150 mM PBS for pH 2.0/2.0 assembled PEMs that resulted in a MB staining matching that of the much stiffer pH 6.5/6.5 samples. SPM-enabled nanoindentation was performed on PEMs incubated in Milli-Q water or 150 mM NaCl solution as described in (Ch. 2.3) to determine whether there was a significant change in the mechanical properties of PAA/PAH assembled PEMs after exposure to aqueous salt solutions. Of all the samples tested, the only PEM that exhibited a significant change in mechanical stiffness was the pH 4.0/4.0 sample assembled on aminosilane treated glass slides. However, the respective salt-exposed pH 4.0/4.0 sample showed a decrease in mechanical stiffness, which does not correlate with a decrease in MB staining. Furthermore, the pH 4.0/4.0 samples had shown a broad range of stiffness values in the past and we did not run multiple assembly batches through this testing regimen. Nevertheless, we did not use the pH 4.0/4.0 samples regularly after this set of experiments, for reasons described previously (Ch. 5.3). While there was some variation in the stiffness values for all samples, none of the other compliant PEMs showed a change in stiffness that approached the stiffness of the pH 6.5/6.5, 3.5/7.5, or 3.5/8.6

samples used for comparison in experiments. Based upon this analysis, we felt confident that results pertaining to cell adhesion that were obtained in low ionic strength solutions (e.g. 150 mM NaCl) could be directly compared to those obtained in Milli-Q water. As noted in earlier (Ch.2, Ch.5), this also prompted us to find a more direct way to assess the relative number of ionizable groups at the PEM interface, since MB staining was clearly affected by the presence of ions.

Assembly pH (PAA/PAH)	E (MPa) H ₂ O	E (MPa) PBS, 37° C
2.0/2.0 Glass slide	3.71 ± 2.1	1.51 ± 0.05
2.0/2.0 Polystyrene slide	2.65 ± 1.77	3.31 ± 2.3
2.0/2.0 Treated glass slide	0.75 ± 0.05	2.04 ± 0.3
4.0/4.0 Glass slide	7.1 ± 2.6	8.9 ± 1.5
4.0/4.0 Polystyrene slide	5.6 ± 4.6	8.5 ± 3.6
4.0/4.0 Treated glass slide	81.4 ± 3.8	6.4 ± 4.6

Table A.4.1 Comparison of E detected via SPM-enabled nanoindentation PEMs incubated in deionized water versus incubation in 150 mM phosphate buffered saline, pH 7.4 for two hours at 37° C. (*treated slide = aminosilane treated glass slide, Sigma-Aldrich.*)

APPENDIX A.5 NOTE ABOUT STATISTICAL ANNOTATION FOR EXPERIMENTAL DATA

All experimental data in this thesis are presented with error bars that represent the standard deviation of the sample mean unless otherwise indicated in the text. When necessary, statistical comparisons between data sets were performed according to the criteria established in Bevington, et al.; Kachigan; and, in later studies, Cumming, et al. (214-216). The standard literature reported parameters for specific statistical tests, such as analysis of variance (ANOVA), are presented both in the text and in the figure captions. Whenever a statistical test such as ANOVA is presented, the type of analytical approach is reported with the relevant statistic (e.g., p-value).

REFERENCES

1. Ofek, I., Hasty, D. L., & Doyle, R. J. (2003) *Bacterial Adhesion* (American Society for Microbiology).
2. Sharma, P. K. & Rao, K. H. (2002) *Advances in colloid and interface science* **98**, 341-463.
3. Brash, J. L. & Wojciechowski, P. W. (1996) *Interfacial Phenomena and Bioproducts* (Marcel Dekker, Inc., Madison).
4. Davies, P. F. & Tripathi, S. C. (1993) *Circ Res* **72**, 239-245.
5. Gupton, S. L. & Waterman-Storer, C. M. (2006) *Cell* **125**, 1361-1374.
6. Bershadsky, A. D., Balaban, N. Q., & Geiger, B. (2003) *Annu Rev Cell Dev Biol* **19**, 677-695.
7. Vogel, V. (2006) *Annu Rev Biophys Biomol Struct* **35**, 459-488.
8. Beckerman, M. (2005) *Molecular and Cellular Signaling* (AIP Press, Springer).
9. Krauss, G. (2003) *Biochemistry of Signal Transduction and Regulation* (Wiley-VCH).
10. Chien, S., Li, S., & Shyy, Y. J. (1998) *Hypertension* **31**, 162-169.
11. Corson, M. A., James, N. L., Latta, S. E., Nerem, R. M., Berk, B. C., & Harrison, D. G. (1996) *Circ Res* **79**, 984-991.
12. Resnick, N., Yahav, H., Shay-Salit, A., Shushy, M., Schubert, S., Zilberman, L. C., & Wofovitz, E. (2003) *Prog Biophys Mol Biol* **81**, 177-199.
13. Nilius, B. & Droogmans, G. (2001) *Physiol Rev* **81**, 1415-1459.
14. Nilsson, L. M., Thomas, W. E., Trintchina, E., Vogel, V., & Sokurenko, E. V. (2006) *J Biol Chem* **281**, 16656-16663.
15. Barbee, K. A., Mundel, T., Lal, R., & Davies, P. F. (1995) *Am J Physiol* **268**, H1765-1772.
16. Davies, P. F., Mundel, T., & Barbee, K. A. (1995) *J Biomech* **28**, 1553-1560.
17. Shukla, A., Dunn, A. R., Moses, M. A., & Van Vliet, K. J. (2004) *Mechanics and Chemistry of Biosystems* **4**.
18. Anishkin, A. & Kung, C. (2005) *Curr Opin Neurobiol* **15**, 397-405.
19. Nilsson, L. M., Thomas, W. E., Sokurenko, E. V., & Vogel, V. (2006) *Appl Environ Microbiol* **72**, 3005-3010.
20. (2007) *Mmwr* **56**, 325-329.
21. Paszek, M. J., Zahir, N., Johnson, K. R., Lakins, J. N., Rozenberg, G. I., Gefen, A., Reinhart-King, C. A., Margulies, S. S., Dembo, M., Boettiger, D., et al. (2005) *Cancer Cell* **8**, 241-254.
22. Thomas, W. E., Nilsson, L. M., Forero, M., Sokurenko, E. V., & Vogel, V. (2004) *Mol Microbiol* **53**, 1545-1557.
23. Thomas, W. E., Trintchina, E., Forero, M., Vogel, V., & Sokurenko, E. V. (2002) *Cell* **109**, 913-923.

24. Bell, G. I. (1978) *Science* **200**, 618-627.
25. Bell, G. I., Dembo, M., & Bongrand, P. (1984) *Biophys J* **45**, 1051-1064.
26. Dustin, M. L., Bromley, S. K., Davis, M. M., & Zhu, C. (2001) *Annu Rev Cell Dev Biol* **17**, 133-157.
27. Zhu, C. (2000) *J Biomech* **33**, 23-33.
28. Zaman, M. H., Kamm, R. D., Matsudaira, P., & Lauffenburger, D. A. (2005) *Biophys J* **89**, 1389-1397.
29. Zaman, M. H., Trapani, L. M., Siemeski, A., Mackellar, D., Gong, H., Kamm, R. D., Wells, A., Lauffenburger, D. A., & Matsudaira, P. (2006) *Proc Natl Acad Sci U S A* **103**, 10889-10894.
30. Schmeichel, K. L., Weaver, V. M., & Bissell, M. J. (1998) *J Mammary Gland Biol Neoplasia* **3**, 201-213.
31. Unger, M. & Weaver, V. M. (2003) *Methods Mol Biol* **223**, 315-347.
32. Wang, F., Weaver, V. M., Petersen, O. W., Larabell, C. A., Dedhar, S., Briand, P., Lupu, R., & Bissell, M. J. (1998) *Proc Natl Acad Sci U S A* **95**, 14821-14826.
33. Weaver, V. M., Lelievre, S., Lakins, J. N., Chrenek, M. A., Jones, J. C., Giancotti, F., Werb, Z., & Bissell, M. J. (2002) *Cancer Cell* **2**, 205-216.
34. Weaver, V. M., Petersen, O. W., Wang, F., Larabell, C. A., Briand, P., Damsky, C., & Bissell, M. J. (1997) *J Cell Biol* **137**, 231-245.
35. Zahir, N., Lakins, J. N., Russell, A., Ming, W., Chatterjee, C., Rozenberg, G. I., Marinkovich, M. P., & Weaver, V. M. (2003) *J Cell Biol* **163**, 1397-1407.
36. Pelham, R. J. & Wang, Y. L. (1997) *P Natl Acad Sci USA* **94**, 13661-13665.
37. Pelham, R. J., Jr. & Wang, Y. (1999) *Mol Biol Cell* **10**, 935-945.
38. Georges, P. C., Miller, W. J., Meaney, D. F., Sawyer, E. S., & Janmey, P. A. (2006) *Biophys J* **90**, 3012-3018.
39. Esue, O., Wirtz, D., & Tseng, Y. (2006) *J Bacteriol* **188**, 968-976.
40. Mendelsohn, J. D., Yang, S. Y., Hiller, J., Hochbaum, A. I., & Rubner, M. F. (2003) *Biomacromolecules* **4**, 96-106.
41. Anderson, D. G., Levenberg, S., & Langer, R. (2004) *Nat Biotechnol* **22**, 863-866.
42. Engler, A. J., Richert, L., Wong, J. Y., Picart, C., & Discher, D. E. (2004) *Surface Science* **570**, 142-154.
43. Schneider, A., Francius, G., Obeid, R., Schwinte, P., Hemmerle, J., Frisch, B., Schaaf, P., Voegel, J. C., Senger, B., & Picart, C. (2006) *Langmuir* **22**, 1193-1200.
44. Schneider, A., Vodouhe, C., Richert, L., Francius, G., Le Guen, E., Schaaf, P., Voegel, J. C., Frisch, B., & Picart, C. (2007) *Biomacromolecules* **8**, 139-145.
45. Thompson, M. T., Berg, M. C., Tobias, I. S., Lichter, J. A., Rubner, M. F., & Van Vliet, K. J. (2006) *Biomacromolecules* **7**, 1990-1995.
46. Thompson, M. T., Berg, M. C., Tobias, I. S., Rubner, M. F., & Van Vliet, K. J. (2005) *Biomaterials* **26**, 6836-6845.
47. Kidambi, S., Lee, I., & Chan, C. (2004) *J Am Chem Soc* **126**, 16286-16287.

48. Zhang, J., Senger, B., Vautier, D., Picart, C., Schaaf, P., Voegel, J. C., & Lavallo, P. (2005) *Biomaterials* **26**, 3353-3361.
49. Engler, A., Bacakova, L., Newman, C., Hategan, A., Griffin, M., & Discher, D. (2004) *Biophys J* **86**, 617-628.
50. Engler, A. J., Griffin, M. A., Sen, S., Bonnemann, C. G., Sweeney, H. L., & Discher, D. E. (2004) *J Cell Biol* **166**, 877-887.
51. Engler, A. J., Sen, S., Sweeney, H. L., & Discher, D. E. (2006) *Cell* **126**, 677-689.
52. Richert, L., Engler, A. J., Discher, D. E., & Picart, C. (2004) *Biomacromolecules* **5**, 1908-1916.
53. Schneider, A., Bolcato-Bellemin, A. L., Francius, G., Jedrzejwska, J., Schaaf, P., Voegel, J. C., Frisch, B., & Picart, C. (2006) *Biomacromolecules* **7**, 2882-2889.
54. Varki, A., Cummings, R., Esko, J., Freeze, H., Hart, G., & Marth, J. *Essentials of Glycobiology* (Cold Spring Harbor Laboratory Press).
55. Dimitriadis, E., Horkay, F., Maresca, J., Kachar, B., & Chadwick, R. (2002) *Biophysical Journal* **82**, 2798-2810.
56. Domke, J., Dannohl, S., Parak, W. J., Muller, O., Aicher, W. K., & Radmacher, M. (2000) *Colloid Surface B* **19**, 367-379.
57. Dubreuil, F., Elsner, N., & Fery, A. (2003) *European Physical Journal E* **12**, 215-221.
58. Andersson, M., Karlsson, L., Svensson, P. A., Ulfhammer, E., Ekman, M., Jernas, M., Carlsson, L. M., & Jern, S. (2005) *J Vasc Res* **42**, 441-452.
59. Berk, B. C., Corson, M. A., Peterson, T. E., & Tseng, H. (1995) *J Biomech* **28**, 1439-1450.
60. Kanai, A. J., Strauss, H. C., Truskey, G. A., Crews, A. L., Grunfeld, S., & Malinski, T. (1995) *Circ Res* **77**, 284-293.
61. Cabeen, M. T. & Jacobs-Wagner, C. (2005) *Nature reviews* **3**, 601-610.
62. Cabeen, M. T. & Jacobs-Wagner, C. (2007) *J Cell Biol*.
63. Shih, Y. L. & Rothfield, L. (2006) *Microbiol Mol Biol Rev* **70**, 729-754.
64. Strohl, W. A., Rouse, H., & Fisher, B. D. eds. (2001) *Microbiology* (Lipincott Williams and Wilkins).
65. (1999) *Jama* **282**, 1123-1125.
66. Klevens, R. M., Edwards, J. R., Richards, C. L., Horan, T. C., Gaynes, R. P., Pollock, D. A., & Cardo, D. M. (2007) *Public Health Rep* **122**, 160-166.
67. Klevens, R. M., Morrison, M. A., Nadle, J., Petit, S., Gershman, K., Ray, S., Harrison, L. H., Lynfield, R., Dumyati, G., Townes, J. M., *et al.* (2007) *Jama* **298**, 1763-1771.
68. *Multilayer thin films: sequential assembly of nanocomposite materials* (2003) (Wiley-VCH, Weinheim).
69. OShiratori, S. S. & Rubner, M. F. (2000) *Macromolecules* **33**, 4213-4219.
70. Yang, S. Y., Berg, M. C., Hammond, P. T., & Rubner, M. F. (2003) in *American Chemical Society*.

71. Yang, S. Y., Mendelsohn, J. D., & Rubner, M. F. (2003) *Biomacromolecules* **4**, 987-994.
72. Yang, S. Y. & Rubner, M. F. (2002) *J Am Chem Soc* **124**, 2100-2101.
73. Significant contribution and/or data acquisition by Jenny A. Lichter
74. Significant contribution and/or data acquisition by Dr. Michael Berg
75. Berg, M. C., Yang, S. Y., Hammond, P. T., & Rubner, M. F. (2004) *Langmuir* **20**, 1362-1368.
76. Cleveland, J. P., Manne, S., Bocek, D., & Hansma, P. K. (1993) *Rev Sci Instrum* **64**, 403-405.
77. Johnson, K. L. (1994) *Contact Mechanics* (Cambridge University Press, Cambridge).
78. Bhattacharya, A. & Nix, W. (1988) *Int. J. Sol. Struc.* **24**, 881-891.
79. Van Vliet, K. J. (2002) in *Materials Science and Engineering* (Massachusetts Institute of Technology, Cambridge).
80. Oommen, B. & Van Vliet, K. J. (2005) *submitted*.
81. Oommen, B. & Van Vliet, K. J. (2006) *Thin Solid Films* **513**, 235-242.
82. Kang, S. & Choi, H. (2005) *Colloid Surface B* **46**, 70-77.
83. Kostler, S., Delgado, A. V., & Ribitsch, V. (2005) *J Colloid Interf Sci* **286**, 339-348.
84. van Oss, C. J. (2003) *J Mol Recognit* **16**, 177-190.
85. Abu-Lail, N. I. & Camesano, T. A. (2006) *Langmuir* **22**, 7296-7301.
86. An, Y. H. & Friedman, R. J. (1998) *J Biomed Mater Res A* **43**, 338-348.
87. Cao, T., Tang, H., Liang, X., Wang, A., Auner, G. W., Salley, S. O., & Ng, K. Y. (2006) *Biotechnol Bioeng* **94**, 167-176.
88. Cerca, N., Pier, G. B., Vilanova, M., Oliveira, R., & Azeredo, J. (2005) *Research in microbiology* **156**, 506-514.
89. Chang, C. C. & Merritt, K. (1992) *J Biomed Mater Res* **26**, 197-207.
90. Fu, J., Ji, J., Yuan, W., & Shen, J. (2005) *Biomaterials* **26**, 6684-6692.
91. Harkes, G., Dankert, J., & Feijen, J. (1992) *J Biomat Sci-Polym E* **3**, 403-418.
92. Harkes, G., Dankert, J., & Feijen, J. (1992) *J Biomater Sci Polym Ed* **3**, 403-418.
93. Katsikogianni, M. & Missirlis, Y. F. (2004) *European cells & materials* **8**, 37-57.
94. Katsikogianni, M., Spiliopoulou, I., Dowling, D. P., & Missirlis, Y. F. (2006) *Journal of Materials Science* **17**, 679-689.
95. Liu, Y., Strauss, J., & Camesano, T. A. (2007) *Langmuir* **23**, 7134-7142.
96. Speranza, G., Gotterdi, G., Pederzoli, C., Lunelli, L., Canteri, R., Pasquardiini, L., Carli, E., Lui, A., Maniglio, D., Brugnara, M., *et al.* (2004) *Biomaterials* **25**, 2029-2037.
97. Teixeira, P., Trindade, A. C., Godinho, M. H., Azeredo, J., Oliveira, R., & Fonseca, J. G. (2006) *J Biomater Sci Polym Ed* **17**, 239-246.

98. Triandafillu, K., Balazs, D. J., Aronsson, B. O., Descouts, P., Tu Quoc, P., van Delden, C., Mathieu, H. J., & Harms, H. (2003) *Biomaterials* **24**, 1507-1518.
99. Tseng, H., Peterson, T. E., & Berk, B. C. (1995) *Circ Res* **77**, 869-878.
100. Verran, J. & Whitehead, K. (2005) *Int J Artif Organs* **28**, 1138-1145.
101. Jockusch, S., Lee, D., Turro, N. J., & Leonard, E. F. (1996) *Proc Natl Acad Sci U S A* **93**, 7446-7451.
102. Shirai, M., Nagatsuka, T., & Tanaka, M. (1977) *Journal of Polymer Science Part a-Polymer Chemistry* **15**, 2083-2095.
103. Dean, D., Han, L., Grodzinsky, A. J., & Ortiz, C. (2006) *J Biomech* **39**, 2555-2565.
104. Rixman, M., Dean, D., Macais, C., & Ortiz, C. (2003) *Langmuir* **19**, 6202-6218.
105. Significant contribution and/or data acquisition by Dr. Alicia Jackson and Prof. Francesco Stellaci
106. Adams, J. C. (2002) *Expert Reviews in Molecular Medicine* **4**, 1-24.
107. Levick, J. R. (2000) *An Introduction to Cardiovascular Physiology* (Arnold/Oxford Press, London, United Kingdom/New York, USA).
108. (1997) *The Endothelium in Clinical Practice: the Source and Target of Novel Therapies* (Marcel Dekker, New York).
109. Adams, J. C. (2002) *Journal of cell science* **115**, 257-265.
110. Alberts, B., Johnson, A., Lewis, J., Martin, R., Roberts, K., & Walter, P. (2002) *Molecular Biology of the Cell* (Garland Science, Taylor and Francis Group, New York).
111. Li, S., Huang, N. F., & Hsu, S. (2005) *Journal of Cellular Biochemistry* **96**, 1110-1126.
112. Adams, J. C. (1997) *Trends Cell Biol* **7**, 107-110.
113. Lin, S. Y. & Corey, D. P. (2005) *Curr Opin Neurobiol* **15**, 350-357.
114. McCue, S., Dajnowiec, D., Xu, F., Zhang, M., Jackson, M. R., & Langille, B. L. (2006) *Circ Res* **98**, 939-946.
115. Beckerle, M. C. (2001) *Cell Adhesion* (Oxford, New York).
116. Discher, D. E., Janmey, P., & Wang, Y. L. (2005) *Science* **310**, 1139-1143.
117. Gailit, J. & Clark, R. A. (1994) *Current Opinion in Cell Biology* **6**, 717-725.
118. Gailit, J., Clarke, C., Newman, D., Tonnesen, M. G., Mosesson, M. W., & Clark, R. A. (1997) *Experimental Cell Research* **232**, 118-126.
119. Feng, X., Clark, R. A., Galanakis, D., & Tonnesen, M. G. (1999) *The Journal of Investigative Dermatology* **113**, 913-919.
120. Ruoslahti, E. (1996) *Annu Rev Cell Dev Biol* **12**, 697-715.
121. Lew, A. M., Glogauer, M., & McUlloch, C. A. (1999) *The Biochemical Journal* **341** (Pt 3), 647-653.
122. Chen, J., Fabry, B., Schiffrin, E. L., & Wang, N. (2001) *American Journal of Physiology* **280**, C1475-1484.
123. Wang, N., Butler, J. P., & Ingber, D. E. (1993) *Science* **260**, 1124-1127.

124. (2000) *Bioprobes: Biochemical Tools for Investigating Cell Function* (Springer).
125. Simmons, C. A., Nikolovski, J., Thornton, A. J., Mattis, S., & Mooney, D. J. (2004) *J Biomech* **37**, 1531-1541.
126. Mermut, O., Lefebvre, J., Gray, D., & Barrett, C. (2003) *Macromolecules* **36**, 8819-8824.
127. Kim, B. S. & Vinogradova, O. I. (2004) *J Phys Chem B* **108**, 8161-8165.
128. Lulevich, V. V., Andrienko, D., & Vinogradova, O. I. (2004) *J Chem Phys* **120**, 3822-3826.
129. Lulevich, V. V. & Vinogradova, O. I. (2004) *Langmuir* **20**, 2874-2878.
130. Vinogradova, O. I., Andrienko, D., Lulevich, V. V., Nordschild, S., & Sukhorukov, G. B. (2004) *Macromolecules* **37**, 1113-1117.
131. Cambrex, B. (2005).
132. Yoo, D., Shiratori, S. S., & Rubner, M. F. (1998) *Macromolecules* **31**, 4309-4318.
133. Bradby, R. ed. (2003) *Comprehensive Desk Reference of Polymer Characterization and Analysis* (Oxford University Press).
134. Pavoov, P. V., Bellare, A., Strom, A., Yang, D. H., & Cohen, R. E. (2004) *Macromolecules* **37**, 4865-4871.
135. Domke, J. & Radmacher, M. (1998) *Langmuir* **14**, 3320-3325.
136. Francius, G., Hemmerle, J., Ball, V., Lavalle, P., Picart, C., Voegel, J. C., Schaaf, P., & Senger, B. (2007) *J. Phys. Chem. C* **111**, 8299-8306.
137. Zheng, H., Berg, M. C., Rubner, M. F., & Hammond, P. T. (2004) *Langmuir* **20**, 7215-7222.
138. (1996) *Interfacial Phenomena and Bioproducts* (Marcel Dekker, Inc., Madison).
139. Linder, A., Weiland, U., & Apell, H. J. (1999) *J Struct Biol* **126**, 16-26.
140. McGregor, W. C. (1996) *Interfacial Phenomena and Bioproducts* (Marcel Dekker, Inc., Madison).
141. Keselowsky, B. G., Collard, D. M., & Garcia, A. J. (2005) *Proc Natl Acad Sci U S A* **102**, 5953-5957.
142. Liao, H., Andersson, A. S., Sutherland, D., Petronis, S., Kasemo, B., & Thomsen, P. (2003) *Biomaterials* **24**, 649-654.
143. Ignatius, A., Peraus, M., Schorlemmer, S., Augat, P., Burger, W., Leyen, S., & Claes, L. (2005) *Biomaterials* **26**, 2325-2332.
144. Andersson, A. S., Backhed, F., von Euler, A., Richter-Dahlfors, A., Sutherland, D., & Kasemo, B. (2003) *Biomaterials* **24**, 3427-3436.
145. Rimmer, S., German, M. J., Maughan, J., Sun, Y., Fullwood, N., Ebdon, J., & MacNeil, S. (2005) *Biomaterials* **26**, 2219-2230.
146. Mukherjee, A., Santra, M. K., Beuria, T. K., & Panda, D. (2005) *Febs J* **272**, 2760-2772.
147. Hersel, U., Dahmen, C., & Kessler, H. (2003) *Biomaterials* **24**, 4385-4415.

148. Lieb, E., Hacker, M., Tessmar, J., Kunz-Schughart, L. A., Fiedler, J., Dahmen, C., Hersel, U., Kessler, H., Schulz, M. B., & Gopferich, A. (2005) *Biomaterials* **26**, 2333-2341.
149. Holland, J., Hersh, L., Bryhan, M., Onyiriuka, E., & Ziegler, L. (1996) *Biomaterials* **17**, 2147-2156.
150. Drumheller, P. D. & Hubbell, J. A. (1994) *Anal Biochem* **222**, 380-388.
151. Boura, C., Muller, S., Vautier, D., Dumas, D., Schaaf, P., Claude Voegel, J., Francois Stoltz, J., & Menu, P. (2005) *Biomaterials* **26**, 4568-4575.
152. Ngankam, A., Mao, G., & Tassel, P. V. (2004) *Langmuir* **20**, 3362-3370.
153. Salloum, D., Olenych, S., Keller, T., & Schlenoff, J. (2005) *Biomacromolecules* **6**, 161-167.
154. Brown, X., Ookawa, K., & Wong, J. (2005) *Biomaterials* **26**, 3123-3129.
155. Picart, C., Elkaim, R., Richert, L., Audoin, T., Arntz, Y., Cardoso, M. D., Schaaf, P., Voegel, J. C., & Frisch, B. (2005) *Adv Funct Mater* **15**, 83-94.
156. Ball, V., Hubsch, E., Schweiss, R., Voegel, J. C., Schaaf, P., & Knoll, W. (2005) *Langmuir* **21**, 8526-8531.
157. Boulmedais, F., Bozonnet, M., Schwinte, P., Voegel, J. C., & Schaaf, P. (2003) *Langmuir* **19**, 9873-9882.
158. Jomaa, H. W. & Schlenoff, J. B. (2005) *Langmuir* **21**, 8081-8084.
159. Kovacevic, D., van der Burgh, S., de Keizer, A., & Stuart, M. A. C. (2002) *Langmuir* **18**, 5607-5612.
160. Kovacevic, D., van der Burgh, S., de Keizer, A., & Stuart, M. A. C. (2003) *J Phys Chem B* **107**, 7998-8002.
161. Forget, G., Latxague, L., Heroguez, V., Labrugere, C., & Durrieu, M. C. (2007) *Conf Proc IEEE Eng Med Biol Soc* **1**, 5107-5110.
162. Sakiyama-Elbert, S. & Hubbell, J. A. (2001) *Annu Rev Mater Res* **31**, 183-201.
163. Shu, X. Z., Ghosh, K., Liu, Y., Palumbo, F. S., Luo, Y., Clark, R. A., & Prestwich, G. D. (2004) *J Biomed Mater Res A* **68**, 365-375.
164. Donlan, R. M. (2001) *Emerging infectious diseases* **7**, 277-281.
165. Costerton, J. W., Stewart, P. S., & Greenberg, E. P. (1999) *Science* **284**, 1318-1322.
166. Tiller, J. C., Lee, S. B., Lewis, K., & Klibanov, A. M. (2002) *Biotechnol Bioeng* **79**, 465-471.
167. Tiller, J. C., Liao, C. J., Lewis, K., & Klibanov, A. M. (2001) *Proc Natl Acad Sci U S A* **98**, 5981-5985.
168. Lee, D., Cohen, R. E., & Rubner, M. F. (2005) *Langmuir* **21**, 9651-9659.
169. Aumswan, N., Heinhorst, S., & Urban, M. W. (2007) *Biomacromolecules* **8**, 713-718.
170. Saygun, O., Agalar, C., Aydinuraz, K., Agalar, F., Daphan, C., Saygun, M., Ceken, S., Akkus, A., & Denkbaz, E. B. (2006) *J Surg Res* **131**, 73-79.
171. Hetrick, E. M. & Schoenfisch, M. H. (2006) *Chem Soc Rev* **35**, 780-789.
172. Kohnen, W., Kolbensschlag, C., Teske-Keiser, S., & Jansen, B. (2003) *Biomaterials* **24**, 4865-4869.

173. Ilker, M. F., Nusslein, K., Tew, G. N., & Coughlin, E. B. (2004) *J Am Chem Soc* **126**, 15870-15875.
174. Ignatova, M., Voccia, S., Gilbert, B., Markova, N., Cossement, D., Gouttebaron, R., Jerome, R., & Jerome, C. (2006) *Langmuir* **22**, 255-262.
175. Hermanson, G. T. (1996) *Bioconjugate Techniques* (Academic Press).
176. Lieberman, J. M. (2003) *The Pediatric infectious disease journal* **22**, 1143-1151.
177. Saubolle, M. A. (2006) *American journal of rhinology* **20**, 667-671.
178. Rothfield, L., Justice, S., & Garcia-Lara, J. (1999) *Annu Rev Genet* **33**, 423-448.
179. Rothfield, L. I. & Justice, S. S. (1997) *Cell* **88**, 581-584.
180. Watters, C. (2006) *CBE life sciences education* **5**, 306-310.
181. Kruse, T., Bork-Jensen, J., & Gerdes, K. (2005) *Mol Microbiol* **55**, 78-89.
182. Kruse, T., Moller-Jensen, J., Lobner-Olesen, A., & Gerdes, K. (2003) *The EMBO journal* **22**, 5283-5292.
183. (1999) *Mechanisms of Microbial Disease* (Lipincott, Williams & Williams).
184. Koch, A. L. (2000) *Critical reviews in microbiology* **26**, 1-35.
185. Koch, A. L. & Woeste, S. (1992) *J Bacteriol* **174**, 4811-4819.
186. Mendez-Vilas, A., Gallardo-Moreno, A. M., & Gonzalez-Martin, M. L. (2006) *Antonie van Leeuwenhoek* **89**, 373-386.
187. Bolshakova, A. V., Kiselyova, O. I., & Yaminsky, I. V. (2004) *Biotechnology progress* **20**, 1615-1622.
188. Yao, X., Jericho, M., Pink, D., & Beveridge, T. (1999) *J Bacteriol* **181**, 6865-6875.
189. Banner, M. A., Cunniffe, J. G., Macintosh, R. L., Foster, T. J., Rohde, H., Mack, D., Hoyes, E., Derrick, J., Upton, M., & Handley, P. S. (2007) *J Bacteriol* **189**, 2793-2804.
190. Veenstra, G. J., Cremers, F. F., van Dijk, H., & Fleer, A. (1996) *J Bacteriol* **178**, 537-541.
191. Thomas, W., Forero, M., Yakovenko, O., Nilsson, L., Vicini, P., Sokurenko, E., & Vogel, V. (2006) *Biophys J* **90**, 753-764.
192. Hung, D. L., Raivio, T. L., Jones, C. H., Silhavy, T. J., & Hultgren, S. J. (2001) *The EMBO journal* **20**, 1508-1518.
193. Otto, K. & Silhavy, T. J. (2002) *Proc Natl Acad Sci U S A* **99**, 2287-2292.
194. Edwards, M. D., Booth, I. R., & Miller, S. (2004) *Current opinion in microbiology* **7**, 163-167.
195. Pivetti, C. D., Yen, M. R., Miller, S., Busch, W., Tseng, Y. H., Booth, I. R., & Saier, M. H., Jr. (2003) *Microbiol Mol Biol Rev* **67**, 66-85, table of contents.
196. Vogel, V. & Sheetz, M. (2006) *Nat Rev Mol Cell Biol* **7**, 265-275.
197. Francois, P., Vaudaux, P., & Lew, P. D. (1998) *Annals of vascular surgery* **12**, 34-40.
198. Tang, H., Cao, T., Wang, A., Liang, X., Salley, S. O., McAllister, J. P., 2nd, & Ng, K. Y. (2007) *J Biomed Mater Res A* **80**, 885-894.

199. Whitehead, K. A., Rogers, D., Colligon, J., Wright, C., & Verran, J. (2006) *Colloids Surf B Biointerfaces* **51**, 44-53.
200. Scheuerman, T. R., Camper, A. K., & Hamilton, M. A. (1998) *J Colloid Interface Sci* **208**, 23-33.
201. Taylor, R. L., Verran, J., Lees, G. C., & Ward, A. J. (1998) *Journal of materials science* **9**, 17-22.
202. de Kerchove, A. J., Weronki, P., & Elimelech, M. (2007) *Langmuir* **23**, 12301-12308.
203. MacKintosh, E. E., Patel, J. D., Marchant, R. E., & Anderson, J. M. (2006) *J Biomed Mater Res A* **78**, 836-842.
204. Murata, H., Koepsel, R. R., Matyjaszewski, K., & Russell, A. J. (2007) *Biomaterials* **28**, 4870-4879.
205. Thome, J., Hollander, A., Jaeger, W., Trick, I., & Oehr, C. (2003) *Surface and Coatings Technology* **174-175**, 584-587.
206. Kugler, R., Bouloussa, O., & Rondelez, F. (2005) *Microbiology (Reading, England)* **151**, 1341-1348.
207. Hutter, J. & Bechhoefer, J. (1993) *Rev. Sci.Instrum.* **64**, 1868–1873.
208. Arnsdorf, M. F. & Knight, B. P. (2006) *Patient Information: Implantable cardio-defibrillators. In: UpToDate.*
209. Walton, E. B., Oommen, B., & Van Vliet, K. J. (2007) in *Engineering in Medicine and Biology*, ed. Layton, B. (Lyon, France).
210. Greenspan, F. S. & Gardner, D. G. (2004) *Basic and Clinical Endocrinology* (Lange Medical Books/McGraw-Hill Publishing).
211. Bachmann, B. J. (1972) *Bacteriological reviews* **36**, 525-557.
212. Sundararaj, S., Guo, A., Habibi-Nazhad, B., Melania Rouani, Stothard, P., Ellison, M., & Wishart, D. S. (2004) *Nucleic Acids Res.* , D293–D295.
213. Taylor, C. E. & Greenough, W. B., 3rd (1989) *Annual review of public health* **10**, 221-244.
214. Bevington, P. R. & Robinson, D. K. (1992) *Data reduction and error analysis for the physical sciences* (WCB/McGraw Hill).
215. Cumming, G., Fidler, F., & Vaux, D. L. (2007) *J Cell Biol* **177**, 7-11.
216. Kachigan, S. K. (1991) *Multivariate Statistical Analysis: A conceptual Introduction* (Radius, New York).